creative commons
COMMONS DEED

저작자표시-비영리-변경금지 2.0 대한민국

이용자는 아래의 조건을 따르는 경우에 한하여 자유롭게

- 이 저작물을 복제, 배포, 전송, 전시, 공연 및 방송할 수 있습니다.

다음과 같은 조건을 따라야 합니다:

저작자표시. 귀하는 원저작자를 표시하여야 합니다.

비영리. 귀하는 이 저작물을 영리 목적으로 이용할 수 없습니다.

변경금지. 귀하는 이 저작물을 개작, 변형 또는 가공할 수 없습니다.

- 귀하는, 이 저작물의 재이용이나 배포의 경우, 이 저작물에 적용된 이용허락조건을 명확하게 나타내어야 합니다.
- 저작권자로부터 별도의 허가를 받으면 이러한 조건들은 적용되지 않습니다.

저작권법에 따른 이용자의 권리는 위의 내용에 의하여 영향을 받지 않습니다.

이것은 이용허락규약(Legal Code)을 이해하기 쉽게 요약한 것입니다.

Disclaimer

dCollection

공학박사 학위논문

Mechanistic understanding and performance simulation of anaerobic digestion of thermally hydrolyzed cattle manure

열가수분해 처리된 우분의 혐기성 소화기작 이해와 성능 모사

2023년 8월

서울대학교 대학원

건설환경공학부

김 승 환

Mechanistic understanding and performance simulation of anaerobic digestion of thermally hydrolyzed cattle manure

지도 교수 김 재 영

이 논문을 공학박사 학위논문으로 제출함
2023년 4월

서울대학교 대학원
건설환경공학부
김 승 환

김승환의 공학박사 학위논문을 인준함
2023년 6월

위 원 장 남 경 필 (인)

부위원장 김 재 영 (인)

위 원 조 진 우 (인)

위 원 최 용 주 (인)

위 원 최 정 권 (인)

Mechanistic understanding and performance simulation of anaerobic digestion of thermally hydrolyzed cattle manure

by
Seunghwan Kim

Advisor: Jae Young Kim

A dissertation submitted in partial fulfillment
of the requirements for the degree of

Doctor of Philosophy

Department of Civil and Environmental Engineering
The Graduate School
Seoul National University

August 2023

Abstract

Mechanistic understanding and performance simulation of anaerobic digestion of thermally hydrolyzed cattle manure

Seunghwan Kim

Department of Civil and Environmental Engineering

The Graduate School

Seoul National university

Livestock manure accounts for 80% (wet weight) of the organic waste generated in Korea. While approximately 86% of this waste is treated through composting, it is expected that the demand for compost will decrease in the future. Anaerobic digestion (AD) is a process that can treat organic waste and produce energy simultaneously and has received considerable attention as a method for treating organic waste in recent decades. Although the energy potential of livestock manure through AD is reported to be approximately 1.7 million tons of oil equivalent per year in Korea, the low anaerobic digestion efficiency of livestock manure limits the process performance. This study aimed to investigate the effect of

thermal hydrolysis pretreatment (THP) on the AD of cattle manure (CM).

The THP was applied to the CM samples under various temperatures and NaOH addition conditions, and biochemical methane potential (BMP) was measured. The generation of recalcitrant and toxic substances (e.g., melanoidins and furfural) that could occur during the THP was determined, and the energy balance of the process was calculated. The results showed that increasing the NaOH concentration decreased the lignin content in the fiber and increased the solubilization of CM. The highest BMP has observed in CM treated at 160 ℃ with 2% NaOH addition, with a value of 227.0 ± 11.0 mL-CH_4/g-Volatile solid(VS), which was 25% higher than that of intact CM samples (182.2 ± 2.5 mL-CH_4/g-VS). The generation of recalcitrant substances and furfural was observed at temperatures above 180 ℃, and the production of recalcitrant substances was also promoted with increasing NaOH addition at temperatures below 180 ℃. Therefore, among the THP conditions without the generation of recalcitrant substances, the highest methane potential was observed in CM treated at 160 ℃ without NaOH addition. When applying THP to the AD of CM, it is predicted that an additional 161.4 ± 39.3 MJ/tonne-CM of energy can be produced.

A lab-scale continuously stirred tank reactor was operated under mesophilic anaerobic conditions for approximately 400 d while gradually reducing the solid retention time (SRT). The THP was performed at 160 ℃ and 6.1 atm for 30 min without the addition of NaOH. The results indicated that the THP-applied AD (THP AD)

exhibited more than 1.4 times higher methane yield and VS removal efficiency than the control AD with the same SRT. Even under the SRT of 13.2 d, the THP AD showed higher performance than the control AD with a 36.0 d of SRT. However, the concentration of volatile fatty acids (VFAs) that could cause inhibition increased from 165 mg/L to 613 mg/L in THP AD as SRT reduced from 36.0 d to 13.2 d, and microbial community shifted towards an inefficient direction for the reactor performance. Thus, the stability of AD could decrease. Regardless of the application of THP, a rapid decrease in methane production was observed after 8.0 d of SRT for both THP AD and control AD. The stable operation was confirmed during the three periods of SRT at 13.2 d in this study, but stability confirmation for long-term operation is required.

ADM1 was enhanced to incorporate changes in biochemical parameters resulting from variations in SRT. Linear regression analysis was used to establish the relationship between the SRT and biochemical parameters, which were then incorporated as variables into the Dynamic ADM1. The model was calibrated using experimental data from an AD of CM and validated by simulating methane production of other reactors operated under different conditions and comparing the results. The accuracy of Dynamic ADM1 was improved by comparing it with the conventional ADM1. The same process was applied to an AD of thermally hydrolyzed CM, and the validity of the model was confirmed. According to model simulations, the application of THP resulted in a 1.5-fold increase in average methane production under SRT conditions ranging from 6.6

to 36.0 d. This was due to an increase in biodegradable substrate and maximum growth rate of microorganisms. Furthermore, THP shortened the SRT condition which demonstrated the highest concentration of microorganisms. The Dynamic ADM1 enables more precise prediction of reactor behavior in response to changes in SRT, offering benefits in determining operational conditions, enhancing design, and reducing operating costs.

Keywords: Anaerobic digestion; Thermal hydrolysis pretreatment; Energy balance; Solid retention time; Microbial community; Anaerobic digestion model no.1

Student Number: 2019-33608

Table of Contents

List of Figures

List of Tables

Chapter 1
Introduction

1.1 Background

Domestication of animals for hunting and protection dates back approximately 10,000 years in history. Later, humans began to domesticate other animals for food, such as sheep, goats, pigs, and cattle. Today, livestock plays an important role in our lives, providing us with food, clothing, and work on farms. However, an immense amount of livestock manure is produced each year. Livestock manure production worldwide exceeds 5.7 billion tons per year by dry weight (wt.) (Chávez-Fuentes et al., 2017). Cattle manure (CM) accounts for most of the total livestock manure production, exceeding swine manure and chicken manure by factors of 9.4 and 6.0, respectively. In South Korea, 51 million tons (by dry wt.) of livestock manure was produced in 2020. which accounts for 80% (by wet wt.) of the three major organic wastes (livestock manure, food waste, and sewage sludge) (Ministry of Environment, 2022). Livestock manure is being treated by composting approximately 87 wt.%, but it can cause environmental pollution when introduced into water systems, such as rivers or lakes (Han et al., 2019; Xing et al., 2021). In addition, the agricultural area, which is the main source of demand for compost, is 1.5 million hectares, a 12% decrease from 2012. Due to the

continuous decrease in agricultural areas, the demand for compost is expected to decrease as well, and this demand also fluctuates significantly depending on the season (Statistics Korea, 2022).

Livestock manure is now recognized as a valuable bioresource that can be harnessed for energy generation using eco-friendly methods such as anaerobic digestion (AD), gasification, and carbonization. AD uses microorganisms to break down organic matter in the absence of oxygen to produce biogas, which is primarily composed of methane and carbon dioxide. Biogas can be used as a source of renewable energy because it can be combusted to generate electricity and heat. However, the treatment of CM can be challenging because of its slow degradation rate. This is due to the pre-degradation of the readily biodegradable parts of the digestive organ of a cow and its high lignocellulose content of approximately 40–50 wt.%. Lignocellulose is a complex mixture of lignin, cellulose, and hemicellulose (LCH), which is difficult for microorganisms to break down. AD of CM is hindered by its slow degradation rate, resulting in long solid retention times and high operating costs.

One of the fundamental issues with AD is the instability of the process. There are limitations to using experiments to understand the changes under various conditions. In order to address this, mechanistic mathematical process modeling is being used, and numerous dynamic models for AD have been developed since the late

1960s (Weinrich & Nelles, 2021a). The Model is divided into several compartments, each representing a specific biochemical reaction or microbial group involved in AD. Reactions are determined by the chemical compounds involved, rather than by each microorganism present. Therefore, the microorganisms metabolizing the same compound are not distinguished from one another and are represented by a single biochemical parameter. In fact, dozens of microbial species participate in AD, and multiple types of microorganisms can participate in the metabolism of the same substrate. For example, various microorganisms (eg., *Pelotomaculum sp., Cloacamonas sp.*) are involved in the degradation of propionate to acetate (Ahlert et al., 2016; Peces et al., 2021; Wu et al., 2022). Each microorganism has a unique set of characteristics that result in different substrate uptake rates and half-saturation constants, resulting in different growth rates. Therefore, biokinetic parameter of the substrate can also change as the microbial composition changes. However, in the conventional ADM1 model, the same parameters are used for simulation under different conditions.

1.2 Objectives

The primary objective of this study was to evaluate the biokinetics of anaerobic digestion of thermally hydrolyzed cattle manure. The specific objectives of this study were:

1) To evaluate the effects of thermal hydrolysis pretreatment conditions on the formation of refractory compounds and energy recovery in the anaerobic digestion of cattle manure
2) To investigate the potential of using thermal hydrolysis pretreatment to reduce the solid retention time in the anaerobic digestion of cattle manure
3) To enhance ADM1 to incorporate the changes in biochemical parameters resulting from variations in solid retention time

1.3 Dissertation structure

This dissertation is composed of six chapters, as illustrated in Figure 1.1. Chapter 1 introduces the background, objectives, and structure of the dissertation. Chapter 2 presents a comprehensive literature review on the occurrence and treatment of cattle manure, anaerobic digestion of cattle manure, and modeling of anaerobic digestion. In Chapter 3, the focus is on analyzing the effects of thermal hydrolysis pretreatment on the physicochemical properties of cattle manure and investigating the digestibility of the pretreated cattle manure through the BMP test. Chapter 4 investigates the performance and stability of anaerobic digestion of thermally hydrolyzed cattle manure in a continuous flow reactor under varied solid retention time. The selection of pretreatment condition is based on the findings from Chapter 3. Chapter 5 proposes an enhanced version of ADM1 that incorporates the changes in biochemical parameters resulting from variations in the solid retention time of the anaerobic digester. The experimental results from Chapter 4 are utilized for the calibration of the ADM1. Finally, Chapter 6 provides a summary and the conclusions of the dissertation.

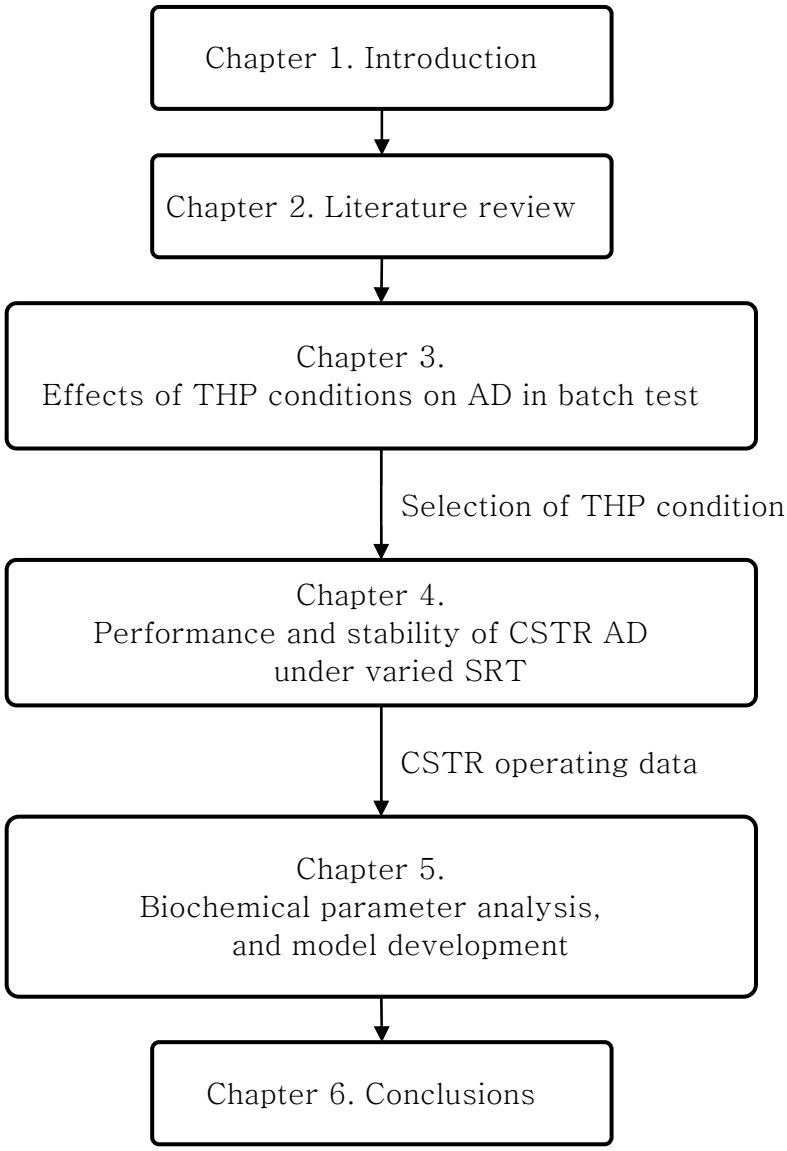

Figure 1.1 Structure of dissertation

References

Ahlert, S., Zimmermann, R., Ebling, J., & König, H. (2016). Analysis of propionate-degrading consortia from agricultural biogas plants. *MicrobiologyOpen*, *5*(6), 1027–1037.

Chávez-Fuentes, J. J., Capobianco, A., Barbušová, J., & Hutňan, M. (2017). Manure from Our Agricultural Animals: A Quantitative and Qualitative Analysis Focused on Biogas Production. *Waste and Biomass Valorization*, *8*(5), 1749–1757.

Han, F., Yun, S., Zhang, C., Xu, H., & Wang, Z. (2019). Steel slag as accelerant in anaerobic digestion for nonhazardous treatment and digestate fertilizer utilization. *Bioresource Technology*, *282*, 331–338.

Ministry of Environment (2022). The state of waste generation and treatment.

Ministry of Trade, Industry and Energy, 2021, New & Renewable energy white paper

Peces, M., Astals, S., Jensen, P. D., & Clarke, W. P. (2021). Transition of microbial communities and degradation pathways in anaerobic digestion at decreasing retention time. *New Biotechnology*, *60*, 52–61.

Wu, D., Li, L., Zhen, F., Liu, H., Xiao, F., Sun, Y., Peng, X., Li, Y., & Wang, X. (2022). Thermodynamics of volatile fatty acid degradation during anaerobic digestion under organic overload stress: The potential to better identify process stability. *Water Research*, *214*.

Xing, T., Yun, S., Li, B., Wang, K., Chen, J., Jia, B., Ke, T., & An, J.

(2021). Coconut-shell-derived bio-based carbon enhanced microbial electrolysis cells for upgrading anaerobic co-digestion of cow manure and aloe peel waste. *Bioresource Technology*, *338*, 125520.

Chapter 2
Literature Review

2.1 Occurrence and treatment of cattle manure

In the last few decades, one of the most remarkable achievements of the world has been the rapid industrialization of agriculture. The number of livestock has continuously increased due to population growth and industrialization (Figure 2.1). According to the Food and Agriculture Organization of the United Nations (FAO), there were about 25.5 billion chickens, 1.5 billion cattle, 1.2 billion sheep, and 0.9 billion pigs (FAO, 2023). Globally, over 5.7 billion tons of livestock manure are produced annually in terms of dry weight (wt.) (Chávez-Fuentes et al., 2017). Most of this production comes from cattle manure, which surpasses pig and chicken manure by 9.4 and 6.0 times, respectively.

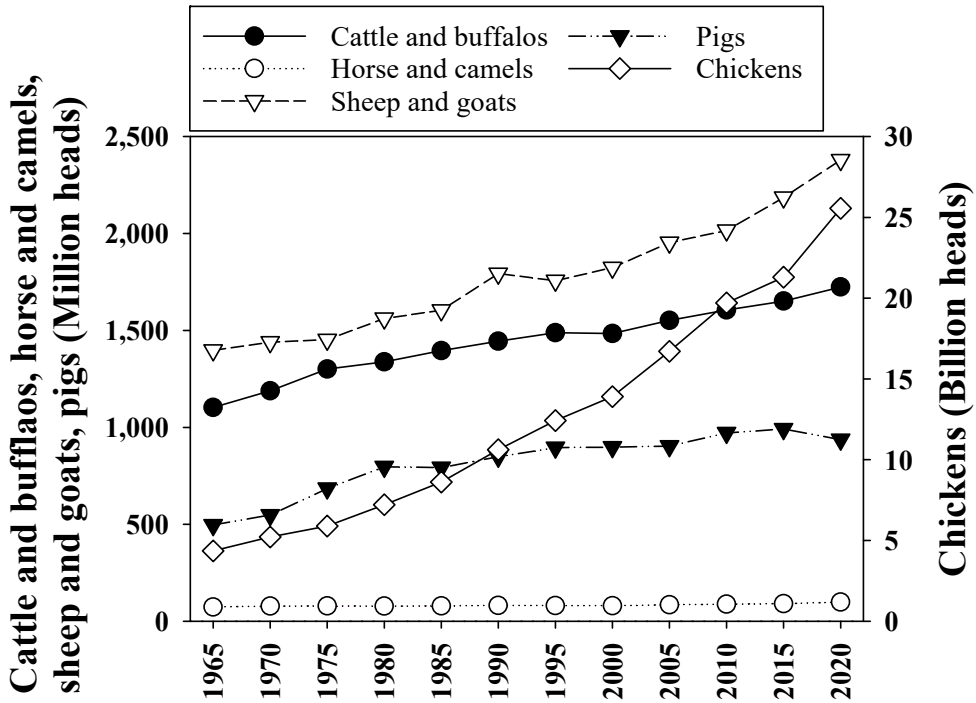

Figure 2.1 Global livestock population growth trend (FAO, 2023)

In 2020, South Korea had 179 million chickens, 6.5 million pigs, and 2.6 million cattle (Statistics Korea, 2023). In South Korea, 51 million tons (wet wt.) of livestock manure are generated, accounting for 80% (wet wt.) of the primary organic waste resources in the country, which including livestock manure, food waste, and sewage sludge (Ministry of Environment, 2022). Livestock manure was previously considered wastewater and was subject to pollution prevention-focused purification policies and treatment processes. After the enactment of the livestock manure management and

utilization act in 2006, the concept of resource recovery was introduced, leading to a significant increase in resource recovery facilities for manure composting and liquid fertilizer production. In 2020, only 13% of livestock manure is being purified and discharged into the water system, while 87% is being processed through composting (Figure 2.2). However, this practice can lead to environmental contamination if the composted manure enters the water bodies like rivers or lakes (F. Han et al., 2019; K. Wang et al., 2021).

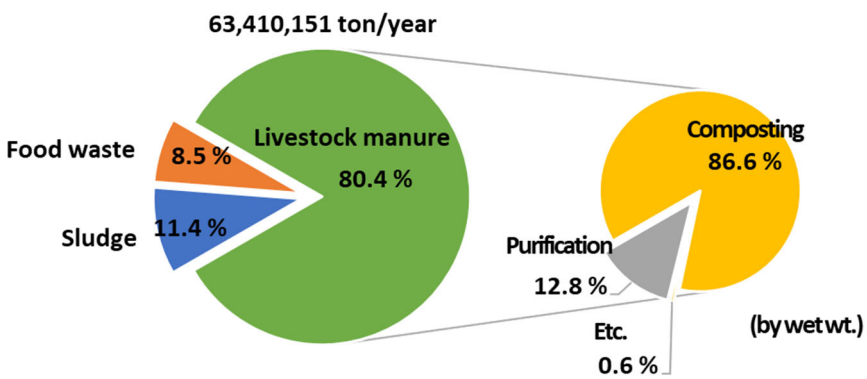

Figure 2.2 Organic waste production and treatment status of livestock manure (Ministry of Environment, 2022)

Moreover, the primary market for compost, agricultural land, has seen a 12% reduction since 2012, now spanning 1.5 million hectares. With the ongoing decrease in agricultural areas, compost demand is anticipated to decline, and its demand also varies

significantly depending on the season (Statistics Korea, 2022). Following this, the government is developing policies to limit the total amount of nutrients entering agricultural land and promoting treatment methods that avoid the use of composting and liquid fertilizer production while recovering energy. In December 2022, the bioenergy promotion act was proposed, which allocates biogas production quotas to businesses that discharge organic waste, aiming to promote the production and utilization of biogas from organic wastes.

According to the New & Renewable energy white paper published by the Ministry of Trade, Industry and Energy, the energy potentials of livestock manure, sewage sludge, and food waste are 1.7, 0.66, 0.48 million TOE/year, respectively (Ministry of Trade, Industry and Energy, 2021). The potential from cow manure alone is 0.8 million TOE/year, accounting for approximately 45.5% of the total potential from livestock manure. In 2021, there were a total of 109 biogas plants across South Korea that processed organic waste. However, it is concerning to note that out of these, only three plants were dedicated to livestock manure. In comparison, there were 25 plants for food waste, 28 for sewage sludge, and 51 for co-digestion (Figure 2.3).

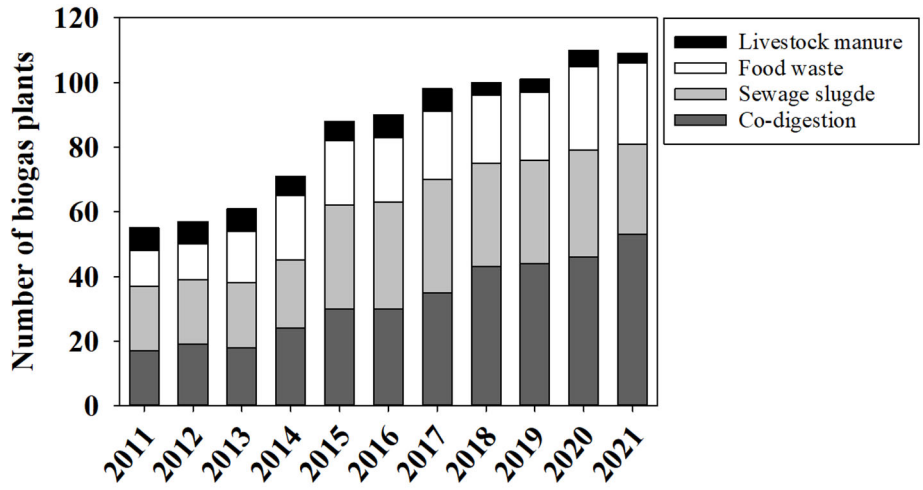

Figure 2.3 Number of biogas plants in South Korea (Ministry of Environment, 2022)

2.2 Anaerobic digestion of cattle manure

2.2.1 Principal of anaerobic digestion

Anaerobic digestion (AD) is a biological process that occurs in the absence of oxygen, where microorganisms break down organic matter into biogas, primarily composed of methane and carbon dioxide. This process is commonly employed for treating various organic wastes, including sewage sludge, food waste, and livestock manure, and generates biogas, which can be used as a renewable energy source. The fundamental stages of anaerobic digestion are hydrolysis, acidogenesis, acetogenesis, and methanogenesis (Figure 2.4).

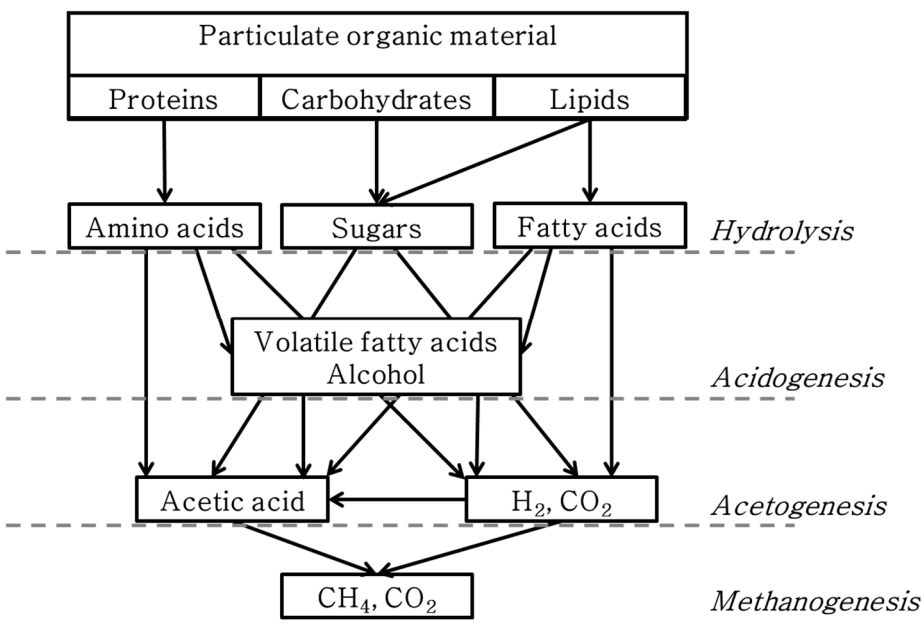

Figure 2.4 Process of anaerobic digestion

In the hydrolysis stage, complex organic compounds such as carbohydrates, proteins, and lipids are broken down into simpler compounds like sugars, amino acids, and fatty acids by hydrolytic enzymes secreted by microorganisms. The hydrolysis of particulate matter can occur through physicochemical reactions. Hydrolysis of slowly decomposable material such as fiber can be a late-limiting stage for AD. During acidogenesis, fermentative bacteria convert the simpler compounds from hydrolysis into volatile fatty acids (VFAs) and other short-chain organic acids, along with alcohol, hydrogen, and carbon dioxide. Acidogenic microbes generally consist of facultative bacteria and obligatory bacteria. In acetogenesis, acetogenic bacteria further break down the products of acidogenesis into acetate, hydrogen, and carbon dioxide. In methanogenesis, methanogenic archaea, a distinct group of microorganisms, convert the acetate, hydrogen, and carbon dioxide produced in the previous stages into methane and carbon dioxide, which are the primary components of biogas. There are three primary pathways in this stage: acetoclastic methanogenesis, where acetate is converted to methane and carbon dioxide, hydrogenotrophic methanogenesis, where hydrogen and carbon dioxide are combined to form methane, and methylotrophic methanogenesis, where methylated compounds are converted to methane and carbon dioxide.

Different species of bacteria and archaea have evolved to

work together in a symbiotic relationship, in which one organism produces a metabolite that the other can use as an energy source. For example, in the acetogenesis stage, some acetogenic bacteria will produce acetic acid and hydrogen as metabolic by-products, which are then used as energy sources by methanogenic archaea. This syntrophic relationship helps to stabilize the AD process, as it ensures that microorganisms can work together in a balanced way.

2.2.2 Effect of solid retention time in anaerobic digestion

AD is a biological process that is sensitive to changes in environmental conditions, such as feedstock type, temperature, and pH, which can lead to digester failure. The application of pretreatment on AD can also change the microbial community by making the organic matter more accessible to microorganisms. Moreover, the solid retention time (SRT) is critical for microbial growth. An insufficient SRT can cause microorganism washout, leading to digester failure. For instance, the methanogenic process fails at an SRT of 2.5–4 d owing to methanogen washout (Lawrence & McCarty, 1969). Reactor failure due to microbial imbalance is a frequent problem, and a clear understanding of the effects of THP and SRT on the microbial community in reactors is vital for maintaining digester stability. Table 2.1 shows a study on the effect of SRT on AD. Zhang et al. (2022) observed a decrease in the microbial diversity in the AD of THP sludge as the SRT decreased from 30 d to 10 d (L. Zhang et al., 2022).

Table 2.1 Study on the effect of SRT on AD

Substrate	SRT (d)	Summary	Reference
Thermally hydrolyzed sludge	20, 10, 5, and 3	−Microorganisms were washed out at SRT of 3 d −Acidogenesis and methanogenesis became the rate−limiting step −VS removal correlated with the methanogenic communities	Wandera et al., 2019
Thermally hydrolyzed sludge	20, and 10	−Relative abundance of *Methanosarcina/Methanosaeta* increased/decreased with THP −Solubility and availability of P decreased after THP and AD	X. Liu et al., 2021
Thermally hydrolyzed sludge	30, 20, 15, and 10	−SRT of AD treating thermal hydrolysis pretreated sewage sludge could be reduced to 15 d −Determinism dominated in THP−AD microbial community assembly while the greater role of stochasticity during the community assembly at longer SRT −Microbial network had lower modularity and stronger interaction at longer SRTs	L. Zhang et al., 2022
Thickened mixed sludge	20, 15, 10, 7.5, 5, and 4	−Typical syntrophic interactions among hydrolytic bacteria, VFA−degrading bacteria, and methanogens were replaced by new interactions at the 5 and 4 d SRT −Decrease in the apparent hydrolysis constant with higher SRT	I. S. Lee et al., 2011
Sugar beet byproduct and pig manure	20, 18, 15, 12, 8, 6, and 5	−The highest methane productivity was obtained at SRT of 6 d −An SRT of 5 d can lead to the accumulation of VFA, system recovery is possible by increasing SRT to 6 d	Aboudi et al., 2015
Cattle manure and food waste	25, 20, 15, 10, 7, 5, and 4	−Complete process failure was taken place at 4 d SRT −Acetoclastic methanogens were largely affected by SRT shortening	Bi et al., 2020

Wandera et al. (2019) reported a decrease in methane yield from 0.28 to 0.12 L-CH_4/g-volatile solids (VS) and an increase in the acetate concentration from 38 to 376 mg/L in the AD of THP sewage sludge as SRT decreased from 20 d to 3 d (Wandera et al., 2019).

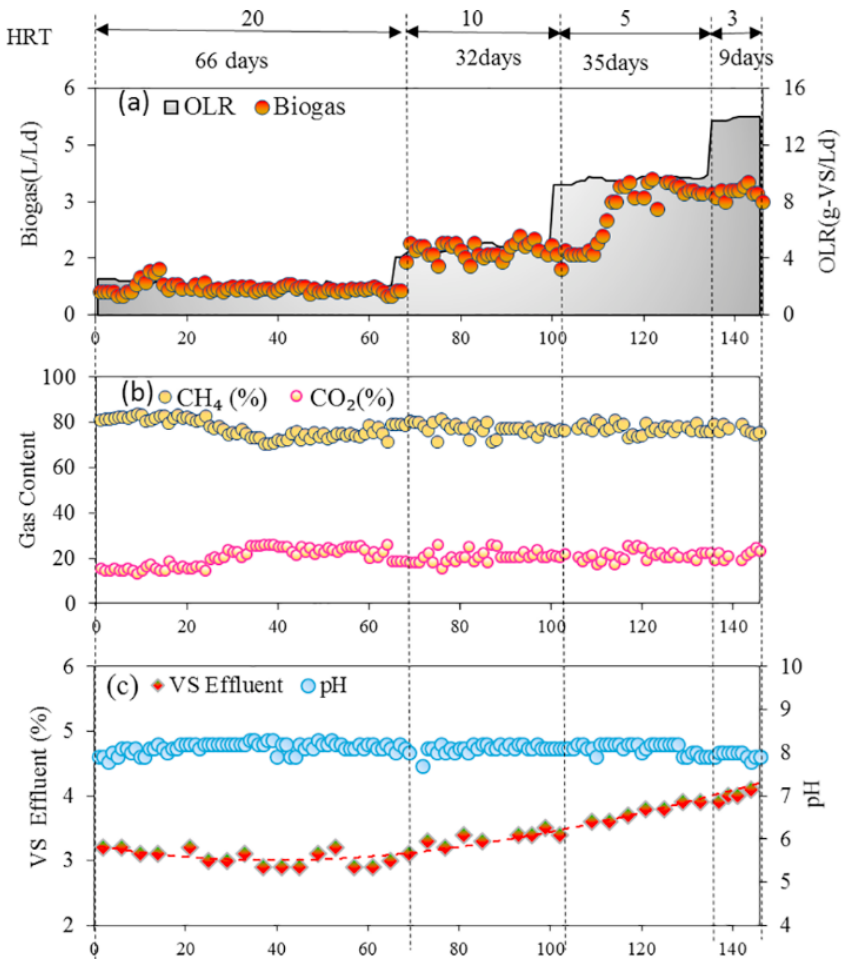

Figure 2.5 The performance of CSTR operated at a HRT from 20 to 3 d (Wandera et al., 2019)

It is worth noting that the behavior of AD may vary significantly depending on the substrate type and operating conditions. However, the effects of THP and SRT on the AD of cattle manure have not been studied.

2.2.3 Characteristics of cattle manure

In cattle farming, feed with high fiber content is mainly used. Due to the characteristics of ruminant animals, easily digestible materials in the feed consumed by cattle are digested during the passage through the digestive organs, and thus, a large amount of undigested fiber is excreted in cattle manure. Additionally, bedding materials such as sawdust, and rice husks are often spread on the floor at a depth of 5 – 10 cm for moisture control and environmental maintenance during cattle farming. Consequently, cattle manure contains around 40 – 60% of lignocellulosic biomass (LCB).

Table 2.2 Characteristic of livestock manure

Sample	TS (wet wt.%)	VS/TS (wt.%)	Lignocellulosic biomass (dry wt.%)				Methane yield ($mL-CH_4/g-VS$)	Reference
			Cellulose	Hemicellulose	Lignin	Total		
Cattle manure	19.6	84.8	21.2	30.4	11.6	63.2	37.5	R. Li et al., 2009
	19.4	93.1	23.5	12.8	8.0	44.3	270.0	K. Li et al., 2015a
	44.3	73.9	17.9	15.7	18.2	51.8	206.9	Shen et al., 2019
	16.8	54.9	22.9	22.9	8.1	53.9	112.1	Zhao et al., 2018
	20.3	86.8	26.7	26.7	11.9	65.3	120.6	Bah et al., 2014
	27.7	84.7	24.2	14.2	10.7	49.1	–	Waszkielis et al., 2022
	15.5	–	21.9	12.5	13.9	48.3	–	Liao et al., 2006
Pig manure	84.5	80.2	32.4	14.6	18.4	65.4	191.4	C. Zhang et al., 2013
	47.5	77.3	15.9	16.7	1.8	34.4	377.0	K. Li et al., 2015a
	25.2	67.9	22.0	22.0	9.8	53.8	111.0	Molinuevo-Salces et al., 2013
	48.8	93.0	11.9	18.8	7.7	38.4	178.7	F. Shen et al., 2019
	28.2	72.4	18.2	21.5	4.8	44.5	187.7	J. Shen et al., 2019b
	18.1	51.9	23.6	21.7	8.4	53.7	245.1	R. Li et al., 2019
Poultry manure	37.5	71.6	37.2	25.5	8.4	71.1	163.2	Wei et al., 2020
	41.9	84.5	44.0	11.8	1.7	57.5	410.0	K. Li et al., 2015a
	24.9	78.1	20.0	23.2	2.3	45.5	260.8	Y. Li et al., 2013
	30.5	66.0	4.4	19	4.2	27.6	158.0	Molinuevo-Salces et al., 2013
	26.8	65.6	14.9	24.3	3.3	42.5	273.9	J. Shen et al., 2019b
	32.5	74.4	24.3	9.9	5.1	39.3	261.7	Rahman et al., 2018

The composition of lignocellulosic biomass (LCB) consists of three biopolymers: cellulose, hemicellulose, and lignin (Figure 2.6). Rather than existing individually, these polymers form lignin–carbohydrate complexes (LCCs) through chemical bonds between lignin and carbohydrates (Azuma & Tetsuo, 1988; Giummarella et al., 2019). It is believed that during the lignification of the cell wall, lignin replaces most of the water. As a result, the hydrophobic and covalent interactions between lignin and carbohydrates make LCB a sturdy and densely packed solid matrix. The presence of LCC bonds in LCB results in a complex structure with intricate physicochemical characteristics and morphology. This complexity of macromolecules in any biomass limits the accessibility of biomolecules during the AD process. The efficiency of enzymatic hydrolysis is thought to be reduced due to the complex structure of LCB (Arslan et al., 2016; Himmel et al., 2007).

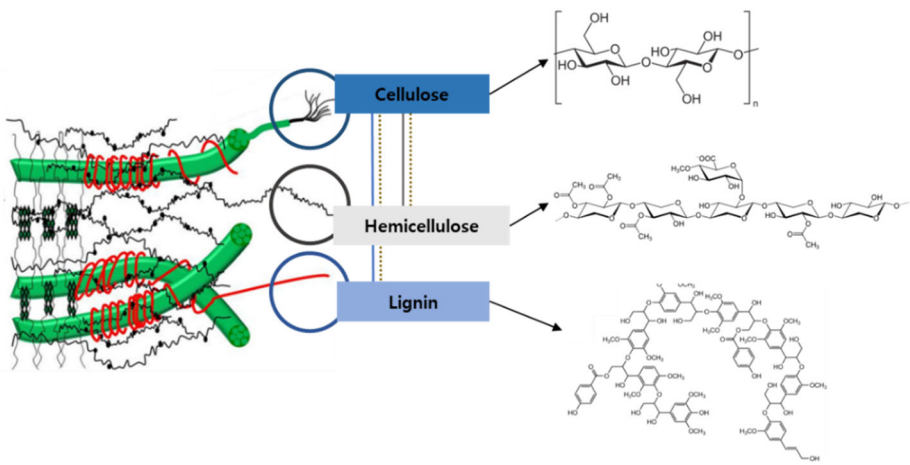

Figure 2.6 Structure of lignocellulosic biomass

2.2.4 Pretreatment of cattle manure for anaerobic digestion

Many pretreatment technologies have been developed with diverse objectives, including acidic, alkaline, ultrasonic, biochemical, mechanical, and integrated processes (Table 2.3). There are several strategies to overcome the low digestion efficiency in AD of CM, including increasing the reaction rate or methane potential. One potential approach involves promoting the hydrolysis step, as known as the rate-limiting step, to enhance the overall reaction rate. Increasing the methane potential involves improving the biodegradability of the substrate. This can be achieved by making previously non-biodegradable materials susceptible to decomposition through pretreatment.

Table 2.3 Type of pretreatments used to improve the biogas production

Pretreatments	Effects on lignocellulosic structure			References
	Cellulose	Hemicellulose	Lignin	
Physical				
Milling	Reduces crystallinity			[1]
Microwave	Increases substrate availability			[2]
Physicochemical				
Steam explosion		Solubilization	Solubilization	[3]
Plasma	Degradation			[4]
CO_2 explosion	Break the structure	Break the structures		[5]
Liquid hot water		Solubilization		[6]
Chemical				
Alkaline		Solubilization	Breck down	[7]
Acid		Solubilization	Breck down	[8]
Organosolv		Solubilization	Solubilization	[9]
Biological				
Microbial consortia, and enzymes	Degradation	Degradation	Degradation	[10]

[1]: Muhammad Nasir & Mohd Ghazi, 2015; [2] Kumar et al., 2009; [3] Agbor et al., 2011; [4] Batista Meneses et al., 2022; [5] Y. Zheng et al., 1995; [6] Taherzadeh & Karimi, 2008; [7] Janker-Obermeier et al., 2012; [8] C. Li et al., 2010; [9] Park et al., 2010; [10] Amin et al., 2017

The physical pretreatment of LCB primarily affects its crystallinity and increases its surface area (Victorin et al., 2020). This increase in the surface area leads to improved accessibility of anaerobic bacteria to the biomass, resulting in an improvement in methane yield. Combining mechanical and chemical pretreatments is an effective method for lignin removal, which can result in improved methane yield and degradability of LCB (Thomas et al., 2019). Acidic pretreatments primarily enhance hemicellulose hydrolysis, with minimal impact on cellulose and lignin removal. However, acidic pretreatments can generate inhibitors that can affect the microorganisms. Hydrothermal pretreatment leads to the breakdown of hemicellulose, modification of lignin, and creation of amorphous regions in cellulose (Ruiz et al., 2013). In addition, alkali-based pretreatment has also been investigated for its effectiveness in AD of LCB and was found to primarily impact the hemicellulose and lignin components (Abraham et al., 2020). Hydrothermal pretreatment is associated with cost-related drawbacks, such as the need to maintain high-temperature and high-pressure conditions, as well as high energy consumption (Liu et al., 2020; Barber, 2016). Additionally, it can lead to the release of ammonium ion from organic matter, and an increase in recalcitrant soluble compounds (Phothilangka et al., 2008; Wilson and Novak, 2009). However, despite these challenges, it has gained attention due to its high pretreatment efficiency.

2.2.5 Thermal hydrolysis pretreatment of cattle manure

Studies on alkaline THP are being conducted to improve the digestibility of livestock manure (Biswas et al., 2015; Khan & Ahring, 2021a; X. Liu et al., 2020; Tsapekos et al., 2016). Some studies have investigated the effects of alkaline THP. Khan and Ahring observed 1.43 times increase in methane yield under mesophilic digestion of digested manure fibers with the addition of 3% (w/w) NaOH to THP (135 ℃ for 1 h) (Khan & Ahring, 2021a). Tsapekos et al. (2016) investigated the effect of alkaline THP (2 – 6% (dry wt.) NaOH at 55 – 121 ℃) on the anaerobic digestion of fibers (Tsapekos et al., 2016). They found that pretreatment using 6% (dry wt.) NaOH at 55 ℃ was the most efficient method as it improved biogas production by 1.26 times than that of the control.

It was discovered that the colored compounds formed during THP are melanoidins, which are products of the Maillard reaction (Dwyer et al., 2008). The Maillard reaction can be accelerated by an increase in pH resulting from the addition of alkaline chemicals (Lund & Ray, 2017; Takashima & Tanaka, 2014).

Table 2.4 Study on the thermal hydrolysis of livestock manure

Feedstock	Temperature (℃)	Chemicals	Summary	Reference
Dairy manure	120	NaOH, CaO, H_2SO_4, HCl, and H_2O_2	−Increasing methane yield from 200 to 350 mL−CH_4/g−VS −Promoting degradation of cellulose and hemicellulose	Jin et al., 2009
Dairy manure	80 and 180	HCl, NaOH, and H_2SO_4	−Alkaline and alkaline hydrogen peroxide pretreatments enhanced methane yield −Sever−acid pretreatment produced furan byproducts and inhibited biogas production	Kim & Karthikeyan, 2021
Digested manure	100 and 135	1 – 3% of NaOH	−The methane yield was increased from 62 ml−CH_4/g−VS to 151 mg−CH_4/g−VS	Khan & Ahring, 2020
Digested diary manure fiber	180	2% of NaOH	−Increased methane yield by 1.43 times then control	Khan & Ahring, 2021
Digested diary manure fiber	55, 90, and 121	2, 4, and 6% of NaOH	−Increased methane yield by 1.26 times than the control	Tsapekos et al., 2016
Swine manure	70 – 190	pH adjusted to 10 and 12 by NaOH	−Temperatures higher than 135 ℃ were necessary to improve the methane potential −THP at pH 12 resulted in a decrease in biodegradability	Carrère et al., 2009

Previous research has investigated the antimicrobial properties of melanoidins and discovered that their ability to chelate metals is responsible for this activity (Figure 2.7)

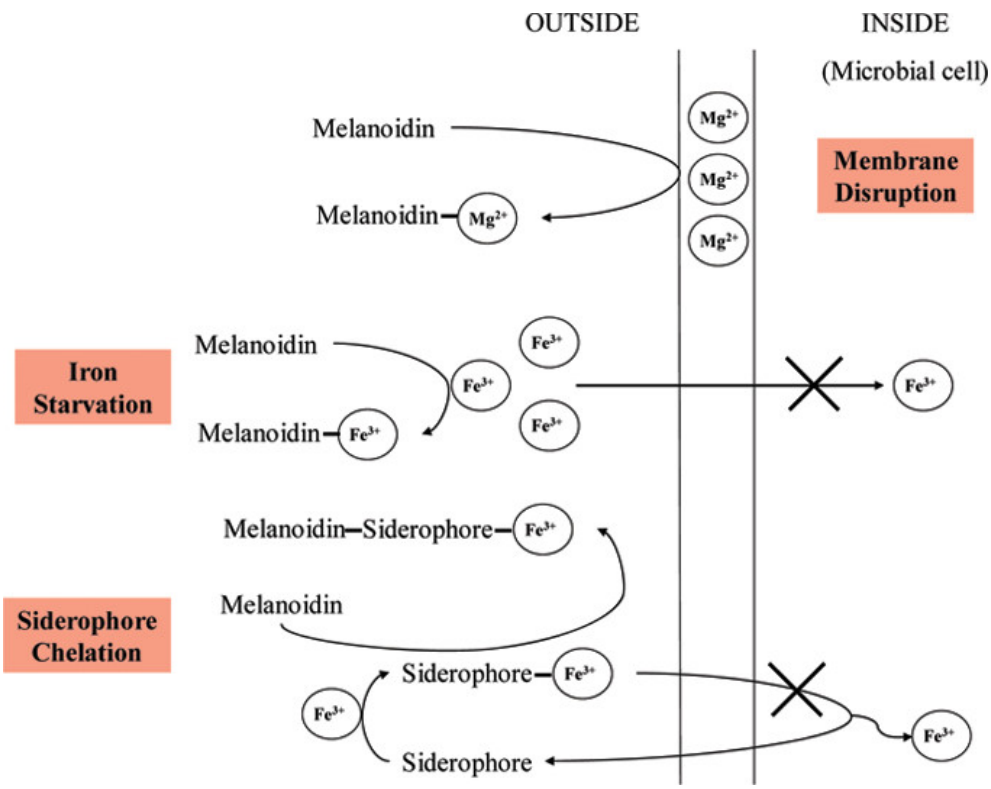

Figure 2.7 Antimicrobial activity of melanoidins (Rufián-Henares & de la Cueva, 2009)

The inhibition effects of THP by-products on microbial processes are summarized in Table 2.1. Melanoidins exhibit limited degradation in the AD process, and can inhibit microbial activity (Chandra et al., 2008). Also in the de-ammonification process, aerobic and anoxic bacteria can be inhibited by the organics present

in THP-AD filtrate (Cao et al., 2022; Tan et al., 2021; Q. Zhang et al., 2018). Also, sugars can be degraded to furan derivatives by caramelization at 120 ℃ or higher (Göncüoğlu Taş & Gökmen, 2017; J.-S. Kim & Lee, 2008; Kroh, 1994). Furan derivatives have the potential to inhibit cell growth and enzymatic activity (Ahmed et al., 2019; Almeida et al., 2009; Palmqvist & Hahn-Hägerdal, 2000; Zhen et al., 2017). For the stable operation of the AD, it is essential to quantitatively determine substances that have the potential to inhibit the process. However, the research on the formation of THP by-products in the broad range of alkaline THP of CM is limited.

Table 2.5 Inhibition effects of THP by-products

Substrate	Precursor	Reaction condition	Concentration	Inhibition	Reference
Melanoidins	Food waste	170℃, 3 h	-	-12% in VFA production	Yin et al., 2019
Melanoidins	Sludge	165 ℃, 30 min	-	-28% in specific anammox activity	Gu et al., 2018
Melanoidins	Sludge	130 ℃, 1 h	8 mmol/L	-33% in methane production	Yang et al., 2023
Melanoidins	Sugar and lysine	120 ℃, 1 h	1,000 mg/L	-44% in oxidative degradation	Jing and Kitts, 2000
Melanoidins	Glucose and tryptophan	80 ℃, 7 d	-	-Not degraded in AD -42% in methane production	S. Wang et al., 2021
Melanoidins	Glucose and glycine	165 ℃, 30 min	-	-26% in methane production	Ortega-Martínez et al., 2021
Furfural	-	-	2,000 mg/L	-69% in methane production	J. R. Kim & Karthikeyan, 2021
HMF[a)]	-	-	2,000 mg/L	-32% in methane production	
Furfural	-	-	1,900 mg/L	-90% in microbial growth rate	Heer & Sauer, 2008
HMF	-	-	3,800 mg/L	-75% in microbial growth rate	

As previously mentioned, the advantage of AD is in its energy-generating process. However, THP consumes large amounts of heat energy compared to other pretreatment processes, such as mechanical, biological, and chemical methods (Carrère et al., 2010). In order to achieve an energetically self-sufficient plant, the THP performance was evaluated based on the energy balance. Energy balance analysis of AD coupled with the pretreatment process has been performed by many researchers. In these studies, the biochemical methane potential, which is an indicator of the ultimate methane production under ideal conditions, was used to calculate the energy generation in AD without considering the removal rate (Cano et al., 2014a; L. He et al., 2017; Huang et al., 2017; Ma et al., 2011; Passos et al., 2015; Yuan et al., 2019). However, a major advantage of THP is the increased methane generation kinetics, which leads to different removal rates in AD. In order to accurately evaluate the effect of THP on the energy balance of the AD process, the change in the methane generation kinetics needs to be considered.

2.3 Modeling of anaerobic digestion

Having a clear understanding of the biochemical and physicochemical changes that occur during a process is crucial for facilitating the design and operation of AD while minimizing any associated risks. Since the late 1960s, there have been numerous dynamic models developed for the simulation of characteristic variables of the AD process (Weinrich & Nelles, 2021a). These models vary in terms of the number and type of components considered, process phases, and physicochemical dependencies. Early models focused on the anaerobic degradation of simple monomers or organic acids, but newer models incorporate more complex substrates such as organic composites or individual nutrients to better represent the entire AD process.

The Anaerobic digestion Model No.1 (ADM1), developed by the International Water Association (IWA), has become the standard model for simulating AD processes by combining relevant approaches (Batstone et al., 2015). The ADM1 encompasses the fundamental degradation pathways and process kinetics, from disintegration or hydrolysis to acetoclastic and hydrogenotrophic methanogenesis (Figure 2.8). The ADM1 is composed of 26 dynamic state concentration variables, 19 biochemical kinetic processes, and 3 gas–liquid transfer kinetic processes. The model is based on first–order kinetics for hydrolysis and Monod kinetics for acidogenesis,

acetogenesis, and methanogenesis. Inhibition of microbial activity by ammonia, hydrogen, pH, and inorganic nitrogen is considered (Batstone et al., 2002).

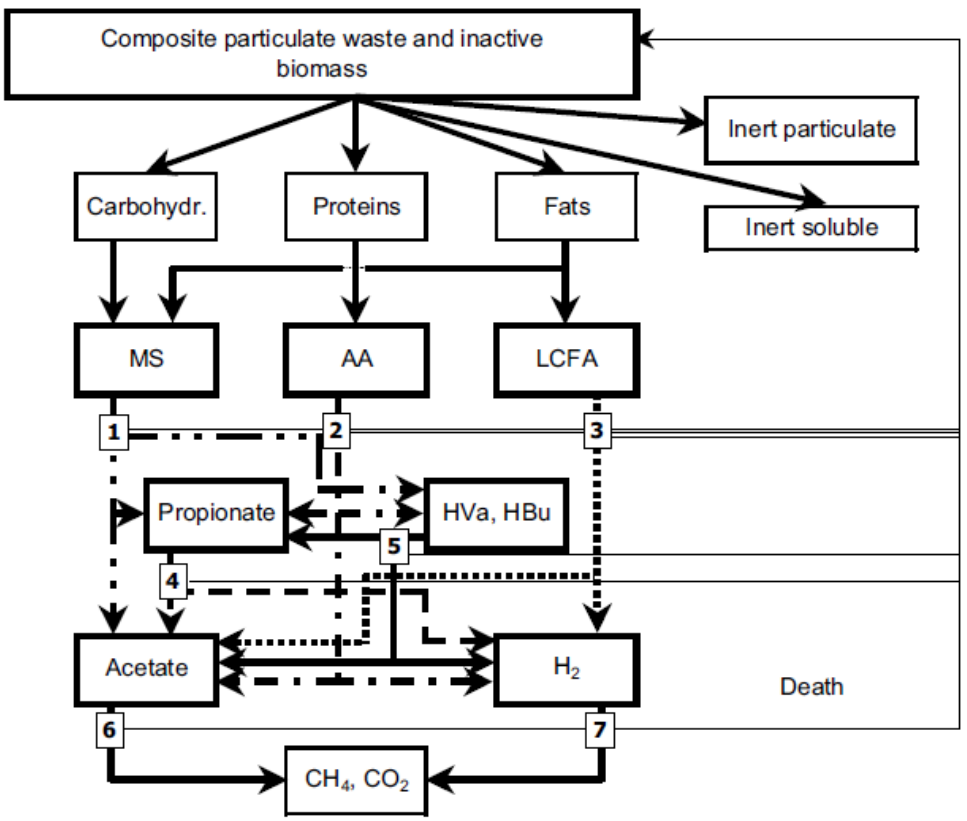

Figure 2.8 Biochemical processes in ADM1 [(1) acidogenesis from sugars; (2) acidogenesis from amino acids; (3) acetogenesis from LCFA; (4) acetogenesis from propionate; (5) acetogenesis from butyrate and valerate; (6) acetoclastic methanogenesis; and (7) hydrogenotrophic methanogenesis (Batstone et al., 2002)]

The original ADM1 framework offers the benefit of providing a basis for further development, resulting in improvements to the model. The ADM1 was initially developed for sewage sludge, and its applicability has been verified for other substrates, such as livestock manure, crops, food waste, and wastewater (Bo Zhang et al., 2009; X. Chen et al., 2016; Fitamo et al., 2016; García-Gen et al., 2015; Page et al., 2008; Phothilangka et al., 2008). Additionally, there have been improvement studies that include the addition of components such as sulfates and phosphorus, which were not previously included in the model, or changes to the model structure (Table 2.6).

Table 2.6 Application and modification of ADM1

Substrate application	Component extension	Structure improvement	Reference
Pig manure	C, N, and P	–	Li et al., 2020
Potato waste	–	Introducing surface area term in hydrolysis	Panaro et al., 2021
Co-digestion of sewage sludge and food waste	–	Introducing surface area term in hydrolysis	Esposito et al., 2011
Sewage sludge	–	Introducing Contois equation in hydrolysis	Bai et al., 2015
Microalgae	–	Introducing Contois equation in hydrolysis	Mairet et al., 2011
Cattle manure	–	Simplification of model structure	Weinrich & Nelles, 2021b
Olive mill wastewater	–	Inhibition of acetogenic methanogenesis by total VFA	Fezzani & Cheikh, 2008
Paper mill	CaCO3	Precipitation of CaCO3	Batstone & Keller, 2003
Green peas	Na	Inhibition of sodium on acetogenic methanogenesis	Hierholtzer & Akunna, 2012

In ADM1, microorganisms that metabolize the same compound are not differentiated from one another and are represented by a single biochemical parameter. However, AD involves dozens of microbial species, and various microorganisms can participate in the metabolism of the same substrate. For instance, *Pelotomaculum sp.*, and *Cloacamonas sp.* are among the microorganisms involved in the breakdown of propionate to acetate (Ahlert et al., 2016; Peces et al., 2021; Wu et al., 2022). Each microorganism possesses a unique set of characteristics that result in different substrate uptake rates and half-saturation constants, resulting in varying growth rates. Consequently, the biochemical parameters of a substrate can change as the microbial composition changes. Indeed, the conventional ADM1 model assumes the same set of biochemical parameters for simulations under different conditions, which can result in increasing prediction errors. For example, when simulating the AD of pig manure using the ADM1 calibrated at an SRT condition of 35 d, the prediction error for methane production increased by 4 and 8% under SRT conditions of 23.3 and 17.5 d, respectively (H. Li et al., 2020).

In order to address this issue, a cellular-level modeling (CLM) approach can be used (Hashemi et al., 2021). Unlike ADM1, which is based on biochemical process modeling (BPM), CLM targets cellular function (Figure 2.9). CLM has previously employed

biotechnology to investigate the impacts of metabolic restriction achieved through either genetic manipulation or physical limitation (Batstone et al., 2019). Nowadays, it is increasingly being utilized to gain a deeper understanding of cellular function at the genome-scale.

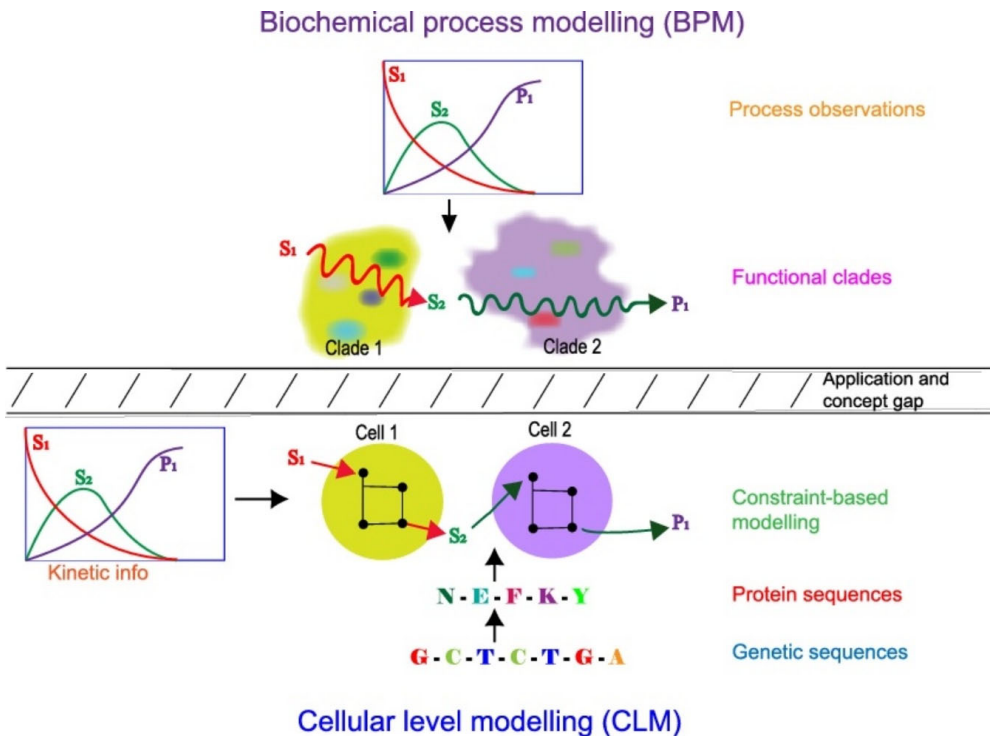

Figure 2.9 Application and concept gap between biochemical process modeling and cellular level modeling (Batstone et al., 2019)

Ramirez et al. (2009) attempted to extend the application of ADM1 to the cellular level in order to model microbial diversity. They divided microorganisms into 10 species within the same functional group, which perform the same reaction (Ramirez et al., 2009). Biokinetic parameters, maximum specific substrate uptake rate, and

half saturation constant, for each species were arbitrarily set to have a same mean of conventional ADM1, but normal bimodal distribution. Detail distribution was established following a curve-fitting process using experimental data. Results showed that the model outperformed the conventional ADM1 in terms of accuracy. Even if the microorganisms involved in each metabolic pathway are divided into 10 species and their biokinetic parameters are modeled using a bimodal distribution, the mean of the biokinetic parameters for all species remains fixed at a certain value. Therefore, there are limitations to simulating changes in the population dynamics constants of microorganisms in response to environmental changes.

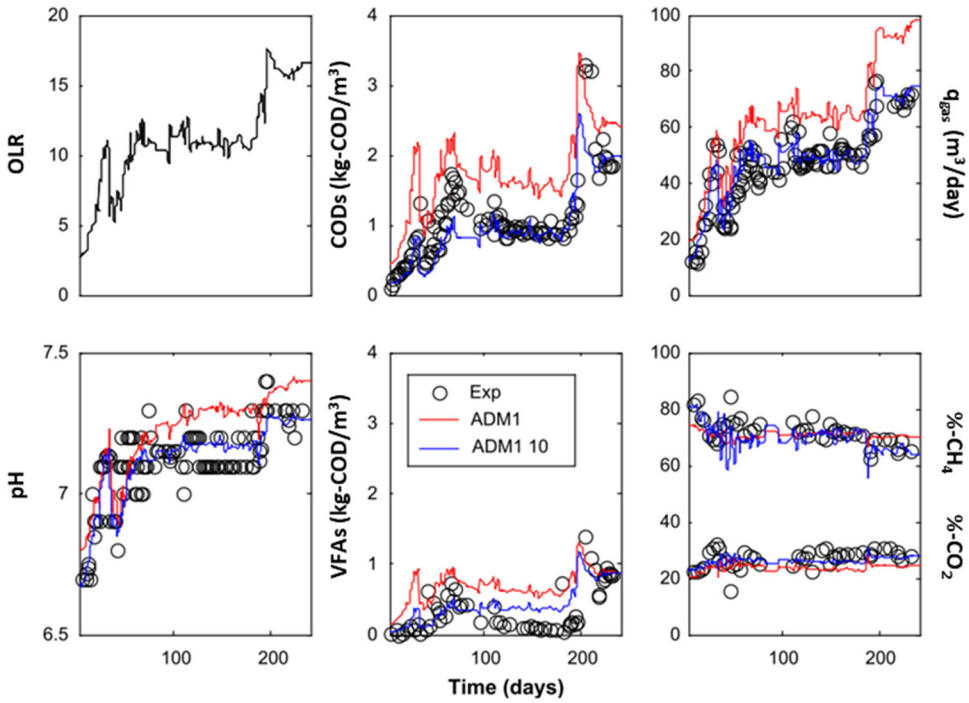

Figure 2.9 Comparison of prediction result from conventional ADM1 and ADM1_10 (ADM1_10 refers to the extension of the ADM1 for microbial diversity with 10 species for each group) (Ramirez et al., 2009)

Although ADM1 is a powerful model with numerous advantages, its inability to incorporate changes in biokinetics of microorganisms in a limitation that leads to a decrease in accuracy as the system deviates from the training conditions. Thus, additional studies are needed to address this limitation.

References

Aboudi, K., Álvarez-Gallego, C. J., & Romero-García, L. I. 2015. Semi-continuous anaerobic co-digestion of sugar beet byproduct and pig manure: Effect of the organic loading rate (OLR) on process performance. *Bioresource Technology*, *194*, 283–290.

Abraham, A., Mathew, A. K., Park, H., Choi, O., Sindhu, R., Parameswaran, B., Pandey, A., Park, J. H., & Sang, B.-I. 2020. Pretreatment strategies for enhanced biogas production from lignocellulosic biomass. *Bioresource Technology*, *301*, 122725.

Agbor, V. B., Cicek, N., Sparling, R., Berlin, A., & Levin, D. B. 2011. Biomass pretreatment: Fundamentals toward application. *Biotechnology Advances*, *29*(6), 675–685.

Ahlert, S., Zimmermann, R., Ebling, J., & König, H. 2016. Analysis of propionate-degrading consortia from agricultural biogas plants. *MicrobiologyOpen*, *5*(6), 1027–1037.

Ahmed, B., Aboudi, K., Tyagi, V. K., álvarez-Gallego, C. J., Fernández-Güelfo, L. A., Romero-García, L. I., & Kazmi, A. A. 2019. Improvement of anaerobic digestion of lignocellulosic biomass by hydrothermal pretreatment. *Applied Sciences (Switzerland)*, *9*(18), 1–17.

Almeida, J. R. M., Bertilsson, M., Gorwa-Grauslund, M. F., Gorsich, S., & Lidén, G. 2009. Metabolic effects of furaldehydes and impacts on biotechnological processes. *Applied Microbiology and Biotechnology*, *82*(4), 625–638.

Amin, F. R., Khalid, H., Zhang, H., Rahman, S. u., Zhang, R., Liu, G., & Chen, C. 2017. Pretreatment methods of lignocellulosic biomass

for anaerobic digestion. *AMB Express*, *7*(1), 72.

Arslan, B., Colpan, M., Ju, X., Zhang, X., Kostyukova, A., & Abu-Lail, N. I. 2016. The Effects of Noncellulosic Compounds on the Nanoscale Interaction Forces Measured between Carbohydrate-Binding Module and Lignocellulosic Biomass. *Biomacromolecules*, *17*(5), 1705–1715.

Azuma, J.-I., & Tetsuo, K. B. T.-M. in E. 1988. Lignin-carbohydrate complexes from various sources. In *Biomass Part B: Lignin, Pectin, and Chitin* (Vol. 161, pp. 12–18). Academic Press.

Bah, H., Zhang, W., Wu, S., Qi, D., Kizito, S., & Dong, R. 2014. Evaluation of batch anaerobic co-digestion of palm pressed fiber and cattle manure under mesophilic conditions. *Waste Management*, *34*(11), 1984–1991.

Bai, J., Liu, H., Yin, B., & Ma, H. 2015. Modeling of enhanced VFAs production from waste activated sludge by modified ADM1 with improved particle swarm optimization for parameters estimation. *Biochemical Engineering Journal*, *103*, 22–31.

Batista Meneses, D., Montes de Oca-Vásquez, G., Vega-Baudrit, J. R., Rojas-Álvarez, M., Corrales-Castillo, J., & Murillo-Araya, L. C. 2022. Pretreatment methods of lignocellulosic wastes into value-added products: recent advances and possibilities. *Biomass Conversion and Biorefinery*, *12*(2), 547–564.

Batstone, D. J., Hülsen, T., & Oehmen, A. 2019. Metabolic modelling of mixed culture anaerobic microbial processes. *Current Opinion in Biotechnology*, *57*, 137–144.

Batstone, D. J., & Keller, J. 2003. Industrial applications of the IWA

anaerobic digestion model No. 1 (ADM1). *Water Science and Technology*, *47*(12), 199–206.

Batstone, D. J., Keller, J., Angelidaki, I., Kalyuzhnyi, S. V., Pavlostathis, S. G., Rozzi, A., Sanders, W. T., Siegrist, H., & Vavilin, V. A. 2002. The IWA Anaerobic Digestion Model No 1 (ADM1). *Water Science and Technology : A Journal of the International Association on Water Pollution Research*, *45*(10), 65–73.

Batstone, D. J., Puyol, D., Flores-Alsina, X., & Rodríguez, J. 2015. Mathematical modelling of anaerobic digestion processes: applications and future needs. *Reviews in Environmental Science and Biotechnology*, *14*(4), 595–613.

Bi, S., Hong, X., Yang, H., Yu, X., Fang, S., Bai, Y., Liu, J., Gao, Y., Yan, L., Wang, W., & Wang, Y. 2020. Effect of hydraulic retention time on anaerobic co-digestion of cattle manure and food waste. *Renewable Energy*, *150*, 213–220.

Biswas, R., Uellendahl, H., & Ahring, B. K. 2015. Wet Explosion: a Universal and Efficient Pretreatment Process for Lignocellulosic Biorefineries. *Bioenergy Research*, *8*(3), 1101–1116.

Bo Zhang, Kathleen R Fowler, Matthew D Grace, Sumona Mondal, & Stefan J Grimberg. 2009. *Optimization of Anaerobic Digestion Model No. 1 (ADM1) : Simulation of Dairy Manure Digestion*. *1*(1), 1–13.

Cano, R., Nielfa, A., & Fdz-Polanco, M. 2014. Thermal hydrolysis integration in the anaerobic digestion process of different solid wastes: Energy and economic feasibility study. *Bioresource*

Technology, *168*, 14–22.

Cao, S., Du, R., Yan, W., & Zhou, Y. 2022. Mitigation of inhibitory effect of THP–AD centrate on partial nitritation and anammox: Insights into ozone pretreatment. *Journal of Hazardous Materials*, *431*, 128599.

Carrère, H., Dumas, C., Battimelli, A., Batstone, D. J., Delgenès, J. P., Steyer, J. P., & Ferrer, I. 2010. Pretreatment methods to improve sludge anaerobic degradability: A review. *Journal of Hazardous Materials*, *183*(1–3), 1–15.

Carrère, H., Sialve, B., & Bernet, N. 2009. Improving pig manure conversion into biogas by thermal and thermo–chemical pretreatments. *Bioresource Technology*, *100*(15), 3690–3694.

Chandra, R., Bharagava, R. N., & Rai, V. 2008. Melanoidins as major colourant in sugarcane molasses based distillery effluent and its degradation. *Bioresource Technology*, *99*(11), 4648–4660.

Chávez–Fuentes, J. J., Capobianco, A., Barbušová, J., & Hutňan, M. 2017. Manure from Our Agricultural Animals: A Quantitative and Qualitative Analysis Focused on Biogas Production. *Waste and Biomass Valorization*, *8*(5), 1749–1757.

Chen, X., Chen, Z., Wang, X., Huo, C., Hu, Z., Xiao, B., & Hu, M. 2016. Application of ADM1 for modeling of biogas production from anaerobic digestion of Hydrilla verticillata. *Bioresource Technology*, *211*, 101–107.

Dwyer, J., Starrenburg, D., Tait, S., Barr, K., Batstone, D. J., & Lant, P. 2008. Decreasing activated sludge thermal hydrolysis temperature reduces product colour, without decreasing

degradability. *Water Research*, *42*(18), 4699–4709.

Esposito, G., Frunzo, L., Panico, A., & Pirozzi, F. 2011. Model calibration and validation for OFMSW and sewage sludge co-digestion reactors. *Waste Management*, *31*(12), 2527–2535.

Fezzani, B., & Cheikh, R. Ben. 2008. Implementation of IWA anaerobic digestion model No. 1 (ADM1) for simulating the thermophilic anaerobic co-digestion of olive mill wastewater with olive mill solid waste in a semi-continuous tubular digester. *Chemical Engineering Journal*, *141*(1–3), 75–88.

Food and Agriculture Organization of the United Nations, fao.org/faostat/en/#data, Accessed 26 April 2023

Fitamo, T., Boldrin, A., Dorini, G., Boe, K., Angelidaki, I., & Scheutz, C. 2016. Optimising the anaerobic co-digestion of urban organic waste using dynamic bioconversion mathematical modelling. *Water Research*, *106*, 283–294.

García-Gen, S., Sousbie, P., Rangaraj, G., Lema, J. M., Rodríguez, J., Steyer, J. P., & Torrijos, M. 2015. Kinetic modelling of anaerobic hydrolysis of solid wastes, including disintegration processes. *Waste Management*, *35*(1), 96–104.

Giummarella, N., Pu, Y., Ragauskas, A. J., & Lawoko, M. 2019. A critical review on the analysis of lignin carbohydrate bonds. *Green Chemistry*, *21*(7), 1573–1595.

Göncüoğlu Taş, N., & Gökmen, V. 2017. Maillard reaction and caramelization during hazelnut roasting: A multiresponse kinetic study. *Food Chemistry*, *221*, 1911–1922.

Gu, Z., Li, Y., Yang, Y., Xia, S., Hermanowicz, S. W., & Alvarez-Cohen,

L. 2018. Inhibition of anammox by sludge thermal hydrolysis and metagenomic insights. *Bioresource Technology*, *270*, 46–54.

Han, F., Yun, S., Zhang, C., Xu, H., & Wang, Z. 2019. Steel slag as accelerant in anaerobic digestion for nonhazardous treatment and digestate fertilizer utilization. *Bioresource Technology*, *282*, 331–338.

Hashemi, S., Hashemi, S. E., Lien, K. M., & Lamb, J. J. 2021. Molecular microbial community analysis as an analysis tool for optimal biogas production. *Microorganisms*, *9*(6), 1162.

He, L., Huang, H., Zhang, Z., Lei, Z., & Lin, B.-L. 2017. Energy Recovery from Rice Straw through Hydrothermal Pretreatment and Subsequent Biomethane Production. *Energy & Fuels*, *31*(10), 10850–10857.

Heer, D., & Sauer, U. 2008. Identification of furfural as a key toxin in lignocellulosic hydrolysates and evolution of a tolerant yeast strain. *Microbial Biotechnology*, *1*(6), 497–506.

Hierholtzer, A., & Akunna, J. C. 2012. Modelling sodium inhibition on the anaerobic digestion process. *Water Science and Technology*, *66*(7), 1565–1573.

Himmel, M. E., Ding, S.-Y., Johnson, D. K., Adney, W. S., Nimlos, M. R., Brady, J. W., & Foust, T. D. 2007. Biomass Recalcitrance: Engineering Plants and Enzymes for Biofuels Production. *Science*, *315*(5813), 804–807.

Huang, W., Zhao, Z., Yuan, T., Huang, W., Lei, Z., & Zhang, Z. 2017. Low-temperature hydrothermal pretreatment followed by dry anaerobic digestion: A sustainable strategy for manure waste

management regarding energy recovery and nutrients availability. *Waste Management*, *70*, 255–262.

Janker-Obermeier, I., Sieber, V., Faulstich, M., & Schieder, D. 2012. Solubilization of hemicellulose and lignin from wheat straw through microwave-assisted alkali treatment. *Industrial Crops and Products*, *39*, 198–203.

Jin, Y., Hu, Z., & Wen, Z. 2009. Enhancing anaerobic digestibility and phosphorus recovery of dairy manure through microwave-based thermochemical pretreatment. *Water Research*, *43*(14), 3493–3502.

Khan, M. U., & Ahring, B. K. 2020. Anaerobic Digestion of Digested Manure Fibers: Influence of Thermal and Alkaline Thermal Pretreatment on the Biogas Yield. *Bioenergy Research*, *14*, 891–900.

Khan, M. U., & Ahring, B. K. 2021. Improving the biogas yield of manure: Effect of pretreatment on anaerobic digestion of the recalcitrant fraction of manure. *Bioresource Technology*, *321*, 124427.

Kim, J. R., & Karthikeyan, K. G. 2021. Effects of severe pretreatment conditions and lignocellulose-derived furan byproducts on anaerobic digestion of dairy manure. *Bioresource Technology*, *340*, 125632.

Kim, J.-S., & Lee, Y.-S. 2008. Effect of pH on the enolization of sugars and antioxidant activity of caramelization products obtained by caramelization browning. *Food Science and Biotechnology*, *17*(5), 931–939.

Kroh, L. W. 1994. Caramelisation in food and beverages. *Food Chemistry*, *51*(4), 373–379.

Kumar, P., Barrett, D. M., Delwiche, M. J., & Stroeve, P. 2009. Methods for Pretreatment of Lignocellulosic Biomass for Efficient Hydrolysis and Biofuel Production. *Industrial & Engineering Chemistry Research*, *48*(8), 3713–3729.

Lawrence, A. W., & Mccarty, P. L. 1969. Kinetics of Methane Fermentation in Anaerobic Treatment. *Water Pollution Control Federateion, 41*(2), 1－17.

Lee, I. S., Parameswaran, P., & Rittmann, B. E. 2011. Effects of solids retention time on methanogenesis in anaerobic digestion of thickened mixed sludge. *Bioresource Technology*, *102*(22), 10266–10272.

Li, C., Knierim, B., Manisseri, C., Arora, R., Scheller, H. V, Auer, M., Vogel, K. P., Simmons, B. A., & Singh, S. 2010. Comparison of dilute acid and ionic liquid pretreatment of switchgrass: Biomass recalcitrance, delignification and enzymatic saccharification. *Bioresource Technology*, *101*(13), 4900–4906.

Li, H., Chen, Z., Fu, D., Wang, Y., Zheng, Y., & Li, Q. 2020. Improved ADM1 for modelling C, N, P fates in anaerobic digestion process of pig manure and optimization approaches to biogas production. *Renewable Energy*, *146*(422), 2330–2336.

Li, K., Liu, R., & Sun, C. 2015. Comparison of anaerobic digestion characteristics and kinetics of four livestock manures with different substrate concentrations. *Bioresource Technology*, *198*, 133–140.

Li, R., Chen, S., & Li, X. 2009. Anaerobic co-digestion of kitchen waste and cattle manure for methane production. *Energy Sources, Part A: Recovery, Utilization and Environmental Effects*, *31*(20), 1848–1856.

Li, R., Tan, W., Zhao, X., Dang, Q., Song, Q., Xi, B., & Zhang, X. 2019. Evaluation on the Methane Production Potential of Wood Waste Pretreated with NaOH and Co-Digested with Pig Manure. *Catalysts, 9(6)*, 539.

Li, Y., Zhang, R., Chen, C., Liu, G., He, Y., & Liu, X. 2013. Biogas production from co-digestion of corn stover and chicken manure under anaerobic wet, hemi-solid, and solid state conditions. *Bioresource Technology*, *149*, 406–412.

Liao, W., Liu, Y., Liu, C., Wen, Z., & Chen, S. 2006. Acid hydrolysis of fibers from dairy manure. *Bioresource Technology*, *97*(14), 1687–1695.

Liu, X., Lee, C., & Kim, J. Y. 2020. Thermal hydrolysis pre-treatment combined with anaerobic digestion for energy recovery from organic wastes. *Journal of Material Cycles and Waste Management*. *22*, 1370-1381.

Liu, X., Wang, Q., Tang, Y., & Pavlostathis, S. G. 2021. Hydrothermal pretreatment of sewage sludge for enhanced anaerobic digestion: Resource transformation and energy balance. *Chemical Engineering Journal*, *410*, 127430.

Lund, M. N., & Ray, C. A. 2017. Control of Maillard Reactions in Foods: Strategies and Chemical Mechanisms. *Journal of Agricultural and Food Chemistry*, *65*(23), 4537–4552.

Ma, J., Duong, T. H., Smits, M., Verstraete, W., & Carballa, M. 2011. Enhanced biomethanation of kitchen waste by different pre-treatments. *Bioresource Technology*, *102*(2), 592–599.

Mairet, F., Bernard, O., Ras, M., Lardon, L., & Steyer, J. P. 2011. Modeling anaerobic digestion of microalgae using ADM1. *Bioresource Technology*, *102*(13), 6823–6829.

Ministry of Environment (2022). The state of waste generation and treatment

Ministry of Trade, Industry and Energy, 2021, New & Renewable energy white paper

Molinuevo-Salces, B., Gómez, X., Morán, A., & García-González, M. C. 2013. Anaerobic co-digestion of livestock and vegetable processing wastes: Fibre degradation and digestate stability. *Waste Management*, *33*(6), 1332–1338.

Muhammad Nasir, I., & Mohd Ghazi, T. I. 2015. Pretreatment of lignocellulosic biomass from animal manure as a means of enhancing biogas production. *Engineering in Life Sciences*, *15*(7), 733–742.

Page, D. I., Hickey, K. L., Narula, R., Main, A. L., & Grimberg, S. J. 2008. Modeling anaerobic digestion of dairy manure using the IWA Anaerobic Digestion Model no. 1 (ADM1). *Water Science and Technology*, *58*(3), 689–695.

Palmqvist, E., & Hahn-Hägerdal, B. 2000. Fermentation of lignocellulosic hydrolysates. II: inhibitors and mechanisms of inhibition. *Bioresource Technology*, *74*(1), 25–33.

Panaro, D. B., Frunzo, L., Mattei, M. R., Luongo, V., & Esposito, G.

2021. Calibration, validation and sensitivity analysis of a surface-based ADM1 model. *Ecological Modelling*, *460*, 109726.

Park, N., Kim, H.-Y., Koo, B.-W., Yeo, H., & Choi, I.-G. 2010. Organosolv pretreatment with various catalysts for enhancing enzymatic hydrolysis of pitch pine (Pinus rigida). *Bioresource Technology*, *101*(18), 7046–7053.

Passos, F., Carretero, J., & Ferrer, I. 2015. Comparing pretreatment methods for improving microalgae anaerobic digestion: Thermal, hydrothermal, microwave and ultrasound. *Chemical Engineering Journal*, *279*, 667–672.

Peces, M., Astals, S., Jensen, P. D., & Clarke, W. P. 2021. Transition of microbial communities and degradation pathways in anaerobic digestion at decreasing retention time. *New Biotechnology*, *60*, 52–61.

Phothilangka, P., Schoen, M. A., Huber, M., Luchetta, P., Winkler, T., & Wett, B. 2008. Prediction of thermal hydrolysis pretreatment on anaerobic digestion of waste activated sludge. *Water Science and Technology*, *58*(7), 1467–1473.

Rahman, Md. A., Møller, H. B., Saha, C. K., Alam, Md. M., Wahid, R., & Feng, L. 2018. Anaerobic co-digestion of poultry droppings and briquetted wheat straw at mesophilic and thermophilic conditions: Influence of alkali pretreatment. *Renewable Energy*, *128*, 241–249.

Ramirez, I., Volcke, E. I. P., Rajinikanth, R., & Steyer, J. P. 2009. Modeling microbial diversity in anaerobic digestion through an extended ADM1 model. *Water Research*, *43*(11), 2787–2800.

Rufián-Henares, J. A., & de la Cueva, S. P. 2009. Antimicrobial

Activity of Coffee Melanoidins—A Study of Their Metal-Chelating Properties. *Journal of Agricultural and Food Chemistry*, *57*(2), 432–438.

Ruiz, H. A., Rodríguez-Jasso, R. M., Fernandes, B. D., Vicente, A. A., & Teixeira, J. A. 2013. Hydrothermal processing, as an alternative for upgrading agriculture residues and marine biomass according to the biorefinery concept: A review. *Renewable and Sustainable Energy Reviews*, *21*, 35–51.

Shen, F., Zhong, B., Wang, Y., Xia, X., Zhai, Z., & Zhang, Q. 2019. Cellulolytic Microflora Pretreatment Increases the Efficiency of Anaerobic Co-digestion of Rice Straw and Pig Manure. *BioEnergy Research*, *12*(3), 703–713.

Shen, J., Zhao, C., Liu, Y., Zhang, R., Liu, G., & Chen, C. 2019a. Biogas production from anaerobic co-digestion of durian shell with chicken, dairy, and pig manures. *Energy Conversion and Management*, *198*, 110535.

Shen, J., Zhao, C., Liu, Y., Zhang, R., Liu, G., & Chen, C. 2019b. Biogas production from anaerobic co-digestion of durian shell with chicken, dairy, and pig manures. *Energy Conversion and Management*, *198*, 110535.

Taherzadeh, M. J., & Karimi, K. 2008. Pretreatment of Lignocellulosic Wastes to Improve Ethanol and Biogas Production: A Review. *International Journal of Molecular Sciences, 9(9),* 1621–1651.

Takashima, M., & Tanaka, Y. 2014. Acidic thermal post-treatment for enhancing anaerobic digestion of sewage sludge. *Journal of Environmental Chemical Engineering*, *2*(2), 773–779.

Tan, Z., Li, X., Yang, C., Liu, H., & Cheng, J. J. 2021. Inhibition and disinhibition of 5-hydroxymethylfurfural in anaerobic fermentation: A review. *Chemical Engineering Journal*, *424*, 130560.

Thomas, H. L., Arnoult, S., Brancourt-Hulmel, M., & Carrère, H. 2019. Methane Production Variability According to Miscanthus Genotype and Alkaline Pretreatments at High Solid Content. *BioEnergy Research*, *12(2)*, 325–337.

Tsapekos, P., Kougias, P. G., Frison, A., Raga, R., & Angelidaki, I. 2016. Improving methane production from digested manure biofibers by mechanical and thermal alkaline pretreatment. *Bioresource Technology*, *216*, 545–552.

Victorin, M., Davidsson, Å., & Wallberg, O. 2020. Characterization of Mechanically Pretreated Wheat Straw for Biogas Production. *BioEnergy Research*, *13(3)*, 833–844.

Wandera, S. M., Westerholm, M., Qiao, W., Yin, D., Jiang, M. M., & Dong, R. 2019. The correlation of methanogenic communities' dynamics and process performance of anaerobic digestion of thermal hydrolyzed sludge at short hydraulic retention times. *Bioresource Technology*, *272*, 180–187.

Wang, K., Yun, S., Xing, T., Li, B., Abbas, Y., & Liu, X. 2021. Binary and ternary trace elements to enhance anaerobic digestion of cattle manure: Focusing on kinetic models for biogas production and digestate utilization. *Bioresource Technology*, *323*, 124571.

Wang, S., Hu, Z.-Y., Geng, Z.-Q., Tian, Y.-C., Ji, W.-X., Li, W.-T., Dai, K., Zeng, R. J., & Zhang, F. 2021. Elucidating the production

and inhibition of melanoidins products on anaerobic digestion after thermal–alkaline pretreatment. *Journal of Hazardous Materials*, *424*(PA), 127377.

Waszkielis, K., Białobrzewski, I., & Bułkowska, K. 2022. Application of anaerobic digestion model No. 1 for simulating fermentation of maize silage, pig manure, cattle manure and digestate in the full-scale biogas plant. *Fuel*, *317*, 123491.

Wei, Y., Yuan, H., Wachemo, A. C., & Li, X. 2020. Impacts of Modification of Corn Stover on the Synergistic Effect and Microbial Community Structure of Co-Digestion with Chicken Manure. *Energy & Fuels*, *34(1)*, 401–411.

Weinrich, S., & Nelles, M. 2021a. *Basics of Anaerobic Digestion: Biochemical Conversion and Process Modelling*. Deutsches Biomasseforschungszentrum gemeinnützige GmbH.

Weinrich, S., & Nelles, M. 2021b. Systematic simplification of the Anaerobic Digestion Model No. 1 (ADM1) – Model development and stoichiometric analysis. *Bioresource Technology*, *333(1)*, 125124.

Wu, D., Li, L., Zhen, F., Liu, H., Xiao, F., Sun, Y., Peng, X., Li, Y., & Wang, X. 2022. Thermodynamics of volatile fatty acid degradation during anaerobic digestion under organic overload stress: The potential to better identify process stability. *Water Research*, *214*, 118187.

Yang, N., Yang, S., Yang, L., Song, Q., & Zheng, X. 2023. Exploration of browning reactions during alkaline thermal hydrolysis of sludge: Maillard reaction, caramelization and humic acid desorption.

Environmental Research, *217*, 114814.

Yin, J., Liu, J., Chen, T., Long, Y., & Shen, D. 2019. Influence of melanoidins on acidogenic fermentation of food waste to produce volatility fatty acids. *Bioresource Technology*, *284*, 121–127.

Yuan, T., Cheng, Y., Zhang, Z., Lei, Z., & Shimizu, K. 2019. Comparative study on hydrothermal treatment as pre- and post-treatment of anaerobic digestion of primary sludge: Focus on energy balance, resources transformation and sludge dewaterability. *Applied Energy*, *239*, 171–180.

Zhang, C., Li, J., Liu, C., Liu, X., Wang, J., Li, S., Fan, G., & Zhang, L. 2013. Alkaline pretreatment for enhancement of biogas production from banana stem and swine manure by anaerobic codigestion. *Bioresource Technology*, *149*, 353–358.

Zhang, L., Guo, K., Wang, L., Xu, R., Lu, D., & Zhou, Y. 2022. Effect of sludge retention time on microbial succession and assembly in thermal hydrolysis pretreated sludge digesters: Deterministic versus stochastic processes. *Water Research*, *209*, 117900.

Zhang, Q., Vlaeminck, S. E., DeBarbadillo, C., Su, C., Al-Omari, A., Wett, B., Pümpel, T., Shaw, A., Chandran, K., Murthy, S., & De Clippeleir, H. 2018. Supernatant organics from anaerobic digestion after thermal hydrolysis cause direct and/or diffusional activity loss for nitritation and anammox. *Water Research*, *143*, 270–281.

Zhao, Y., Sun, F., Yu, J., Cai, Y., Luo, X., Cui, Z., Hu, Y., & Wang, X. 2018. Co-digestion of oat straw and cow manure during anaerobic digestion: Stimulative and inhibitory effects on fermentation. *Bioresource Technology*, *269*, 143–152.

Zhen, G., Lu, X., Kato, H., Zhao, Y., & Li, Y. Y. 2017. Overview of pretreatment strategies for enhancing sewage sludge disintegration and subsequent anaerobic digestion: Current advances, full-scale application and future perspectives. In *Renewable and Sustainable Energy Reviews, 69*, 559-577.

Zheng, Y., Lin, H.-M., Wen, J., Cao, N., Yu, X., & Tsao, G. T. 1995. Supercritical carbon dioxide explosion as a pretreatment for cellulose hydrolysis. *Biotechnology Letters*, *17(8)*, 845–850.

Chapter 3
Effects of thermal hydrolysis pretreatment on the formation of refractory compounds and energy balance

3.1 Introduction

Livestock manure from ruminants (i.e., cows) contains a large amount of recalcitrant materials, such as lignocellulose. Among the livestock manures (swine, cattle, chicken, and rabbit), cattle manure (CM) has the lowest biodegradability and methane yield due to its high fiber content (K. Li et al., 2015b). A pretreatment to increase biodegradability is required to treat CM with AD. Anaerobic digestion can be divided into four steps: hydrolysis, acidogenesis, acetogenesis, and methanogenesis (McCarty, 1964; McCarty & Smith, 1986; Rittmann & McCarty, 2001; Tang et al., 2022). Hydrolysis is a rate-limiting step in AD. The pretreatment process for AD has been studied extensively, and several processes have been applied in the industry such as shredding, microwave, ultrasonic, oxidation, and biological treatments (Hernández-Beltrán et al., 2019; Poddar et al., 2021). Among them, thermal hydrolysis pretreatment (THP) exhibits the most superior pretreatment effects, including increased biogas yield, enhanced degradation kinetics, pathogen reduction, and ability to handle higher loading rates in AD (Barber, 2016; Cano et al., 2014b;

Devos et al., 2021; Xue et al., 2015a). THP involves treating a substrate at high temperature (120 – 230 ℃) and high pressure (corresponding to the vapor pressure of water at the treatment temperature). Hydrolysis is accelerated by hydronium ions generated by the autoionization of water under high temperature and pressure conditions during THP (Bandura & Lvov, 2006).

Cattle manure contains approximately 40 – 50% lignocellulose by dry weight (Tsapekos et al., 2016). Lignocellulose is a major constituent of plants and is composed of cellulose, hemicellulose, and lignin. Cellulose is a homopolymer compound composed of D−glucose connected by beta−1, 4 glycosidic bonds. Hemicellulose is a heteropolymeric structure composed of short−chain polysaccharides, such as pentose and hexose. Lignin is a three−dimensional, highly cross−linked macromolecule composed of sinapyl, coniferyl, and p−coumaryl alcohols. Lignocellulose contains many polysaccharides; and it has a high digestion potential, but hydrolysis by enzymes is difficult because of the complex bonds between cellulose, hemicellulose, and lignin. The biodegradability of lignocellulose can be improved by removing the lignin from the lignocellulose structure, which increases substrate availability (polysaccharides) to hydrolytic enzymes. The removal of lignin from lignocellulose has been extensively studied in the pulp industry, and it depends on the type of chemical used: kraft (NaOH and Na_2S),

sulfite (alkaline earth metal sulfite), soda (NaOH), and organosolv (organic solvents) processes are well known (José Borges Gomes et al., 2020). Among them, alkali reagents are also being used for the pretreatment of lignocellulosic materials for depolymerization using saponification (Carrère et al., 2009; Khan & Ahring, 2021b).

Studies on alkaline THP are being conducted to improve the digestibility of livestock manure (Biswas et al., 2015; Khan & Ahring, 2021a; X. Liu et al., 2020; Tsapekos et al., 2016). Some studies have investigated the effects of alkaline THP. Khan and Ahring observed 1.43 times increase in methane yield under mesophilic digestion of digested manure fibers with the addition of 3 wt.% NaOH to THP (135 ℃ for 1 h) (Khan & Ahring, 2021a). Tsapekos et al. (2016) investigated the effect of alkaline THP (2 – 6 wt.% NaOH at 55 – 121 ℃) on the anaerobic digestion of fibers (Tsapekos et al., 2016). They found that pretreatment using 6 wt.% NaOH at 55 ℃ was the most efficient method as it improved biogas production by 1.26 times than that of the control. An increase in pH caused by the addition of alkaline chemicals can accelerate the Maillard reaction, resulting in the formation of refractories in the THP of carbohydrates and proteins (Lund & Ray, 2017; Takashima & Tanaka, 2014). The formation of refractories in THP is crucial because it can decrease biodegradability. The Maillard reaction is a chemical reaction that takes place between a reducing sugar and amino group at high

temperature, resulting in formation of dark-colored polymers that absorb UV light and are resistant to biodegradation (Maillard, 1912). Melanoidins, product of the Maillard reaction, inhibited methane production by around 35% in batch AD (Cao et al., 2022; J. Li et al., 2021; S. Wang et al., 2021). However, the research on the formation of refractory compounds in the broad range of alkaline THP of CM is limited.

As previously mentioned, the advantage of AD is in its energy-generating process. However, THP consumes large amounts of heat energy compared to other pretreatment processes, such as mechanical, biological, and chemical methods (Carrère et al., 2010). In order to achieve an energetically self-sufficient plant, the THP performance was evaluated based on the energy balance. Energy balance analysis of AD coupled with the pretreatment process has been performed by many researchers. In these studies, the biochemical methane potential, which is an indicator of the ultimate methane production under ideal conditions, was used to calculate the energy generation in AD without considering the removal rate (Cano et al., 2014a; L. He et al., 2017; Huang et al., 2017; Ma et al., 2011; Passos et al., 2015; Yuan et al., 2019). However, a major advantage of THP is the increased methane generation kinetics, which leads to different removal rates in AD. In order to accurately evaluate the effect of THP on the energy balance of the AD process, the change

in the methane generation kinetics needs to be considered. The primary novelty of this chapter is the investigation of the influence of THP on the formation of by-products, as well as its implications from energy perspectives.

The objective of this study was to evaluate the effect of alkaline THP conditions on the formation of refractory compounds and energy recovery in the AD of CM. To this end, the biochemical methane potential and refractory compound formation were analyzed before and after the alkaline THP of CM samples. The energy gain was calculated considering the change in methane generation kinetics, and the sensitivity of the factors used for the energy gain calculation was analyzed.

3.2 Materials and Methods

3.2.1 Substrate and inoculum

The cattle manure samples were collected from 12 farms located in Cheonan, South Korea. The collected cattle manure was mixed homogeneously and stored at −20 ℃ until use. Table 3.1 shows the characteristics of cattle manure. Anaerobic sludge was collected from a mesophilic anaerobic digester treating 9,000 tonne/day of 52, 45, and 3 wt.% of sewage sludge, septage, and food waste leachate, respectively, located in Seoul, South Korea. The anaerobic sludge was filtered through a sieve with 0.5 mm openings and stored at 4 ℃ until use. The concentration of total solids (TS) and volatile solids (VS) of anaerobic sludge were 2.7 ± 0.2, and 1.2 ± 0.1 wt.%, respectively.

Table 3.1. Physicochemical characteristics of the intact cattle manure sample

		Cattle manure
TS (% by wet wt.)		24.9 ± 0.4
VS (% by wet wt.)		18.8 ± 0.3
TCOD (g/L)		147.2 ± 23.6
SCOD (g/L)		24.8 ± 2.3
NH_4 (mg-N/L)		1,485 ± 93
Elemental composition (% by dry wt.)	C	38.8
	H	4.7
	O	26.5
	N	2.2
	S	0.7
Lignocellulose composition (% by dry wt. in fiber)	Cellulose	31.6 ± 2.1
	Hemicellulose	14.6 ± 2.2
	Lignin	53.8 ± 10.5

*A ± B indicates average ± standard deviation
*n=3, except for elemental composition

3.2.2 Thermal hydrolysis pretreatment

Thermal hydrolysis pretreatment of CM was performed using a 2 L stainless steel autoclave (HR-S-2000, Ilshin Autoclave, South Korea). In order to achieve a homogeneous mixture and a dilute condition that does not hinder the mass transfer due to high TS content, the intact CM sample was diluted with deionized water to adjust the TS to 5 wt.%. After 1 L of CM mixture was loaded into the autoclave, 1 M of NaOH solution was added according to the designed treatment conditions. The THP was conducted under five temperature conditions (120, 140, 160, 180, and 200 ℃) and four NaOH concentrations (0, 2, 4, and 6% (dry wt.) to TS of CM). The upper limit of NaOH concentration was set to avoid the potential inhibitory effect of sodium ion on microorganisms (Fang et al., 2011; Hierholtzer & Akunna, 2012; McCarty, 1964).

In the THP of sewage sludge, the concentrations of SCOD, soluble carbohydrates, and soluble proteins remained relatively stable over time after 10 min at the target temperature, whereas with increasing temperature, these concentrations showed a sharp increase (Xue et al., 2015b). The generation of refractory organics is also predominantly influenced by temperature in the case of sewage sludge (Barber, 2016). Therefore, the reaction time was set at 30 min, which is generally used in an industrial THP plant and suggested by many researchers (Ngo et al., 2021; Yousefifar et al.,

2017). The pressure was maintained at a thermodynamic equilibrium condition (2.0 – 15.5 atm) corresponding to the temperature. Therefore, a total of 20 THP conditions for CM were used. All thermally hydrolyzed substrates were referred to as 'THP–Temperature–% of NaOH', where 'THP' is the thermally hydrolyzed sample, 'Temperature' indicates the temperature condition, and '% of NaOH' indicates the amount of NaOH addition. For example, THP–120–2 indicates that the sample was thermally hydrolyzed at 120 ℃ with the addition of 2% (dry wt.) NaOH.

3.2.3 Biochemical methane potential (BMP) test

In order to evaluate biochemical methane potential, a BMP test was conducted on intact and thermally hydrolyzed CM samples. The experiment was conducted following the BMP protocol for solid organic wastes (Angelidaki et al., 2009). Briefly, 10 mL of inoculum and substrate (corresponding to 0.5 g−VS of substrate/g−VS of inoculum), and 90 mL of medium were mixed in 250 mL of serum bottles. The reactors were stored under mesophilic (35 ± 1 ℃) conditions after purging nitrogen gas to create anaerobic conditions, and methane generation was monitored for 50 d. Biogas generation was calculated using the ideal gas equation and the pressure of the headspace in the serum bottle. The pressure was measured using a needle pressure gauge. Biodegradability was calculated as the ratio of the biochemical methane generation to the theoretical methane potential. The chemical formula was determined based on the elemental composition, and the theoretical methane potential was calculated using Eq. 3.1 (Buswell & Mueller, 1952).

$$C_aH_bO_cN_d + \left(\frac{4a-b-2c+3d}{4}\right)H_2O \rightarrow \left(\frac{4a+b-2c-3d}{8}\right)CH_4 + \left(\frac{4a-b+2c+3d}{8}\right)CO_2 + dNH_3 \quad \text{Eq. 3.1}$$

The methane generation kinetics were analyzed using a first−order kinetic model (Eq. 3.2), which is based on the hypothesis that hydrolysis is the rate−limiting step in the AD process (Friesen & Friesen, 2010; Prajapati et al., 2018).

$$M = M_{max} \times \left(1 - e^{-kt}\right) \quad \text{Eq. 3.2}$$

where M is the cumulative methane production ($mL-CH_4/g-VS$), M_{max} is the maximum methane production ($mL-CH_4/g-VS$), e is the mathematical constant, k is the kinetic constant (d^{-1}), and t is the time (d). The maximum methane production was calculated from the ultimate methane production measured in the BMP test.

3.2.4 Energy analysis

In order to quantitatively compare the effects of the THP on AD, the energy gain was compared. The energy requirements for substrate heating, and methane generation were considered. It was assumed that the energy required to maintain the digester temperature, and electrical cost for the other equipment were the same, regardless of the pretreatment conditions. The energy consumption of the THP was calculated using Eq. 3.3 (L. He et al., 2017).

$$E_{in,THP} = C_{p,\mathrm{CM}}(T_{THP} - T_{CM}) - \phi C_{p,\mathrm{CM}}(T_{THP} - T_{AD}) \quad \text{Eq. 3.3}$$

where $E_{in,THP}$ is the energy consumption of THP (MJ/tonne-CM), $C_{p,CM}$ is the specific heat of CM (MJ/tonne-CM/℃), T_{THP} is the THP temperature (℃), T_{CM} is the temperature of CM (℃), ϕ is the heat recovery ratio, and T_{AD} is the digester temperature (℃). The CM and digester temperatures were assumed to be 25 and 35 ℃, respectively. The heat recovery ratio was set to 0.85 (L. He et al., 2017). The specific heat of 3.53 MJ/tonne-CM/℃, calculated from the VS concentration of CM using the equation suggested by Achkari-Begdouri et al. (1992), was used (Achkari-Begdouri & Goodrich, 1992). In the case of anaerobic digestion without THP, the energy consumption required to heat the substrate to the digestion temperature was considered (Eq. 3.4).

$$E_{in,heating} = C_{p,\mathrm{CM}}(T_{AD} - T_{CM}) \quad \text{Eq. 3.4}$$

where, $E_{in,heating}$ is the energy consumption of feed heating (MJ/tonne−CM). The amount of energy generated in the digester was calculated using an equation derived from an analytical solution of a continuous stirred−tank reactor (CSTR) assuming the first−order reaction in a steady state (Eq. 3.5).

$$E_{out} = \eta M_{max} r_{VS} \left(1 - \frac{1}{1+k\tau}\right) \xi_{CH_4} \quad \text{Eq. 3.5}$$

where, E_{out} is the energy generated in the digester (MJ/tonne−CM), η is the energy conversion ratio from methane to energy, r_{VS} is the mass ratio of VS to CM, τ is the hydraulic retention time (d), and ξ_{CH_4} is the lower heating value of methane (MJ/m^3−CH_4). The hydraulic retention time was assumed to be 20 d, which is the typical hydraulic retention time of the AD of CM (Rico et al., 2011; Tufaner & Avşar, 2016). The lower heating value of methane, and energy conversion rate were assumed to be 35.8 MJ/m^3−CH_4 and 0.9, respectively (Yuan et al., 2019). The net energy production was calculated by subtracting the energy consumption (for feed heating or the THP process) from the energy generated in the digester, as shown in Eq. 3.6.

$$E_{net} = E_{out} - E_{in} \quad \text{Eq. 3.6}$$

where E_{net} is the net energy production (MJ/tonne−CM). The energy gain by applying THP was calculated by subtracting the net energy production in the AD without THP from the net energy production in the AD with THP (Eq. 3.7).

$$E_{gain} = E_{net,THP} - E_{net,w/o\ THP}$$ Eq. 3.7

where E_{gain} represents the energy gain (MJ/tonne−CM). A positive energy gain indicates that the additional energy generation by applying THP to AD can cover the energy usage in the THP process. In order to compare the energy gain with the conventional method, which is assumed 100% removal of biodegradable substrate, the energy gain was calculated using Eq. 3.7, while using Eq. 3.8 in place of Eq. 3.5.

$$E_{out,100\%\ remv.} = \eta M_{max} \xi_{CH_4}$$ Eq. 3.8

where $E_{out,100\%\ remv.}$ is the energy generated in the digester calculated under the assumption of 100% removal of a biodegradable substrate (MJ/tonne−CM).

A sensitivity analysis was performed to investigate the factors that contributed significantly to the energy gain. The BMP after THP, VS concentration of CM, first−order kinetic constant, and HRT were changed from −60 to +60% from the initial value (or assumption). The heat recovery ratio was changed from −60 to +17% with the value at which the heat recovery rate became 1.0, which is the upper limit.

3.2.5 Analysis of melanoidins

Melanoidin is a polymer that can exist in various molecular weights, and it undergoes diverse reaction pathways, making quantitative measurement challenging (Arimi et al., 2015; H. Y. Wang et al., 2011). Melanoidins can be quantitatively measured using their optical properties (Brands et al., 2002; Martins & Van Boekel, 2003; D. Zhang et al., 2020). In the case of heterogeneous samples, there may be some errors due to the background absorption of other dissolved organic compounds, However, utilizing the optical properties of melanoidins remains the simplest method for semi-quantitative analysis of Maillard reaction products. This approach has been widely utilized in studies involving solid waste samples such as sludge and food waste (Dwyer et al., 2008; J. Liu et al., 2018; N. Yang et al., 2022).

In order to make melanoidins model compound, a mixture was prepared by adding 0.5 mol of glucose, and glycine into a 1,000 mL solution of 0.05 M Na_2CO_3. The mixture was then heated at 120 ℃ for 3 h using an autoclave to synthesize melanoidin. The melanoidin solution was freeze-dried, and obtained powder was used as a standard melanoidin compound. UV absorbance was measured spectrophotometrically as absorbance at 420 nm using a UV-visible spectrometer. The three-dimensional excitation-emission matrix (3-D EEM) fluorescence spectra were measured using a

fluorescence spectrophotometer (Cary Eclipse, Agilent Technologies, USA) with a quartz cuvette. The scanning range of excitation and emission wavelengths was 200 – 400 nm at 5 nm increments and 250 – 550 nm at 5 nm increments, respectively. The excitation and emission slits were set to 5 nm, and the scanning speed was 9,600 nm/min. All samples were diluted to a final dissolved organic carbon (DOC) concentration of 1 mg-C/L using deionized water to normalize the fluorescence intensity. The EEM intensity of the sample was divided by the intensity of the Raman peak of deionized water to standardize the fluorescence intensity, which may vary depending on the humidity and temperature (Goletz et al., 2011). The 3D-EEM matrix is divided into five regions (region Ⅰ, Ⅱ: aromatic protein-like fluorophores (tyrosine, and tryptophan); region Ⅲ: fulvic acid-like fluorophores; region Ⅳ: soluble microbial product-like fluorophores; and region Ⅴ: humic acid-like fluorophores) based on the excitation and emission wavelength.

3.2.6 Analytical methods

The water quality parameters were analyzed colorimetrically using the dichromate, persulfate digestion, salicylate, and molybdovanadate methods to measure the chemical oxygen demand (COD), total nitrogen (TN), ammonium ions (NH_4^+), and total phosphorus (TP), according to standard methods for the examination of water and wastewater 5200-C, 4500-N, 4500-NH_3-G, and 4500-P-H, respectively (APHA, 2012). Structural carbohydrates (cellulose and hemicellulose) and lignin (acid-soluble and acid-insoluble lignin) were measured using the laboratory analytical procedure (LAP) developed by the National Renewable Energy Laboratory (NREL) (Sluiter et al., 2008). Carbohydrates (i.e., glucose and xylose) were analyzed using ion chromatography (ISC-5000 plus, Dionex, Germany) equipped with an electron capture detector. The gas composition (i.e., CH_4 and CO_2) was measured using gas chromatography (Acme 6100, Young Lin, South Korea) equipped with a thermal conductivity detector. Volatile fatty acids were analyzed using gas chromatography (7890B, Agilent Technologies, USA) equipped with a flame ionization detector. Statistical analysis was performed using the SigmaPlot 14.0 (Systat Software Inc., USA) with a significance level of 0.05 for the *t*-test, and analysis of variance (ANOVA) test.

3.3 Results and discussion

3.3.1 Physicochemical properties of cattle manure

VS content of CM after THP was shown in Figure 3.1. It was statistically confirmed that the VS concentration did not change after THP (p = 0.766 using t-test). The VS concentration decreased by dilution during THP with steam injection heating, which is mainly applied at an industrial scale (Barber, 2016; Pérez-Elvira & Fdz-Polanco, 2012). However, it was confirmed that VS concentration did not decrease during the THP by conduction heating applied in this study (Xue et al., 2015b; T. Zheng et al., 2021).

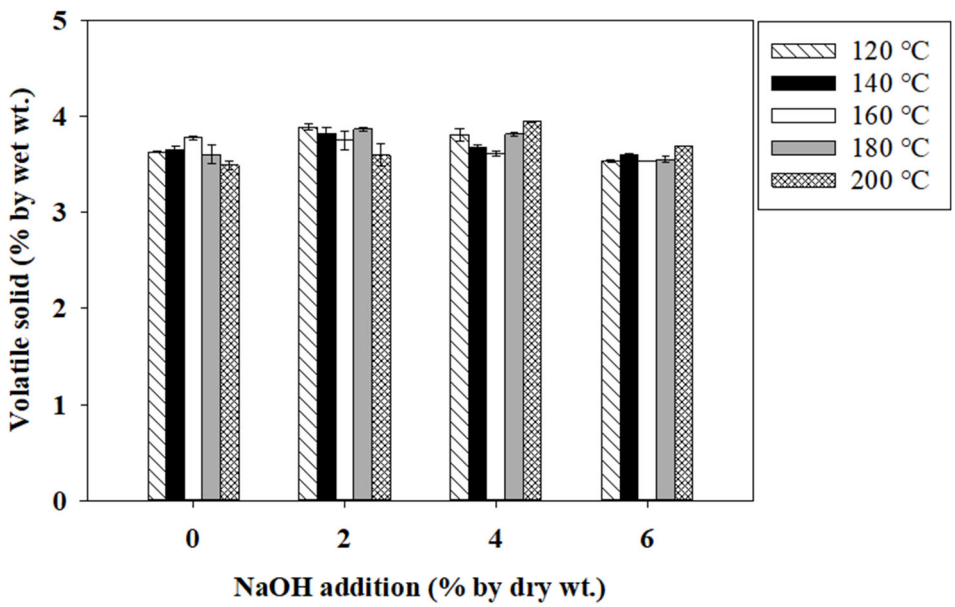

Figure 3.1 Volatile solid content of cattle manure after thermal hydrolysis

The pH of CM after THP is shown in Figure 3.2. Before the

THP, the pH was increased from 8.45 to 10.07, 11.75, and 12.24 upon the addition of 2, 4, and 6% (dry wt.) of NaOH, respectively. After the THP, the pH decreased in all treatments, with a greater decrease observed at higher THP temperatures. The decrease in pH was mainly caused by the release of organic acids from the solid phase through hydrolysis or organic matter (Khan & Ahring, 2021a; J. Lee & Park, 2020; Nuchdang et al., 2018). The concentration of total volatile fatty acids was increased from 225 mg/L in the intact CM sample to 1,580 – 3,509 mg/L with increasing THP temperature and NaOH addition, and over 60% of the VFA was acetate (Figure 3.3).

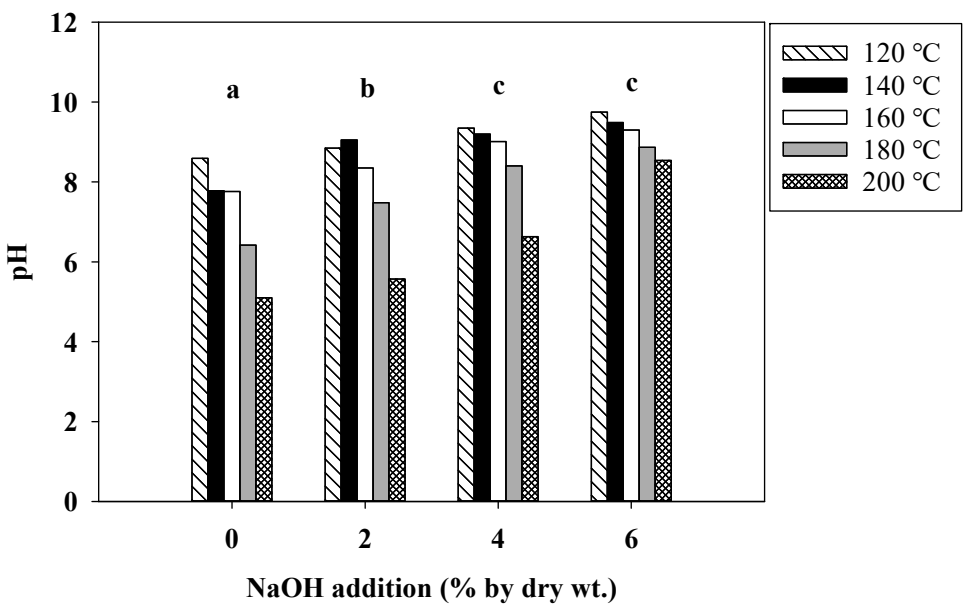

Figure 3.2 The pH of cattle manure after thermal hydrolysis pretreatment [different letters (a, b, and c) represent significant differences in average pH between NaOH concentration groups

according to paired t−test ($p < 0.05$)]

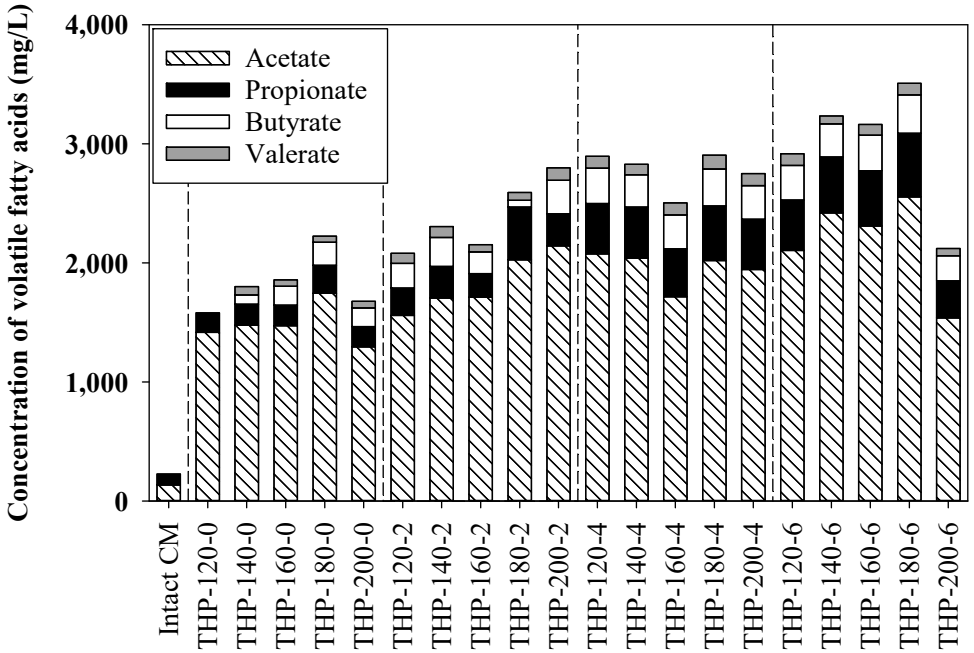

Figure 3.3 Concentration of volatile fatty acids of intact cattle manure sample and after thermal hydrolysis

Soluble COD (sCOD) of CM after THP is shown in Figure 3.4. Comparing the average sCOD values at various temperatures for the same NaOH addition, there was no significant difference in average sCOD between the group with 2% (dry wt.) NaOH addition and the group without NaOH addition (p = 0.494 using paired t−test). However, for the 4 and 6% (dry wt.) NaOH addition groups, the average sCOD was increased by 1.34 and 1.42 times, respectively, compared to the control group (p = 0.006 and 0.001, respectively, using paired t−test). There was no significant difference in the sCOD

between the 4 and 6% (dry wt.) NaOH addition groups (p = 0.28 using paired t-test). As for the average sCOD values at various NaOH addition for the same temperature, the average sCOD concentration increased in a stepwise manner by 7.0, 23.9, and 13.4% as the THP temperature increased from 120 to 140, 160, and 180 ℃, respectively, and it decreased by 15.8% when the THP temperature increased from 180 to 200 ℃. Overall, under the experimental conditions, sCOD increased with increasing NaOH addition. However, it increased with increasing THP temperature until 180 ℃ and then decreased. Therefore, the temperature was more sensitive to sCOD than NaOH in tested conditions. A similar trend was observed in the concentration of soluble carbohydrates and proteins (Figure 3.5 and Figure 3.6).

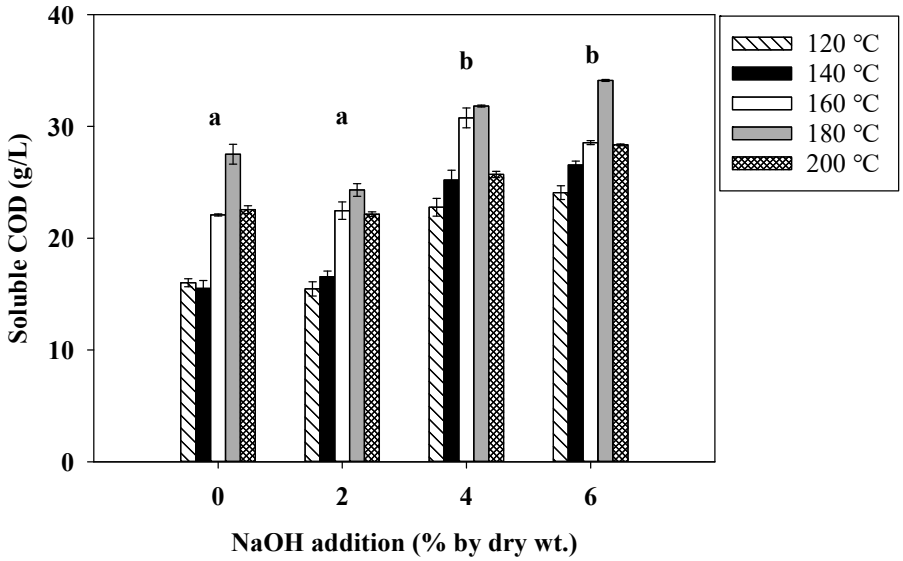

Figure 3.4 The soluble COD of cattle manure after thermal hydrolysis [different letters (a, and b) represent significant differences in average pH between NaOH concentration groups according to paired t-test ($p < 0.05$))

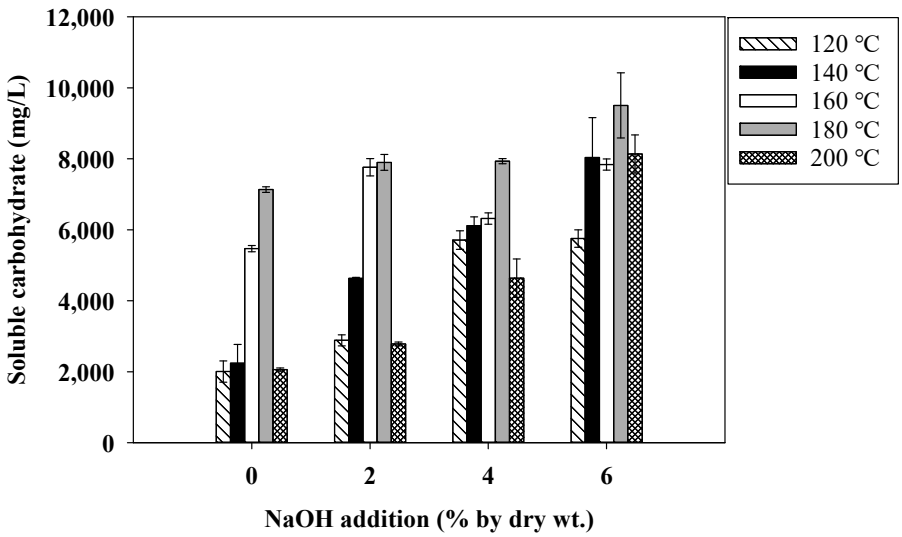

Figure 3.5 The concentration of soluble carbohydrates in cattle manure after thermal hydrolysis

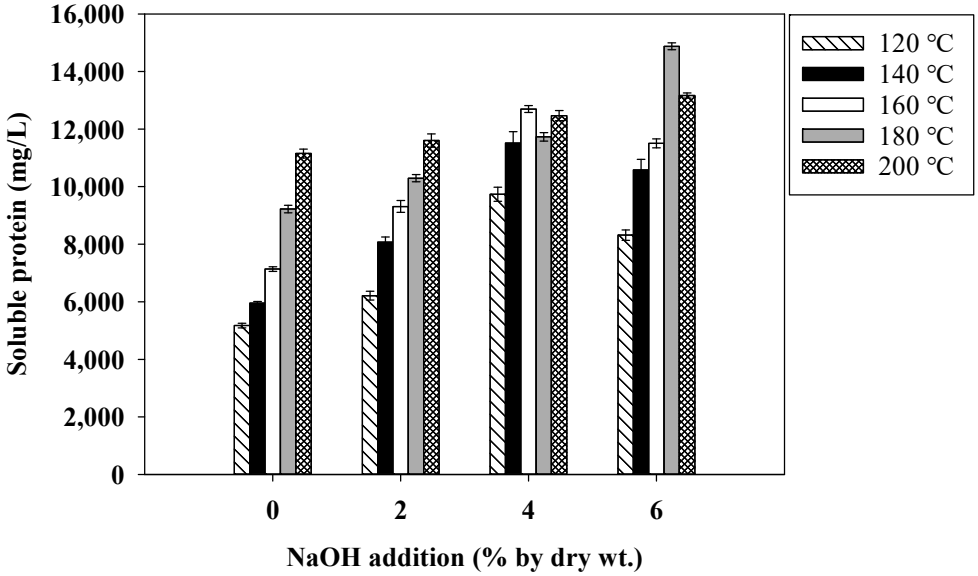

Figure 3.6 The concentration of soluble protein in cattle manure after thermal hydrolysis

Lignin content in the fiber from CM after THP is shown in Figure 3.7. Comparing the average lignin content at various temperatures for the same NaOH addition, it was decreased by 10.0 and 13.3% (dry wt.) in 2 and 4% (dry wt.) NaOH addition groups, respectively, compared to the control group (p = 0.001, and 0.022, respectively, using paired t−test). There was no significant difference in the average lignin content between the 4 and 6% (dry wt.) NaOH addition groups (p = 0.847 using paired t−test). Cellulose and hemicellulose, which are polymers of hexose (mannose, galactose, and glucose) and pentose (arabinose and xylose), can be degraded during the AD process (Usmani et al., 2020). However,

lignin acts as a physical barrier to microbial enzymes and inhibits the AD of lignocellulose by forming lignin–carbohydrate complexes (H. Chen et al., 2017; Eich–Greatorex et al., 2018; Zhao et al., 2020). Alkali agents can remove lignin from lignocellulose by causing saponification of the ester and ether bond in the lignin–carbohydrate complex, leading to an increase in the internal surface area and accessibility of enzymes to carbohydrates (Chandra et al., 2012; M. Liu et al., 2021). Overall, as the NaOH concentration increased up to 4% (dry wt.), the lignin removal efficiency also increased, but there was no further increase beyond that concentration. However, the change in lignin content due to the THP temperature was not confirmed ($p > 0.2$ between all THP temperature pairs using paired t–test).

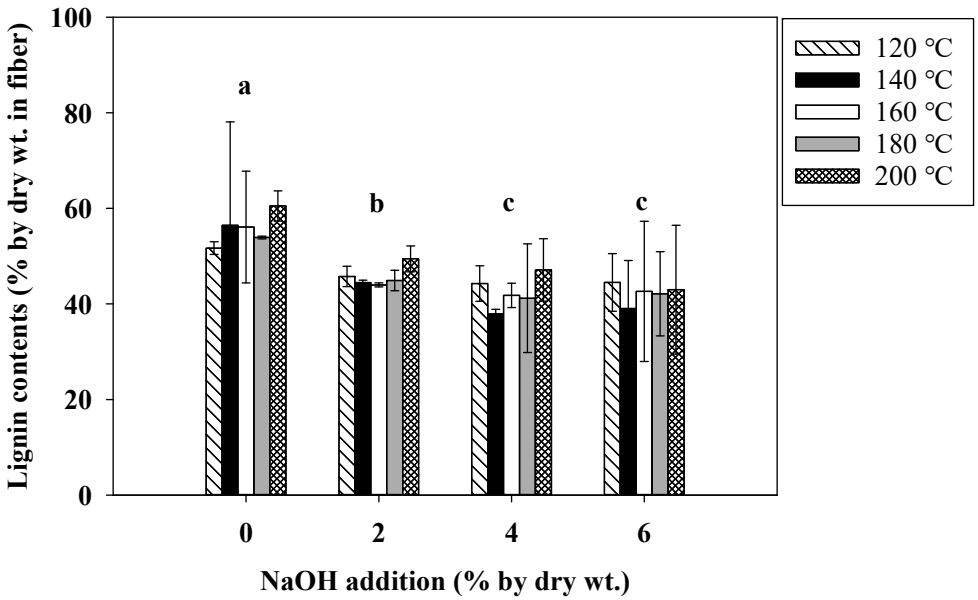

Figure 3.7 Lignin contents in the fiber from cattle manure samples after thermal hydrolysis pretreatment [different letters (a, b, and c) represent significant differences in average lignin content between NaOH concentration groups according to paired t-test ($p < 0.05$)]

Pentose and hexose, which are the decomposition products of cellulose and hemicellulose, respectively, can be degraded to furan derivatives by caramelization at 150 ℃ or higher (Göncüoğlu Taş & Gökmen, 2017). Furan derivatives can potentially inhibit cell growth and enzymatic activity (Almeida et al., 2009; Palmqvist & Hahn-Hägerdal, 2000). The formation of furfural was identified in the THP-180-0 and THP-180-2 treatments, and all samples under THP of 200 ℃ (Table 3.2). Lee et al. (2020) also confirmed that the furfural was formed in the THP of lignocellulose materials at temperatures higher than 180 ℃ (J. Lee & Park, 2020). The 5-

hydroxymethylfurfural was not found in all samples.

Table 3.2 Furfural concentrations after thermal hydrolysis

Thermal hydrolysis temperature (℃)	Furfural (mg/L)			
	NaOH addition (% by dry wt.)			
	0	2	4	6
120	ND	ND	ND	ND
140	ND	ND	ND	ND
160	ND	ND	ND	ND
180	40.8	25.8	ND	ND
200	53.1	41.4	41.1	34.6

*ND= not detected

Figure 3.8 shows the 3D-EEM matrix of CM after THP, and four regions are shown in the graph at the top left corner (THP-200-0 samples). A fulvic acid-like peak (region Ⅲ) was observed in all samples. After THP, the intensity of the aromatic protein-like peak increased (region Ⅰ, Ⅱ). In the case of the THP-200-0 treatment, the intensity of the aromatic protein-like peak (region Ⅰ, Ⅱ) decreased, and the intensity of the humic acid-like peak (region Ⅴ) increased. The increase in the humic acid-like peak is due to the generation of melanoidins by the Maillard reaction. Melanoidins are a polymer that contains nitrogen and furan rings, has a high molecular weight, and is typically brown in color. It can have various functional groups including carbonyl, carboxyl, amine, amide, pyrrole, indole,

methyleneimine, ester, anhydride, ether, methyl, and hydroxyl groups (Ames et al., 1993; Ledl & Schleicher, 1990). When proteins are carbonylated, they produce a fluorescent material (Baisier & Labuza, 1992). Humic acid is an aromatic quinone polymeric organic substance made up of humic, fulvic, and xanthic acids. It contains many oxygen-containing functional groups like carboxyl, phenolic hydroxyl, alcohol hydroxyl, methoxy, and carbonyl (Amir et al., 2004). The nitrogen element in humic acid is primarily derived from protein-like substances and produces a fluorescent effect (Boyd et al., 1980). Therefore, the fluorescent characteristics of melanoidins produced during the Maillard reaction are very similar to those of humic acid. During the THP of sewage sludge, the humic acid-like peak increased owing to the formation of melanoidins by the Maillard reaction (S. Wang et al., 2021; N. Yang et al., 2022).

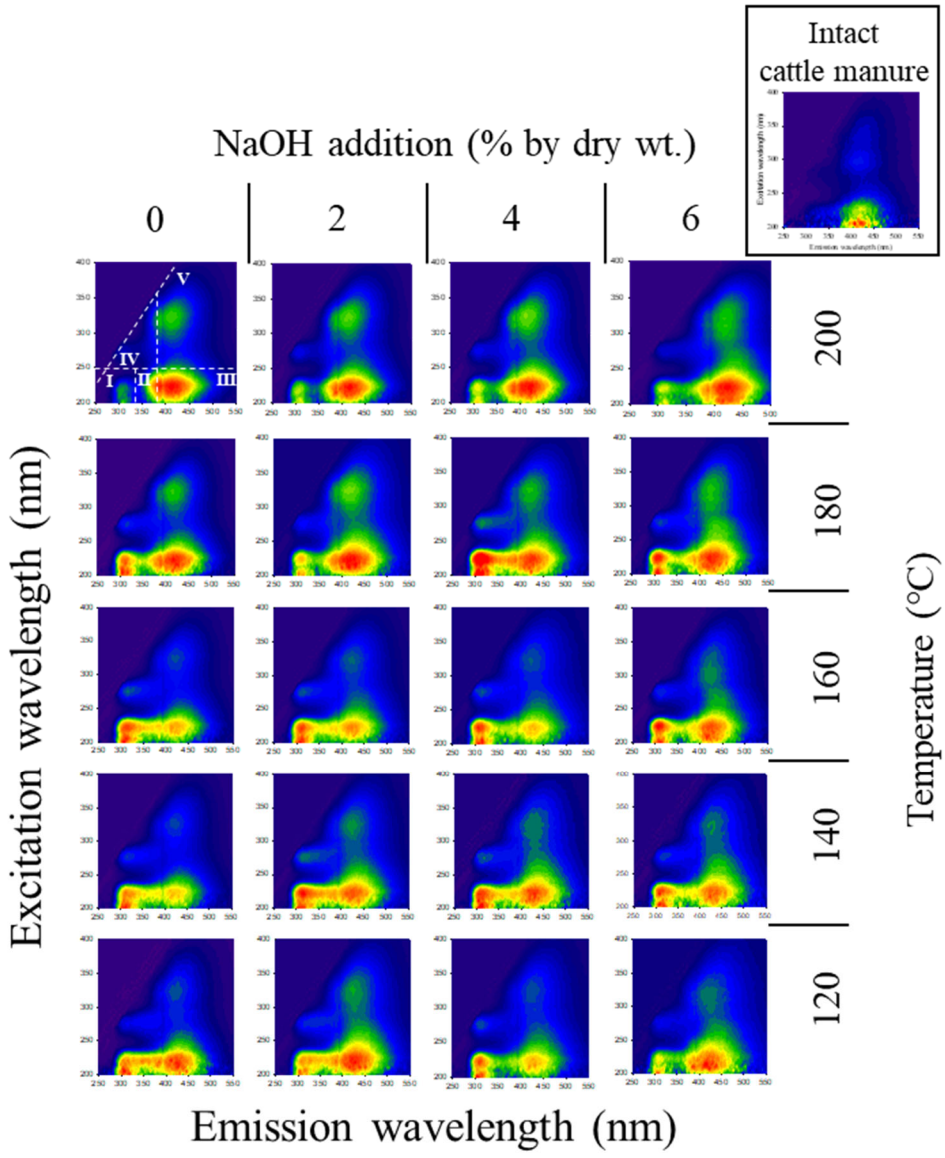

Figure 3.8 Three-dimensional excitation-emission matrix images of intact cattle manure sample and after thermal hydrolysis pretreatment (graph position in a row and column means the condition of temperature and NaOH addition, respectively)

Figure 3.9 illustrate the melanoidins concentration before and after THP. The concentration of melanoidins in intact cattle manure was measured to be 16.4 mg/g−VS of CM. After THP, the concentration of melanoidins significantly increased, ranging from 52.6 – 135.3 mg/g−VS of CM. The formation of melanoidins was found to be gradually enhanced by increasing THP temperature and adding NaOH. The Maillard reaction is stimulated not only at high temperatures but also at high pH because the reactive form of precursors (the open−chain form of sugar and unprotonated form of the amino group) are favored at higher pH (Martins et al., 2000; Takashima & Tanaka, 2014). Before the addition of NaOH, there was a clear increase in melanoidins concentration with the rising THP temperature. However, following the addition of NaOH, melanoidins were generated even at the temperature of 120 ℃, surpassing 85.4 ± 1.0 mg/g−VS of CM. Therefore, it can be inferred that avoiding the addition of NaOH would be beneficial for reducing melanoidin concentration.

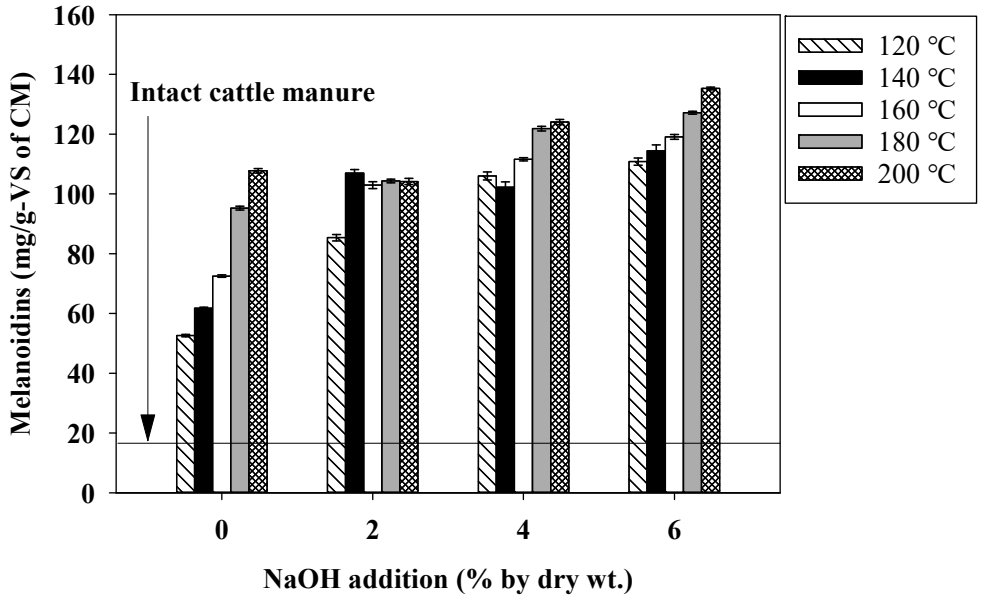

Figure 3.9 The concentration of melanoidins after thermal hydrolysis

The contour graph of melanoidins concentration by THP conditions was shown in Figure 3.10. In the contour graph, when the plot lines are closely spaced, it indicates a rapid change in values. From the NaOH addition range of 0 to 2% by dry wt. and temperature range of 120 to 180 ℃, a significant change in melanoidins concentration can be observed, suggesting a sharp transition.

The unit of melanoidins concentration was initially presented as mass-based concentration. In order to assess the level of inhibition, the concentration can be converted to a volume-based concentration by using the organic loading rate (OLR; g-VS of CM/L-reactor/d) of the reactor. The OLR guide for CSTR AD of

livestock manure is 1 – 3 g-VS/L/d (NIER, 2017). Melanoidins are known to be hardly degraded during the digestion process (Chandra et al., 2008). Under steady-state conditions, the expected concentration of melanoidins in the digester can be ranged from 52.6 – 405.9 mg/L, considering a melanoidins concentration of 52.6 – 135.3 mg/g-VS in CM. In a study by Jing and Kitts (2000), it was reported that a concentration of 1,000 mg/L of melanoidins resulted in a 44% inhibition in the oxidative degradation of proteins (Jing & Kitts, 2000). Melanoidins, which are produced through THP of food waste at a temperature of 170 ℃, have been shown to cause a 12% decrease in VFA production during the fermentation process (S. Wang et al., 2021). Furthermore, Gu et al. (2018) found that melanoidins generated through THP of sewage sludge at a temperature of 165 ℃ exhibited a 28% inhibition in specific anammox activity (Gu et al., 2018). Therefore, the melanoidins concentration in this study cannot be ruled out as a potential factor contributing to the inhibition of microbial activity.

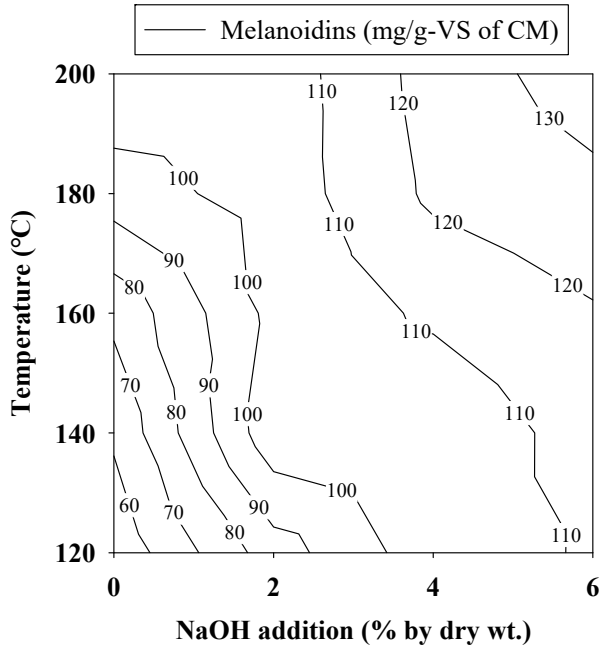

Figure 3.10 Contour graph of melanoidins concentration

3.3.2 Biochemical methane potential of cattle manure

The BMP of cellulose measured using the seeding sludge in this experiment was 401 ± 6 mL−CH_4/g−VS, and it was confirmed that the activity of the seeding sludge was optimal (Holliger et al., 2016). Figure 3.11 shows the BMP of CM samples after THP. The calculated theoretical methane potential of the CM sample was 535.1 mL−CH_4/g−VS using Eq. 3.1. The BMP of the intact CM sample was 182.2 ± 2.5 mL−CH_4/g−VS, and biodegradability was 33.6 ± 1.6% (wt.). This BMP value matches well with the values, 130 – 220 mL−CH4/g−VS, reported in the literature (Roger Kim & G. Karthikeyan, 2021; Triolo et al., 2011; Tufaner & Avşar, 2016). The THP−160−2 treatment showed the highest BMP of 227.0 ± 11.0 mL−CH_4/g−VS, and biodegradability was 42.4 ± 2.1%. The increase in biodegradability due to THP was approximately 8.8%, which is higher than the 2% increase observed in ultrasound treatment for CM (Luste & Luostarinen, 2011). The BMP showed a significant decrease when the THP temperature was increased from 160 ℃ to 180 and 200 ℃ regardless of NaOH addition (p = 0.010, and 0.000 for 160 vs. 180 ℃ and 180 vs. 200 ℃ groups, respectively, using paired t−test). The BMP was lower than that of the intact CM sample in the THP−200−0, and THP−200−2 treatments. This appears to be due to the formation of refractory compounds such as humic acid−like substances and furfural. In the food industry, studies have been

conducted to inhibit or regulate the Maillard reaction that produces refractory compounds. The Maillard reaction can be inhibited by controlling the pH, using chemical inhibitors such as SO_2, and decreasing the temperature (Fox et al., 1983; Nursten, 2005). According to Yang et al. (2022), the use of sulfites for the THP of the sewage sludge reduces the production of melanoidin by 67.4 wt.% compared with the control (N. Yang et al., 2022) This was attributed to the carbonyl group in the reducing sugar, which is the precursor of the Maillard reaction, being scavenged by the bisulfate ion. As the Maillard reaction decreases, the refractory compounds decrease, and the polysaccharides and protein concentrations increase; therefore, the BMP can be further improved.

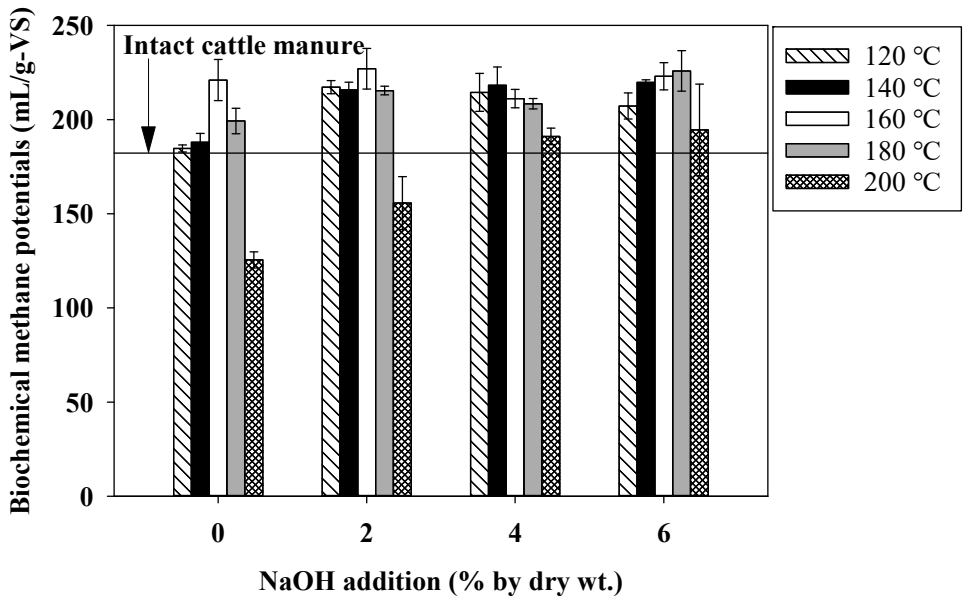

Figure 3.11 Biochemical methane potentials of cattle manure samples after thermal hydrolysis pretreatment

The first-order kinetic constant of anaerobic digestion is shown in Figure 3.12. The intact CM sample showed a kinetic constant of 0.0719 d^{-1}, and the highest kinetic constant of 0.2058 d^{-1} was observed in the THP-200-6 treatment. As the THP intensity increased (high temperature, and high NaOH addition), the kinetic constant also increased. Disintegration of particulate organic matter by THP leads to increasing kinetic constant because it is considered a bottleneck of AD process (Meyer & Edwards, 2014; Ormaechea et al., 2018).

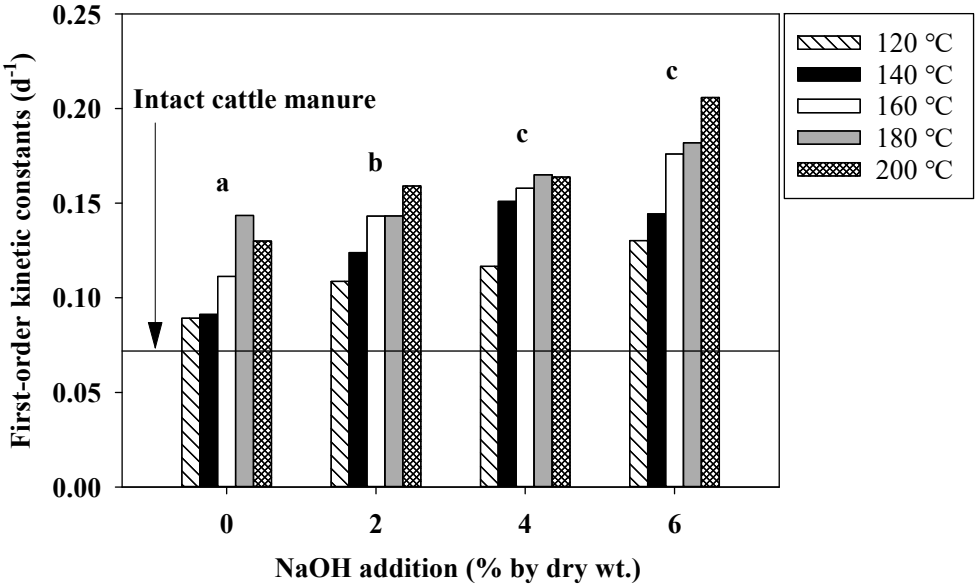

Figure 3.12 First-order kinetic constants of cattle manure samples after thermal hydrolysis pretreatment (different letters (a, b) represent significant differences in average kinetic constant between NaOH concentration groups according to paired t-test ($p < 0.05$))

3.3.3 Energy balance analysis

Energy generation and consumption are summarized in Table 3.3. The energy consumption of the AD process increased from 39.2 MJ/tonne−CM to 89.2 – 136.2 MJ/tonne−CM on applying THP. Therefore, the ratio of energy consumption to energy generation in AD increased from 7% in AD without THP to 11 – 29% in AD with THP. Figure 3.13 shows the energy gains of AD of CM coupled with THP. A positive energy gain was observed in all the treatments except for THP−200−0 and THP−200−2. This appears to be due to the decrease in BMP. THP−180−6 treatment showed the highest energy gain of 278.2 ± 43.9 MJ/tonne−CM.

Table 3.3 Energy generation and production in anaerobic digestion of cattle manure samples after thermal hydrolysis pretreatment

THP conditions		$E_{in,heating}$ (J/tonne−CM)	$E_{in,THP}$ (MJ/tonne−CM)	E_{out} (MJ/tonne−CM)	E_{net} (MJ/tonne−CM)
NaOH (% by dry wt.)	Temperature (℃)				
w/o TH		39.2	−	561.1 ± 7.7	521.9 ± 7.7
0	120	−	89.2	617.7 ± 6.3	528.5 ± 6.3
	140	−	100.9	633.8 ± 15.7	532.9 ± 15.7
	160	−	112.7	795.9 ± 39.3	683.2 ± 39.3
	180	−	124.4	771.4 ± 26.1	647.0 ± 26.1
	200	−	136.2	473.0 ± 16.1	336.9 ± 16.1
2	120	−	89.2	776.3 ± 12.6	687.1 ± 12.6
	140	−	100.9	802.7 ± 14.8	701.8 ± 14.8
	160	−	112.7	878.3 ± 41.9	765.6 ± 41.9
	180	−	124.4	833.6 ± 8.9	709.1 ± 8.9
	200	−	136.2	618.2 ± 55.9	482.0 ± 55.9
4	120	−	89.2	783.4 ± 36.8	694.2 ± 36.8
	140	−	100.9	855.6 ± 38.3	754.7 ± 38.3
	160	−	112.7	836.9 ± 19.5	724.2 ± 19.5
	180	−	124.4	834.9 ± 11.1	710.4 ± 11.1
	200	−	136.2	764.1 ± 17.5	627.9 ± 17.5
6	120	−	89.2	781.5 ± 26.2	692.3 ± 26.2
	140	−	100.9	852.0 ± 5.2	751.1 ± 5.2
	160	−	112.7	906.4 ± 29.2	793.8 ± 29.2
	180	−	124.4	924.6 ± 43.9	800.1 ± 43.9
	200	−	136.2	816.9 ± 102.2	680.7 ± 102.2

* A ± B indicates average ± standard deviation

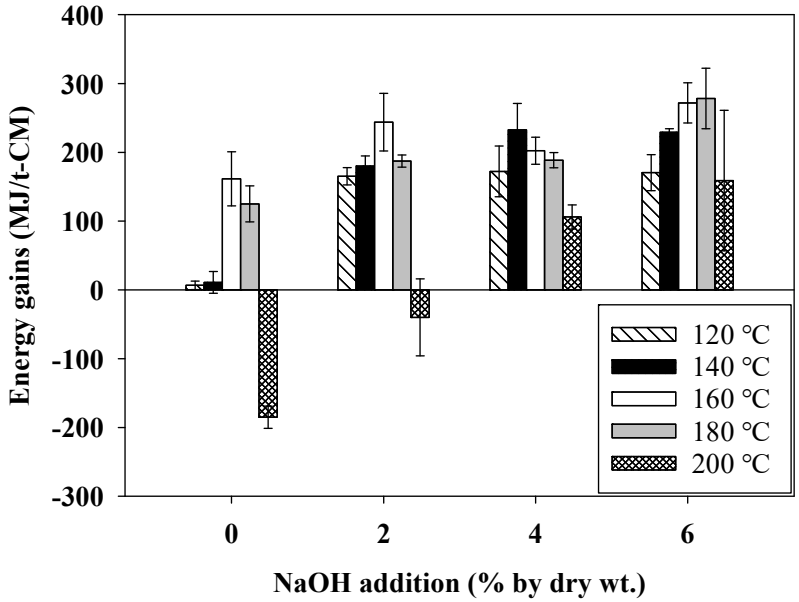

Figure 3.13 Energy gain of anaerobic digestion of cattle manure samples with thermal hydrolysis pretreatment

The difference in energy gain compared to the energy gain calculated under the assumption of 100% removal of the biodegradable substrate (without the consideration of methane generation kinetics) is shown in Figure 3.14. In all THP conditions, the energy gain was higher than that calculated under the assumption of 100% removal. Intact CM has low degradation kinetic compared to hydrolyzed CM. The removal rate of intact CM will be lower than that of hydrolyzed CM with limited digestion time. So, the energy generation of AD without THP can be overestimated if the energy balance is calculated under the assumption of the same removal rate. This leads to an underestimation of the energy gain effect of THP application.

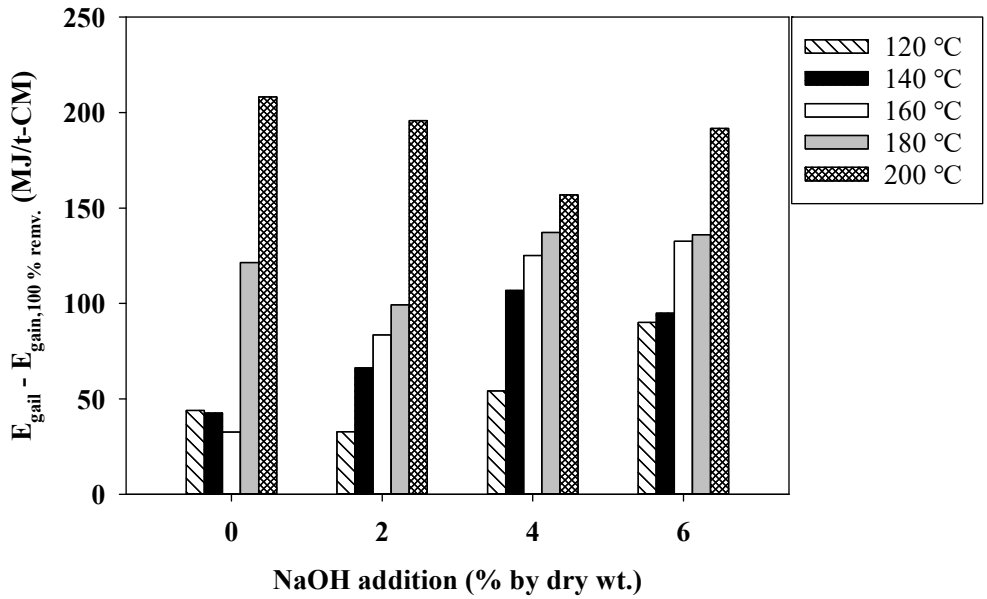

Figure 3.14 Difference in energy gain compared to the energy gain calculated under the assumption of complete removal of biodegradable substrate

The increase in energy gain showed a similar trend to the increase in methane generation kinetics (Figure 3.12). Through this, the effect of THP on methane generation kinetics was included in the energy gain. The results of the sensitivity analysis of the energy gain according to the changes in the parameters are shown in Figure 3.15. The BMP of CM after the THP had a significant influence on the energy gain. It varied from –316 to 639 MJ/tonne−CM as the BMP of CM increased from 0.4 to 1.6 times the initial BMP (from 88.4 to 353.6 mL−CH_4/g−VS). The heat recovery ratio, which was assumed to be 0.85, had a considerable influence on the energy gain change

following the BMP of CM. The energy gain varied from −88 to 235 MJ/t−CM as the heat recovery ratio increased from 0.4 to 1.18 times the initial value (from 0.35 to 1.0). Improving the BMP of substrate would be a suitable way to improve the energy gain of AD with THP. In addition to BMP, the heat recovery ratio is also an important factor.

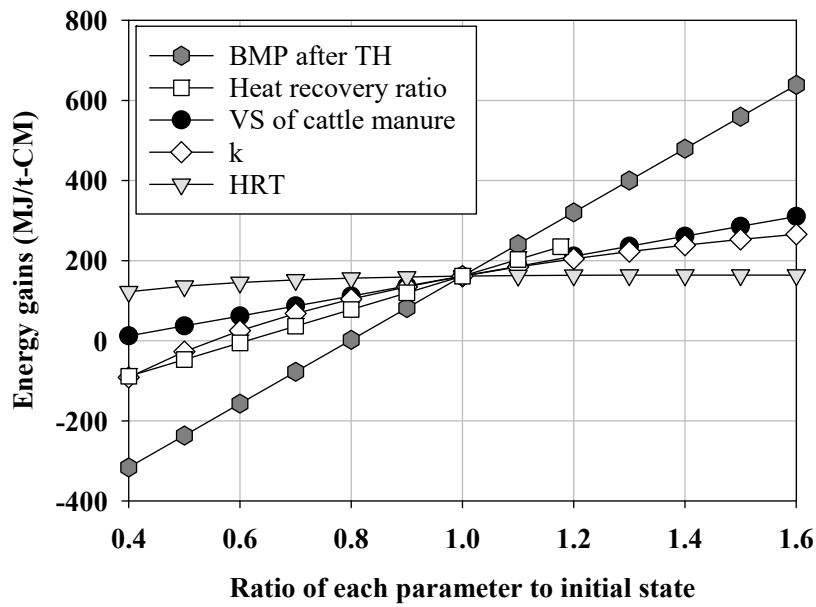

Figure 3.15 Sensitivity of parameters on energy gain

Figure 3.16 illustrates a contour graph of net energy gain by THP conditions. As the addition of NaOH increases, the net energy gain tends to increase; however, it also promotes the formation of refractory compounds (Figure 3.10). To minimize the inhibition effects caused by these compounds, it is recommended to avoid

NaOH addition. In such cases, the THP at 160 ℃ without NaOH addition exhibits the highest net energy gain of 163 ± 39.3 MJ/tonne-CM.

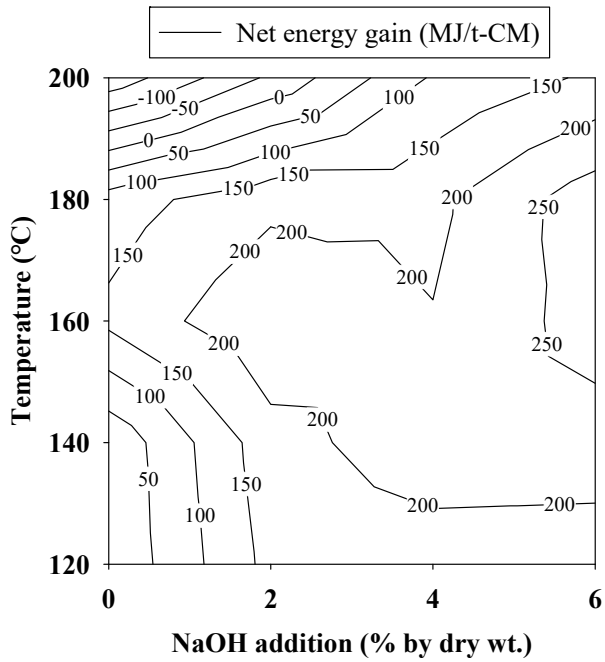

Figure 3.16 Contour graph of net energy gain

3.4 Summary

Thermal hydrolysis treatment was conducted on CM to investigate the changes in physicochemical and biochemical characteristics. The application of THP significantly enhanced the BMP and energy gain in the AD of CM. The concentration of melanoidins exhibited a significant increase with higher THP temperatures, and the addition of NaOH. Notably, THP conducted at 180 ℃ with 6% NaOH addition resulted in the highest net energy gain. Among the THP conditions without NaOH addition, aimed at reducing by-product formation, the THP at 160 ℃ demonstrated the highest net energy gain.

References

Achkari-Begdouri, A., & Goodrich, P. R. 1992. Bulk density and thermal properties of Moroccan dairy cattle manure. *Bioresource Technology*, *40*(2), 149–156.

Almeida, J. R. M., Bertilsson, M., Gorwa-Grauslund, M. F., Gorsich, S., & Lidén, G. 2009. Metabolic effects of furaldehydes and impacts on biotechnological processes. *Applied Microbiology and Biotechnology*, *82*(4), 625–638.

Ames, J. M., Apriyantono, A., & Arnoldi, A. 1993. Low molecular weight coloured compounds formed in xylose-lysine model systems#. In *Food Chemistry, 46*(2), 121-1227.

Amir, S., Hafidi, M., Merlina, G., Hamdi, H., & Revel, J. C. 2004. Elemental analysis, FTIR and 13C-NMR of humic acids from sewage sludge composting. *Agronomie*, *24*(1), 13–18.

Angelidaki, I., Alves, M., Bolzonella, D., Borzacconi, L., Campos, J. L., Guwy, A. J., Kalyuzhnyi, S., Jenicek, P., & Van Lier, J. B. 2009. Defining the biomethane potential (BMP) of solid organic wastes and energy crops: A proposed protocol for batch assays. *Water Science and Technology*, *59*(5), 927–934.

APHA. 2012. *Standard methods for the examination of water and wastewater*. American public health association Washington, DC.

Arimi, M. M., Zhang, Y., Götz, G., & Geißen, S. U. 2015. Treatment of melanoidin wastewater by anaerobic digestion and coagulation. *Environmental Technology*, *36*(19), 2410–2418.

Baisier, W. M., & Labuza, T. P. 1992. Maillard browning kinetics in a

liquid model system. *Journal of Agricultural and Food Chemistry, 40*(5), 707−713.

Bandura, A. V., & Lvov, S. N. 2006. The ionization constant of water over wide ranges of temperature and density. *Journal of Physical and Chemical Reference Data*, *35*(1), 15–30.

Barber, W. P. F. 2016. Thermal hydrolysis for sewage treatment: A critical review. *Water Research*, *104*, 53–71.

Biswas, R., Uellendahl, H., & Ahring, B. K. 2015. Wet Explosion: a Universal and Efficient Pretreatment Process for Lignocellulosic Biorefineries. *Bioenergy Research*, *8*(3), 1101–1116.

Boyd, S. A., Sommers, L. E., & Nelson, D. W. 1980. Changes in the humic acid fraction of soil resulting from sludge application. *Soil Science Society of America Journal*, *44*(6), 1179–1186.

Brands, C. M. J., Wedzicha, B. L., & Van Boekel, M. A. J. S. 2002. Quantification of melanoidin concentration in sugar − casein systems. *Journal of Agricultural and Food Chemistry*, *50*(5), 1178–1183.

Buswell, A. M., & Mueller, H. F. 1952. Mechanism of Methane Fermentation. *Industrial & Engineering Chemistry*, *44*(3), 550–552.

Cano, R., Nielfa, A., & Fdz−Polanco, M. 2014a. Thermal hydrolysis integration in the anaerobic digestion process of different solid wastes: Energy and economic feasibility study. *Bioresource Technology*, *168*, 14–22.

Cano, R., Nielfa, A., & Fdz−Polanco, M. 2014b. Thermal hydrolysis integration in the anaerobic digestion process of different solid

wastes: Energy and economic feasibility study. *Bioresource Technology*, *168*, 14–22.

Cao, S., Du, R., Yan, W., & Zhou, Y. 2022. Mitigation of inhibitory effect of THP–AD centrate on partial nitritation and anammox: Insights into ozone pretreatment. *Journal of Hazardous Materials*, *431*(5), 128599.

Carrère, H., Dumas, C., Battimelli, A., Batstone, D. J., Delgenès, J. P., Steyer, J. P., & Ferrer, I. 2010. Pretreatment methods to improve sludge anaerobic degradability: A review. *Journal of Hazardous Materials*, *183*(1–3), 1–15.

Carrère, H., Sialve, B., & Bernet, N. 2009. Improving pig manure conversion into biogas by thermal and thermo–chemical pretreatments. *Bioresource Technology*, *100*(15), 3690–3694.

Chandra, R., Takeuchi, H., Hasegawa, T., & Kumar, R. 2012. Improving biodegradability and biogas production of wheat straw substrates using sodium hydroxide and hydrothermal pretreatments. *Energy*, *43*(1), 273–282.

Chen, H., Liu, J., Chang, X., Chen, D., Xue, Y., Liu, P., Lin, H., & Han, S. 2017. A review on the pretreatment of lignocellulose for high–value chemicals. *Fuel Processing Technology*, *160*, 196–206.

Chen, W., Westerhoff, P., Leenheer, J. A., & Booksh, K. 2003. Fluorescence Excitation–Emission Matrix Regional Integration to Quantify Spectra for Dissolved Organic Matter. *Environmental Science and Technology*, *37*(24), 5701–5710.

Devos, P., Haddad, M., & Carrère, H. 2021. Thermal Hydrolysis of Municipal Sludge: Finding the Temperature Sweet Spot: A Review.

Waste and Biomass Valorization, *12*(5), 2187–2205.

Dwyer, J., Starrenburg, D., Tait, S., Barr, K., Batstone, D. J., & Lant, P. 2008. Decreasing activated sludge thermal hydrolysis temperature reduces product colour, without decreasing degradability. *Water Research*, *42*(18), 4699–4709.

Eich-Greatorex, S., Vivekanand, V., Estevez, M. M., Schnürer, A., Børresen, T., & Sogn, T. A. 2018. Biogas digestates based on lignin-rich feedstock–potential as fertilizer and soil amendment. *Archives of Agronomy and Soil Science*, *64*(3), 347–359.

Fang, C., Boe, K., & Angelidaki, I. 2011. Anaerobic co-digestion of desugared molasses with cow manure; focusing on sodium and potassium inhibition. *Bioresource Technology*, *102*(2), 1005–1011.

Fox, M., Loncin, M., & Weiss, M. 1983. Investigations into the influence of water activity, pH and heat treatment on the velocity of the Maillard reaction in foods. *Journal of Food Quality*, *6*(2), 103–118.

Friesen, W. O., & Friesen, J. A. 2010. Existing Empirical Kinetic Models in Biochemical Methane Potential (BMP) Testing, Their Selection and Numerical Solution. *NeuroDynamix II*, 216–218.

Goletz, C., Wagner, M., Grübel, A., Schmidt, W., Korf, N., & Werner, P. 2011. Standardization of fluorescence excitation-emission-matrices in aquatic milieu. *Talanta*, *85*(1), 650–656.

Göncüoğlu Taş, N., & Gökmen, V. 2017. Maillard reaction and caramelization during hazelnut roasting: A multiresponse kinetic study. *Food Chemistry*, *221*, 1911–1922.

He, L., Huang, H., Zhang, Z., Lei, Z., & Lin, B.-L. 2017. Energy Recovery from Rice Straw through Hydrothermal Pretreatment and Subsequent Biomethane Production. *Energy & Fuels*, *31*(10), 10850–10857.

Hernández-Beltrán, J. U., Hernández-De Lira, I. O., Cruz-Santos, M. M., Saucedo-Luevanos, A., Hernández-Terán, F., & Balagurusamy, N. 2019. Insight into pretreatment methods of lignocellulosic biomass to increase biogas yield: Current state, challenges, and opportunities. *Applied Sciences, 9*(18), 3721.

Hierholtzer, A., & Akunna, J. C. 2012. Modelling sodium inhibition on the anaerobic digestion process. *Water Science and Technology*, *66*(7), 1565–1573.

Holliger, C., Alves, M., Andrade, D., Angelidaki, I., Astals, S., Baier, U., Bougrier, C., Buffière, P., Carballa, M., De Wilde, V., Ebertseder, F., Fernández, B., Ficara, E., Fotidis, I., Frigon, J. C., De Laclos, H. F., Ghasimi, D. S. M., Hack, G., Hartel, M., … Wierinck, I. 2016. Towards a standardization of biomethane potential tests. *Water Science and Technology*, *74*(11), 2515–2522.

Huang, W., Zhao, Z., Yuan, T., Huang, W., Lei, Z., & Zhang, Z. 2017. Low-temperature hydrothermal pretreatment followed by dry anaerobic digestion: A sustainable strategy for manure waste management regarding energy recovery and nutrients availability. *Waste Management*, *70*, 255–262.

José Borges Gomes, F., de Souza, R. E., Brito, E. O., & Costa Lelis, R. C. 2020. A review on lignin sources and uses. *Journal of Applied Biotechnology & Bioengineering*, *7*(C), 100–105.

Khan, M. U., & Ahring, B. K. 2020. Anaerobic Digestion of Digested Manure Fibers: Influence of Thermal and Alkaline Thermal Pretreatment on the Biogas Yield. *Bioenergy Research, 14*, 891–900.

Khan, M. U., & Ahring, B. K. 2021. Improving the biogas yield of manure: Effect of pretreatment on anaerobic digestion of the recalcitrant fraction of manure. *Bioresource Technology*, *321*, 124427.

Ledl, F., & Schleicher, E. 1990. New Aspects of the Maillard Reaction in Foods and in the Human Body. In *Angewandte Chemie International Edition in English, 29*(6), 565–594.

Lee, J., & Park, K. Y. 2020. Impact of hydrothermal pretreatment on anaerobic digestion efficiency for lignocellulosic biomass: Influence of pretreatment temperature on the formation of biomass–degrading byproducts. *Chemosphere*, *256*, 127116.

Li, J., Hao, X., van Loosdrecht, M. C. M., & Liu, R. 2021. Relieving the inhibition of humic acid on anaerobic digestion of excess sludge by metal ions. *Water Research*, *188*, 116541.

Li, K., Liu, R., & Sun, C. 2015. Comparison of anaerobic digestion characteristics and kinetics of four livestock manures with different substrate concentrations. *Bioresource Technology*, *198*, 133–140.

Liu, J., Yin, J., He, X., Chen, T., & Shen, D. 2018. Three–Dimensional Excitation and Emission Fluorescence–Based Method for Evaluation of Maillard Reaction Products in Food Waste Treatment. *Journal of Chemistry*, 2018, 6758794

Liu, M., Wei, Y., & Leng, X. 2021. Improving biogas production using additives in anaerobic digestion: A review. *Journal of Cleaner Production*, *297*, 126666.

Liu, X., Lee, C., & Kim, J. Y. 2020. Thermal hydrolysis pre-treatment combined with anaerobic digestion for energy recovery from organic wastes. *Journal of Material Cycles and Waste Management*.

Lund, M. N., & Ray, C. A. 2017. Control of Maillard Reactions in Foods: Strategies and Chemical Mechanisms. *Journal of Agricultural and Food Chemistry*, *65*(23), 4537–4552.

Luste, S., & Luostarinen, S. 2011. Enhanced methane production from ultrasound pre-treated and hygienized dairy cattle slurry. *Waste Management*, *31*(9–10), 2174–2179.

Ma, J., Duong, T. H., Smits, M., Verstraete, W., & Carballa, M. 2011. Enhanced biomethanation of kitchen waste by different pre-treatments. *Bioresource Technology*, *102*(2), 592–599.

Maillard, L. C. 1912. Action des acides amines sur les sucres: formation des melanoidines par voie methodique. *CR Acad Sci*, *154*, 66–68.

Martins, S. I. F. S., Jongen, W. M. F., & van Boekel, M. A. J. S. 2000. A review of Maillard reaction in food and implications to kinetic modelling. *Trends in Food Science & Technology*, *11*(9), 364–373.

Martins, S. I. F. S., & Van Boekel, M. A. J. S. 2003. Melanoidins extinction coefficient in the glucose/glycine Maillard reaction. *Food Chemistry*, *83*(1), 135–142.

McCarty, P. L. 1964. Anaerobic Waste Treatment Fundamentals. *Public Works*, *95*, 91–94.

McCarty, P. L., & Smith, D. P. 1986. Anaerobic wastewater treatment. *Environmental Science and Technology*, *20*(12), 1200–1206.

Meyer, T., & Edwards, E. A. 2014. Anaerobic digestion of pulp and paper mill wastewater and sludge. *Water Research*, *65*, 321–349.

Neyens, E., & Baeyens, J. 2003. A review of thermal sludge pre-treatment processes to improve dewaterability. In *Journal of Hazardous Materials, 98*(1-3), 51-67

Ngo, P. L., Udugama, I. A., Gernaey, K. V., Young, B. R., & Baroutian, S. 2021. Mechanisms, status, and challenges of thermal hydrolysis and advanced thermal hydrolysis processes in sewage sludge treatment. *Chemosphere*, *281*, 130890.

Nuchdang, S., Frigon, J. C., Roy, C., Pilon, G., Phalakornkule, C., & Guiot, S. R. 2018. Hydrothermal post-treatment of digestate to maximize the methane yield from the anaerobic digestion of microalgae. *Waste Management*, *71*, 683–688.

Nursten, H. E. 2005. *The Maillard reaction: chemistry, biochemistry and implications.* Royal Society of Chemistry, Cambridge.

Ormaechea, P., Castrillón, L., Suárez-Peña, B., Megido, L., Fernández-Nava, Y., Negral, L., Marañón, E., & Rodríguez-Iglesias, J. 2018. Enhancement of biogas production from cattle manure pretreated and/or co-digested at pilot-plant scale. Characterization by SEM. *Renewable Energy*, *126*, 897–904.

Palmqvist, E., & Hahn-Hägerdal, B. 2000. Fermentation of lignocellulosic hydrolysates. II: inhibitors and mechanisms of inhibition. *Bioresource Technology*, *74*(1), 25–33.

Passos, F., Carretero, J., & Ferrer, I. 2015. Comparing pretreatment

methods for improving microalgae anaerobic digestion: Thermal, hydrothermal, microwave and ultrasound. *Chemical Engineering Journal*, *279*, 667–672.

Pérez-Elvira, S. I., & Fdz-Polanco, F. 2012. Continuous thermal hydrolysis and anaerobic digestion of sludge. Energy integration study. *Water Science and Technology*, *65*(10), 1839–1846.

Poddar, B. J., Nakhate, S. P., Gupta, R. K., Chavan, A. R., Singh, A. K., Khardenavis, A. A., & Purohit, H. J. 2021. A comprehensive review on the pretreatment of lignocellulosic wastes for improved biogas production by anaerobic digestion. *International Journal of Environmental Science and Technology*, 19, 3429-3456.

Prajapati, K. K., Pareek, N., & Vivekanand, V. 2018. Pretreatment and multi-feed anaerobic co-digestion of agro-industrial residual biomass for improved biomethanation and kinetic analysis. *Frontiers in Energy Research*, *6*, 1–18.

Rico, C., Rico, J. L., Tejero, I., Muñoz, N., & Gómez, B. 2011. Anaerobic digestion of the liquid fraction of dairy manure in pilot plant for biogas production: Residual methane yield of digestate. *Waste Management*, *31*(9–10), 2167–2173.

Rittmann, B. E., & McCarty, P. L. 2001. *Environmental biotechnology: principles and applications*. McGraw-Hill Education.

Roger Kim, J., & G. Karthikeyan, K. 2021. Solubilization of Lignocellulosic Biomass Using Pretreatments for Enhanced Methane Production during Anaerobic Digestion of Manure. *ACS ES&T Engineering*, *1*(4), 753-760.

Sluiter, A., Hames, B., Ruiz, R., Scarlata, C., Sluiter, J., Templeton, D.,

& Crocker, D. 2008. Determination of structural carbohydrates and lignin in biomass. *Laboratory Analytical Procedure*, *1617*(1), 1–16.

Takashima, M., & Tanaka, Y. 2014. Acidic thermal post-treatment for enhancing anaerobic digestion of sewage sludge. *Journal of Environmental Chemical Engineering*, *2*(2), 773–779.

Tang, T., Liu, M., Du, Y., & Chen, Y. 2022. Deciphering the internal mechanisms of ciprofloxacin affected anaerobic digestion, its degradation and detoxification mechanism. *Science of The Total Environment*, *842*, 156718.

Triolo, J. M., Sommer, S. G., Møller, H. B., Weisbjerg, M. R., & Jiang, X. Y. 2011. A new algorithm to characterize biodegradability of biomass during anaerobic digestion: Influence of lignin concentration on methane production potential. *Bioresource Technology*, *102*(20), 9395–9402.

Tsapekos, P., Kougias, P. G., Frison, A., Raga, R., & Angelidaki, I. 2016. Improving methane production from digested manure biofibers by mechanical and thermal alkaline pretreatment. *Bioresource Technology*, *216*, 545–552.

Tufaner, F., & Avşar, Y. 2016. Effects of co-substrate on biogas production from cattle manure: a review. *International Journal of Environmental Science and Technology*, *13*(9), 2303–2312.

Usmani, Z., Sharma, M., Gupta, P., Karpichev, Y., Gathergood, N., Bhat, R., & Gupta, V. K. 2020. Ionic liquid based pretreatment of lignocellulosic biomass for enhanced bioconversion. *Bioresource Technology*, *304*, 123003.

Wang, H. Y., Qian, H., & Yao, W. R. 2011. Melanoidins produced by the Maillard reaction: Structure and biological activity. *Food Chemistry*, *128*(3), 573–584.

Wang, S., Hu, Z.-Y., Geng, Z.-Q., Tian, Y.-C., Ji, W.-X., Li, W.-T., Dai, K., Zeng, R. J., & Zhang, F. 2021. Elucidating the production and inhibition of melanoidins products on anaerobic digestion after thermal–alkaline pretreatment. *Journal of Hazardous Materials*, *424*(PA), 127377.

Xue, Y., Liu, H., Chen, S., Dichtl, N., Dai, X., & Li, N. 2015a. Effects of thermal hydrolysis on organic matter solubilization and anaerobic digestion of high solid sludge. *Chemical Engineering Journal*, *264*, 174–180.

Xue, Y., Liu, H., Chen, S., Dichtl, N., Dai, X., & Li, N. 2015b. Effects of thermal hydrolysis on organic matter solubilization and anaerobic digestion of high solid sludge. *Chemical Engineering Journal*, *264*, 174–180.

Yang, N., Yang, S., & Zheng, X. 2022. Inhibition of Maillard reaction during alkaline thermal hydrolysis of sludge. *Science of the Total Environment*, *814*, 152497.

Yousefifar, A., Baroutian, S., Farid, M. M., Gapes, D. J., & Young, B. R. 2017. Fundamental mechanisms and reactions in non–catalytic subcritical hydrothermal processes: A review. *Water Research*, *123*, 607–622.

Yuan, T., Cheng, Y., Zhang, Z., Lei, Z., & Shimizu, K. 2019. Comparative study on hydrothermal treatment as pre– and post–treatment of anaerobic digestion of primary sludge: Focus on

energy balance, resources transformation and sludge dewaterability. *Applied Energy*, *239*, 171–180.

Zhang, D., Feng, Y., Huang, H., Khunjar, W., & Wang, Z. W. 2020. Recalcitrant dissolved organic nitrogen formation in thermal hydrolysis pretreatment of municipal sludge. *Environment International*, *138*, 105629.

Zhao, Y., Shakeel, U., Saif Ur Rehman, M., Li, H., Xu, X., & Xu, J. 2020. Lignin–carbohydrate complexes (LCCs) and its role in biorefinery. *Journal of Cleaner Production*, *253*, 120076.

Zheng, T., Zhang, K., Chen, X., Ma, Y., Xiao, B., & Liu, J. 2021. Effects of low– and high–temperature thermal–alkaline pretreatments on anaerobic digestion of waste activated sludge. *Bioresource Technology*, *337*, 125400.

Chapter 4
Performance and stability of continuous reactor under varied solid retention time

4.1 Introduction

The treatment of CM can be challenging because of its slow degradation rate. This is due to the pre-degradation of the readily biodegradable parts of the digestive organ of a cow and its high lignocellulose content of approximately 40–50 wt.% (Tsapekos et al., 2016). Lignocellulose is a complex mixture of lignin, cellulose, and hemicellulose (LCH), which is difficult for microorganisms to break down (Ahring et al., 2015; Koyama et al., 2017). In order to enhance the efficiency of AD, various pretreatment methods, including physical, chemical, and biological ones, can be applied (Carrère et al., 2010; Orlando & Borja, 2020). Among these methods, thermal hydrolysis pretreatment (THP), which hydrolyzes a substrate at high temperature and pressure (approximately 160 ℃ and 6.1 atm), has been shown to enhance the degradation rates and increase the biochemical methane potential (BMP) of organic matter (Devos et al., 2021; J. Lee & Park, 2020; Xue et al., 2015a). However, AD is a biological process that is sensitive to changes in environmental conditions, such as feedstock type, temperature, and pH, which can lead to digester failure. The application of pretreatment on AD can

also change the microbial community by making organic matter more accessible to microorganisms.

Solid retention time (SRT) is a crucial factor in the operation of AD. In a typical AD process with a continuous stirred-tank reactor (CSTR), an increase in SRT improves the removal efficiency but also results in increased operational costs. Additionally, the SRT plays a critical role in microbial growth. An insufficient SRT can cause microorganisms to wash out, leading to digester failure. Reactor failure due to microbial imbalance is a frequent problem, and a clear understanding of the effects of THP and SRT on the microbial community in reactors is vital for maintaining digester stability. For instance, Zhang et al. (2022) observed a decrease in the microbial diversity in the AD of THP sludge as the SRT decreased from 30 d to 10 d (L. Zhang et al., 2022). In another study, Wandera et al. (2019) reported a decrease in methane yield from 0.28 to 0.12 L-CH_4/g-volatile solids (VS) and an increase in the acetate concentration from 38 to 376 mg/L in the AD of THP sewage sludge as SRT decreased from 20 d to 3 d (Wandera et al., 2019). It is worth noting that the behavior of AD may vary significantly depending on the substrate type and operating conditions. As mentioned earlier, studies have been conducted on the influence of SRT on thermally hydrolyzed sludge. However, the effects of THP and SRT on the AD of CM have not been studied.

The objective of this study was to investigate the potential of using THP to reduce the SRT in the AD of CM. To achieve this, two continuously stirred tank reactors (CSTRs) were operated for 398 d and fed with intact CM, and THP CM. Their performance in terms of biogas yield, VS removal, reaction kinetics, and microbial community dynamics was evaluated.

4.2 Materials and methods

4.2.1 Substrate and inoculum

Intact CM samples were collected from six farms in Cheonan, South Korea. The collected CM was mixed homogeneously and stored at −20 ℃ until use. The THP process was carried out using an autoclave (HR−S−2000, Ilshin Autoclave, South Korea) at 160 ℃ and 6.1 atm for 30 min. AD sludge was obtained from the wastewater treatment plant in Seoul, South Korea, filtered through a 0.5 mm sieve, and used as inoculum. Table 4.1 shows the characteristics of the inoculum, intact cattle manure, and thermally hydrolyzed cattle manure samples.

Table 4.1 Characteristics of inoculum, intact cattle manure, and thermally hydrolyzed cattle manure

	Inoculum	Intact cattle manure	Thermally hydrolyzed cattle manure
TS (% by wet wt.)	4.2 ± 0.3	27.4 ± 1.9	25.5 ± 1.3
VS (% by wet wt.)	3.2 ± 0.3	18.7 ± 0.8	18.0 ± 1.2
BMP ($mL-CH_4/g-VS_{in}$)	–	182.2 ± 2.5	221.0 ± 11.0
pH	7.2	8.45	7.37
TCOD (g-COD/L)	–	231.7 ± 51.3	212.9 ± 10.2
SCOD (g-COD/L)	–	25.2 ± 8.5	56.3 ± 6.9
NH_4^+ (mg-N/L)	–	1,260 ± 495	1,795 ± 254
Total VFA (mg/L)	–	2,247 ± 488	10,729 ± 2,146
Carbohydrates (% by dry wt.)	–	39.2	38.9
Proteins (% by dry wt.)	–	16.8	16.9
Lipids (% by dry wt.)	–	7.2	7.4

4.2.2 Reactor operation

Two CSTRs were operated; one with THP (THP AD) and the other without THP (control AD), each with a total and working volume of 8 L and 6 L, respectively. Due to the nature of a CSTR where sludge concentration or membranes are not employed, the SRT and hydraulic retention time (HRT) were equivalent. The reactors were operated in a mesophilic (35 ± 1 ℃) constant-temperature room for 398 d. In order to acclimate the inoculum to the substrate, intact CM samples were fed to both reactors for 100 d, with an increase in the organic loading rate (OLR) from 1.5 to 1.94 and 2.5 g-VS/L/d under an SRT of 36.0 d (Table 4.2).

Table 4.2 Operating conditions of Control AD, and THP AD

Elapsed time (d)	SRT (d)	OLR (g-VS/L/d)	Substrate		
			Control AD	THP AD	
0 - 52	36.0	1.5	Intact cattle manure	Intact cattle manure	Start-up
53 - 71		1.9			
72 - 100		2.5			
101 - 212				Thermally hydrolyzed cattle manure	Phase 1
213 - 294	21.8	4.1			Phase 2
295 - 355	13.2	6.8			Phase 3
356 - 398	8.0	11.3			Phase 4

Tap water was used to dilute the CM and adjust the target OLR and SRT to the desired levels. After the start-up, the VS concentration in the CM remained at 8.0 wt.% using the same dilution rate throughout the experiment (phases 1-4). At day 101, the thermally hydrolyzed CM was fed into a treatment reactor (THP AD). The SRT was subsequently decreased from 36.0 to 21.8, 13.2, and 8 d to evaluate the impact of SRT on the reactor performance and microbial community. The reactors were operated for at least 3.1 SRT cycles under each condition to confirm the steady-state operation. The OLR increased from 2.5 to 4.1, 6.8, and 11.3 g-VS/L/d as the SRT decreased. Data collected within one SRT cycle after changing the operating conditions were not used to evaluate the reactor performance (methane yield, VS removal, and reaction kinetics). The biogas generated in the reactors was collected in a gas sampling bag and its volume and composition were analyzed.

4.2.3 Kinetic analysis

The first-order rate constant for VS removal was calculated using the rate expressions (Eq. 4.1), and the mass balance of a CSTR at a steady state (Eq. 4.2).

$$\frac{dS}{dt} = -k_{VS}S \quad \text{Eq. 4.1}$$

$$0 = Q(S_0 - S) + \frac{dS}{dt}V \quad \text{Eq. 4.2}$$

where S is the effluent concentration of substrate (mg/L for VS), k_{VS} is the VS removal rate constant (d^{-1}), Q is the flow rate (L/d), S_0 is the influent concentration of substrate (mg/L for VS), and V is the reactor volume (L). The VS removal rate constant was determined by combining Eq. 4.1 and Eq. 4.2 as Eq. 4.3.

$$k_{VS} = \frac{Q(S_0 - S)}{S\,V} \quad \text{Eq. 4.3}$$

Some of the biochemical methane potential of the substrate was released as gas and the rest was released as effluent. This can be expressed using Eq. 4.4.

$$M_{max} = Y + M \quad \text{Eq. 4.4}$$

where M_{max} is the biochemical methane potential (BMP) of the influent ($mL-CH_4/g-VS_{in}$), Y is the methane yield of the reactor ($mL-CH_4/g-VS_{in}$), M is the BMP of effluent ($mL-CH_4/g-VS_{in}$). The BMP decrease rate is equal to methane generation rate; therefore, the first-order rate constant for methane generation was calculated using the rate expression (Eq. 4.5), and the mass balance for the

CSTR at steady state (Eq. 4.6).

$$\frac{dM}{dt} = -k_{CH_4}M \quad \text{Eq. 4.5}$$

$$0 = Q(M_{max} - M) + \frac{dM}{dt}V \quad \text{Eq. 4.6}$$

where k_{CH_4} is the methane generation rate constant (d^{-1}). The methane generation rate constant was determined by combining Eq. 4.4, 4.5, and 4.6 as shown in Eq. 4.7.

$$k_{CH_4} = \frac{Q\,Y}{(M_{max}-Y)V} \quad \text{Eq. 4.7}$$

The influent biochemical methane potential was measured in a previous study (Kim et al., 2023). To eliminate data from the transient period, only the data after one SRT cycle from the condition changes were used for modeling.

4.2.4 Analytical methods

The gas compositions, including CH_4, CO_2, and N_2, were analyzed by gas chromatography with a thermal conductivity detector (Young Lin, Republic of Korea). The total solids (TS) and VS were determined using standard methods (APHA, 2012). Chemical oxygen demand (COD) and ammonium ions (NH_4^+) were measured using colorimetric methods with dichromate and salicylate, respectively, in accordance with standard methods. Volatile fatty acids (VFAs) were analyzed via gas chromatography using a flame ionization detector (Agilent Technologies, CA, USA). The alkalinity was determined using a titration method with a pH endpoint of 4.5 (APHA, 2012).

DNA for taxonomic profiling of the microbiome was extracted from the digestate of both CSTRs collected at the end of each operating condition (215, 290, 349, and 390 d). DNA was extracted using the FastDNA Spin Kit for Soil (MP Biomedicals, OH, USA). The taxonomic profile of the microbiome was identified using 16S rRNA-based microbiome analysis, targeting the V4 and V5 regions for archaea and the V3 and V4 regions for bacteria, using the MiSeq platform (Illumina, CA, USA). The sequencing was carried out at CJ Bioscience, Inc. (Seoul, Republic of Korea). The taxonomic ranks of each sequence read were determined based on their similarity to species (≥ 97%), genus (97≥ x≥ 94.5%), family (94.5≥ x≥ 86.5%), order (86.5≥ x≥ 82%), class (82≥ x≥ 78.5%), and phylum

(78.5≥ x≥ 75%) using the EzBiocloud 16S rRNA database. The operational taxonomic units (OUTs) were 97% identical. The diversity of microbial communities was calculated using Shannon and Simpson indices. The relative abundances of bacteria and archaea were calculated as a percentage of the total number of sequences in each sample, with a threshold of at least 1%. Sequence data from this article have been deposited with the GenBank Data Libraries supported by U.S National Center for Biotechnology Information under the accession number of PRJNA965919.

An analysis of non-metric multidimensional scaling (NMDS) based on the Bray-Curtis distance was performed using the *vegan* package in R software to investigate beta diversity between samples. Statistical analysis was conducted using SigmaPlot (Systat Software Inc., CA, USA) with a significance level of 0.05 for *t*-test and analysis of variance (ANOVA) test.

4.3 Results and discussion

4.3.1 Reactor stability

The daily methane production of the control AD and THP AD is shown in Figure 4.1. The application of THP resulted in 1.5 ± 2 times higher methane production in THP AD compared to control AD after 100 d, as indicated by a pared t-test ($p < 0.001$). This appeared to be due to solubilization and an increase in the BMP of CM by THP (Table 4.1). Continuous methane generation without reactor failure was confirmed while decreasing the SRT from 36.0 to 13.2 d in both control AD and THP AD. Methane production in both control AD and THP AD rapidly decreased under an SRT condition of 8.0 d, potentially due to the decrease of methanogenic microorganisms with slow growth rates. The limiting value of the SRT for preventing the washout of acetoclastic methanogens was reported to be 4 d (Rittmann & McCarty, 2001). In the AD of sewage sludge, decreased methane production resulted from the washout of methanogens by decreasing the SRT by 3–4 d (I. S. Lee et al., 2011; Wandera et al., 2019). The criteria for washout SRT can vary depending on the environment and substrate (Schmidt et al., 2014), and decomposition rate of CM is slower compared to other organic waste due to the presence of lignocellulose materials (Tufaner & Avşar, 2016). In the case of co-digestion of cattle manure with food waste to improve

efficiency, stable operation was achieved up to an HRT of 5 d (Bi et al., 2020).

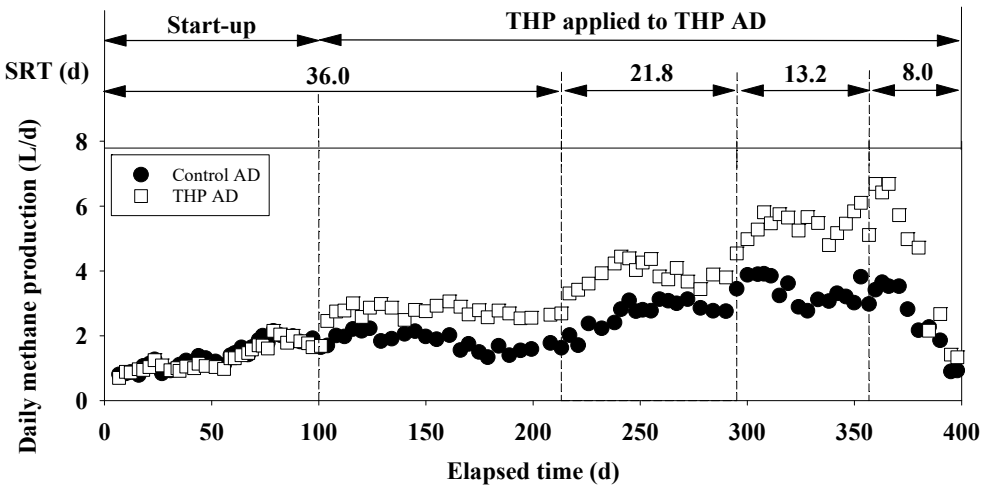

Figure 4.1 Daily methane production of control AD, and THP AD

VFA, intermediate products of the AD process, may accumulate in the digester in the case of overloading or insufficient methanogenesis (Björnsson et al., 1997; Wu et al., 2022). The accumulation of VFAs can lead to process inhibition via two major mechanisms. One is by lowering the pH of the digester owing to acid accumulation, which decreases the rate of enzyme activity and biochemical reactions of microorganisms (Rittmann & McCarty, 2001; Russell & Dombrowski, 1980). The other is caused by direct inhibition by VFAs. The undissociated forms of acids (e.g., acetic acid

and propionic acid) can easily diffuse into the cell membrane and dissociate, disrupting the proton motive force and homeostasis of microorganisms (Henderson, 1973; Shi et al., 2017; Wainaina et al., 2019). The concentrations of the VFAs are shown in Figure 4.2. Both control AD and THP AD maintained VFA concentrations below 165 mg/L under the SRT condition of 36.0 d, except for the data measured at the elapsed time of 85 d. This temporal VFA accumulation seems to be due to the OLR increase from 1.9 to 2.5 g-VS/L/d after an elapsed time of 72 d. At the SRT conditions of 21.8 d and 13.2 d the VFA concentration increased to 551 mg/L and 613 mg/L in the control AD and THP AD, respectively. The ratio of acetate in VFAs was 70 ± 10 and 81 ± 9 wt.% in the control AD and THP AD, respectively. At the SRT condition of 8 d, the VFA concentration increased up to 1,214 in the control AD and 1,332 mg/L in THP AD, where propionate was dominant (56 ± 14 wt.% in the control AD and 49 ± 14 wt.% in THP AD). Propionate accumulates easily because of its much slower acetogenic rate than that of other VFAs (L. Wang et al., 2006). Propionate accumulation is often correlated with the failure of overloaded digesters (Y. Yang et al., 2018). Therefore, an increase in the propionate concentration means that the instability of the AD increased under the SRT condition of 8.0 d. The concentration of undissociated VFAs at an SRT of 8 d was calculated to be 30.3 and 19.9 mg/L for control AD and THP AD, respectively, based on the

dissociation constant of VFA and reactor pH. While the inhibitory effect of undissociated VFA was minimal under these conditions, it could increase with a further decrease in pH.

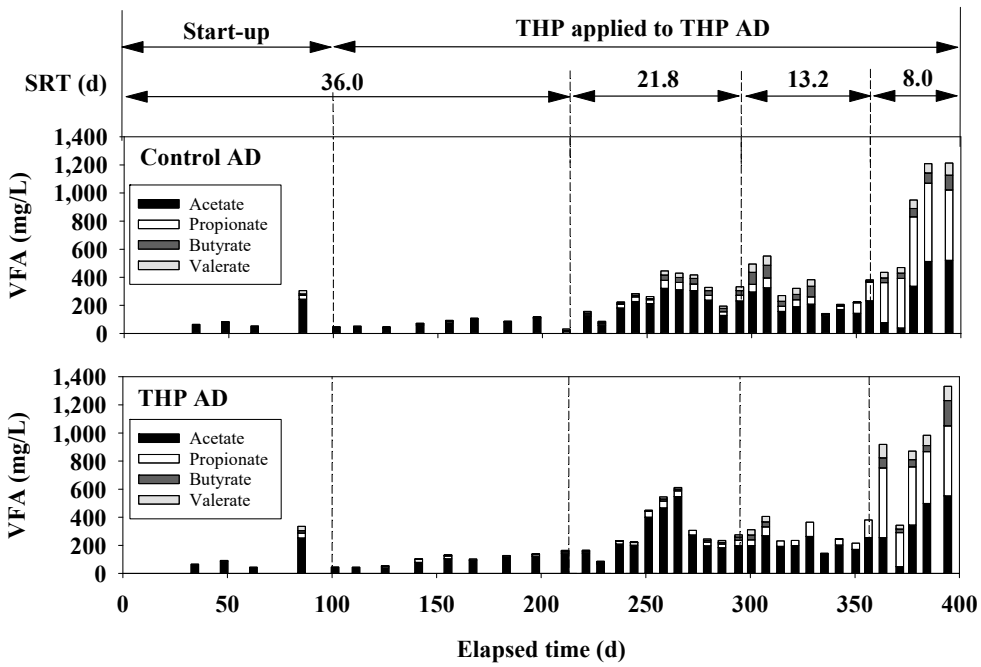

Figure 4.2 VFA concentration of control AD (top) and THP AD (bottom)

The inhibitory effect of VFA on microbial activity was determined by the pH and VFA concentration. The ratio of the VFA concentration to alkalinity was used as an indicator of reactor stability (Huang et al., 2017; Y. Q. Li et al., 2018). . It has been suggested that a VFA/alkalinity ratio of 0.3 or higher may lead to reactor instability, although this threshold can vary depending on the case (Hernández et al., 2014; Steinmetz et al., 2016). Figure 4.3

shows VFA/alkalinity ratio. This ratio was maintained lower than 0.1 during the reducing SRT condition from 36.0 d to 13.2 d. At an SRT of 8 d, the ratio increased dramatically to 0.3. By increasing VFA/alkalinity, the pH of control AD and THP AD decreased to 6.42 and 6.66, respectively.

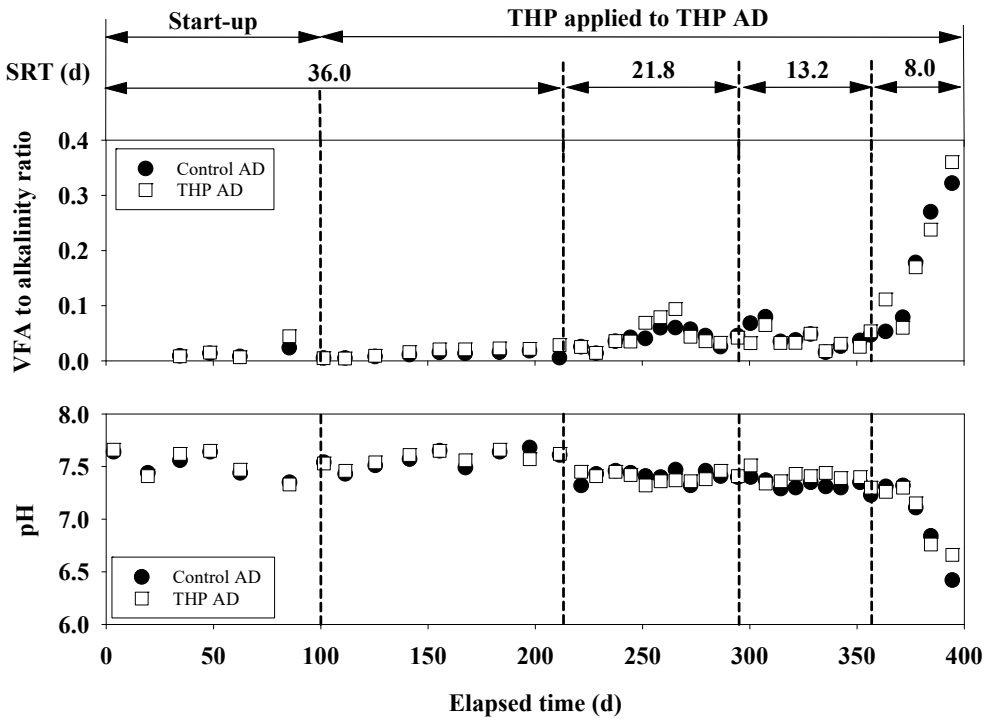

Figure 4.3 VFA to alkalinity ratio (top) and pH (bottom) of control AD and THP AD

The high concentration of ammonia can inhibit the activity of methanogenic microorganisms, and inhibitory levels of total ammonium nitrogen (TAN) have been reported to range from 2,500 to 11,000 mg-N/L (Y. Yang et al., 2018). Figure 4.4 illustrates the

concentration of total ammonium nitrogen in control AD, and THP AD. Despite the increase in ammonia concentration due to THP (Table 4.1), the ammonia concentration in THP AD was kept below 1,200 mg−N/L. However, an increase in pH can lead to an increase in free ammonia, which is more toxic and can inhibit methane production.

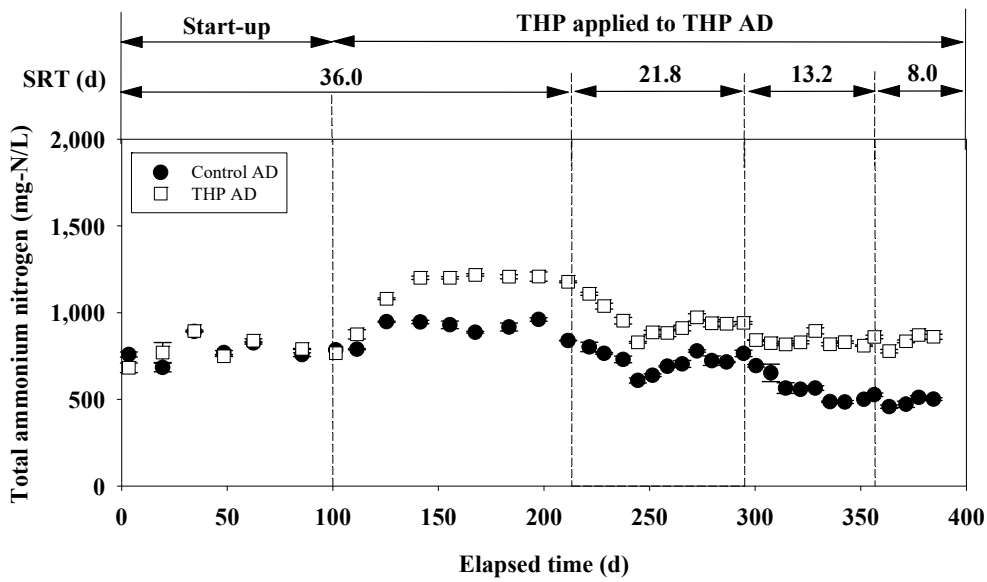

Figure 4.4 Total ammonium nitrogen of control AD, and THP AD

4.3.2 Reactor performance

Figure 4.5 illustrates the methane yield of the control AD, and THP AD. The results indicated that THP AD exhibited 1.6, 1.4, and 1.7 times higher methane yields than the control AD at SRT of 36.0, 21.8, and 13.2 d, respectively ($p < 0.05$). Moreover, the methane yield of THP AD decreased by 26.0% upon reducing the SRT from 36.0 d to 13.2 d, whereas it decreased by 28.7% in the control AD ($p < 0.05$). In the THP AD, methane yield at SRT of 21.8, and 13.2 d was 0.162, and 0.135 L/g−VS of raw CM. These values are lower than the methane yields of thermally hydrolyzed sludge at SRT of 20, and 10 d, which were 0.095, and 0.280 L/g−VS, respectively (Quiao et al., 2011).

Figure 4.6 illustrates the VS removal ratio of the control and THP AD. THP AD had 1.4, 1.9, and 2.0 times higher VS removal ratio than control AD at SRT conditions of 36.0, 21.8, and 13.2 d, respectively ($p < 0.05$). While the VS removal ratio of the THP AD did not significantly change during the reduction of the SRT from 36.0 d to 13.2 d, that of the control AD decreased by 30.6% ($p < 0.05$). Remarkably, THP AD with a shorter SRT (13.2 d) outperformed the control AD with a longer SRT (36.0 d in terms of both methane yield and VS removal ratio).

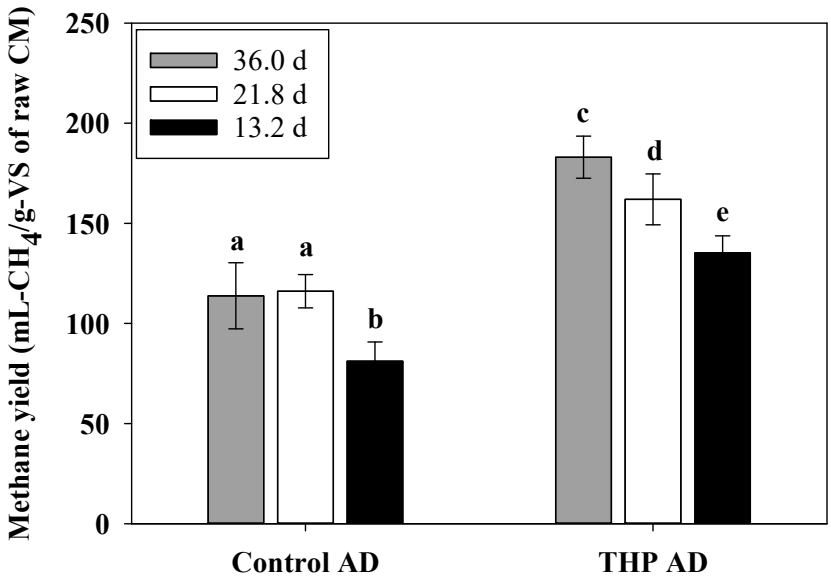

Figure 4.5 Methane yield of control AD and THP AD

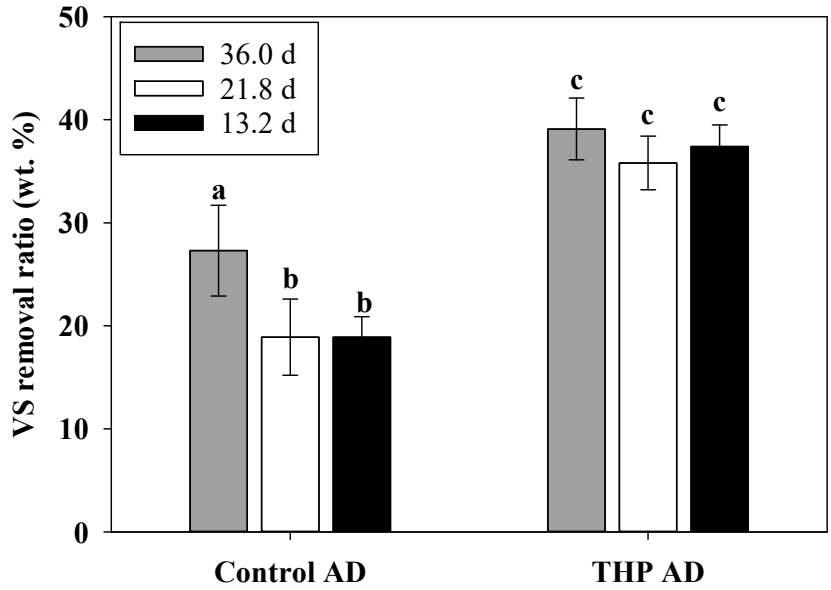

Figure 4.6 VS removal ratio of control AD and THP AD

Table 4.3 summarizes the first-order rate constants for methane generation and VS removal. The methane generation rate constant of THP AD ranged from 0.120 to 0.129 d^{-1}, whereas it ranged from 0.048 to 0.084 d^{-1} in the control AD. The VS removal rate constant of the THP AD ranged from 0.020 to 0.047 d^{-1}, whereas it ranged from 0.010 to 0.018 d^{-1} in the control AD. THP AD had a higher reaction rate than the control AD in terms of methane generation and VS removal. The VS removal rate constants of CSTR AD fed with sewage sludge ranged from 0.066 to 0.118 d^{-1} at SRT of 20 d to 4 d (I. S. Lee et al., 2011), whereas the hydrolysis rate of carbohydrates in the primary sludge ranged from 0.153 to 0.428 d^{-1} in CSTR AD at SRT of 3 d to 15 d (Miron et al., 2000). In the case of methane generation, the rate constant of CSTR AD fed with food waste was 0.329 d^{-1} at an SRT of 16 d (Nagao et al., 2012). The relatively low-rate constant for CM was probably due to the pre-digestion of readily biodegradable substances in the cow's digestive system, and the high content of lignocellulosic materials in CM (Muhammad Nasir and Mohd ghazi, 2015; Tsapekos et al., 2016). With decreasing SRT, the rate constant showed an increasing trend, particularly for the VS removal rate. This can be explained by the heterogeneity of the CM samples. If the CM is homogeneous, the removal ratio with increase as reaction time increases under the same reaction rate. However, in the case of CM samples, readily

degradable and slowly degradable substrates are mixed. At short SRTs, the rapidly degrading substrates were predominantly degraded. At long SRTs, slowly degrading substrates were also degraded, therefore, the substrate removal ratio and methane yield increased (Figure 4.6), but the overall reaction rate decreased. The AD of sewage sludge showed an increasing trend in the reaction rate with decreasing SRT (I. S. Lee et al., 2011). This effect was greater in THP AD than in control AD owing to the increasing concentrations of SCOD and VFA, which are rapidly degrading substrates, by THP Table 4.1). Due to the accelerated substrate degradation by THP, a significant portion of the removable VS had already been removed at an SRT of 13.2 d. As a result, the reaction rate increased at shorter SRT conditions, and it became difficult to observe differences in VS removal ratio under the SRT conditions of 13.2 – 36.0 d due to experimental error.

Table 4.3 The first-order rate constant of methane generation, and VS degradation

SRT (d)	CH_4 generation rate constant (d^{-1})		VS removal rate constant (d^{-1})	
	Control AD	THP AD	Control AD	THP AD
36.0	0.053 (± 0.023)	0.121 (±0.067)	0.012 (±0.003)	0.020 (±0.003)
21.8	0.085 (± 0.013)	0.132 (±0.040)	0.010 (±0.003)	0.026 (±0.003)
13.2	0.065 (± 0.013)	0.145 (±0.019)	0.018 (±0.002)	0.047 (±0.003)

4.3.3 Microbial community

During a reduction of SRT from 36.0 d to 21.8, 13.2, and 8.0 d, the dominant bacterial genus in control AD remained as *AC160630_g*, while the dominant bacterial genus in THP AD shifted from *BBZD_g* to *AC160630_g*, and *Proteiniphilum*. Figure 4.7 shows the relative abundances of *Firmicutes* and *Bacteroidetes*. *Bacteroidetes* and *Firmicutes* are bacterial phyla that are frequently found in the AD of organic waste (C. Lee et al., 2023; Wandera et al., 2019). The abundance ratio of *Firmicutes* to *Bacteroidetes* was used as an indicator of AD stability in terms of bacterial structure (Cayetano et al., 2020, 2021; S. Chen et al., 2016). In the AD of livestock manure, the relative abundance of *Bacteroidetes*, has a positive correlation with VFA concentrations, which is a potential inhibitor, whereas *Firmicutes* showed the opposite trend (S. Chen et al., 2016). In the AD of wasted activated sludge, the relative abundance ratio of *Firmicutes* to *Bacteroidetes* had a significantly positive correlation with reactor stability, implying that as the ratio increased, the efficiency increased (Cayetano et al., 2021). By applying THP, it can be inferred that stability decreased owing to a decrease in the relative abundance ratio of *Firmicutes* to *Bacteroidetes* (p = 0.029).

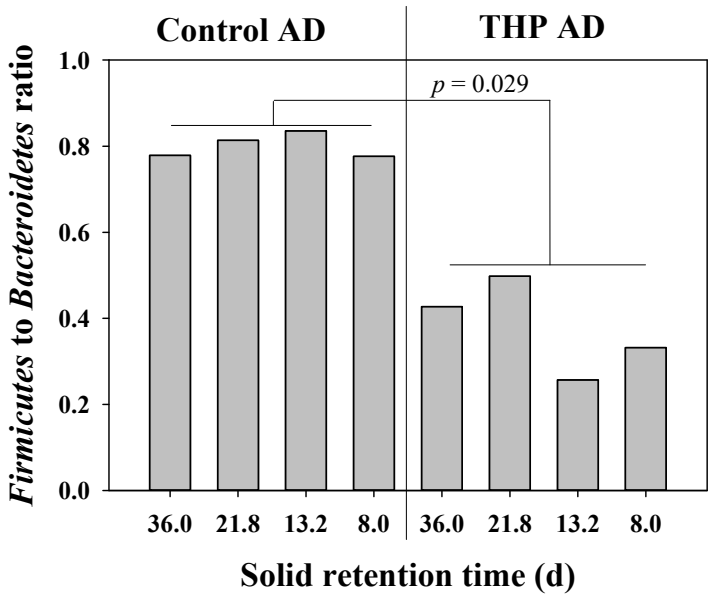

Figure 4.7 Effect of SRT and THP on the *Firmicutes* to *Bacteroidetes* ratio

Regardless of the SRT conditions, the dominant archaeal genus was *AF424768_g*, which belongs to the phylum *Bathyarchaeota*. In the inoculum, the relative abundances of *Bathyarchaeota* were 5%. Within the methanogenic archaea, the dominant genus in control AD shifted from *Methanosaeta* to *Methanocorpusculum*, *Methanogranum*, and then back to *Methanosaeta* during the period of SRT shortening from 36.0 d to 21.8, 13.2, and 8.0 d. However, in the THP AD, the dominant genus shifted from *Methanogranum* to *Methanosaeta* when the SRT was below 13.2 d. Methanogenesis can be divided into acetoclastic, hydrogenotrophic, and methylotrophic processes, depending on the substrates (Madigan et al., 2018). Acetoclastic methanogens (genera

Methanosarcina and Methanosaeta) use acetic acid, hydrogenotrophic methanogens (orders *Methanobacteriales*, *Methanococcales*, *Methanomicrobiales*, etc.) use H_2 and CO_2, and methylotrophic methanogens (*Methanogranum*, *Methanimicrococcus, Methanomassiliicoccus*, etc.) use methyl compounds such as methanol, methylamines, and methylsulfides (Madigan et al., 2018). Figure 4.8 shows the relative abundance of methanogens. The application of THP increased the relative abundance ratio of methylotrophic methanogens (p = 0.02, paired t−test), by 16%, 28%, and 13% under SRT conditions of 36.0, 21.8, and 13.2 d, respectively. As mentioned above, CM contains large amounts of lignocellulose, which is composed of cellulose, hemicellulose, and lignin. Lignin is a macromolecule composed of methylated alcohols (sinapyl, coniferyl, and p−coumaryl alcohol). The THP treatment was found to promote the hydrolysis of lignin in livestock manure fiber and the degradation by anaerobic digestion (Ahring et al., 2015; Khan & Ahring, 2021a; X. Liu et al., 2020). Hydrolysis by THP increases the accessibility of methylated compounds to microorganisms, resulting in a higher ratio of methylotrophic methanogens in THP AD than in control AD.

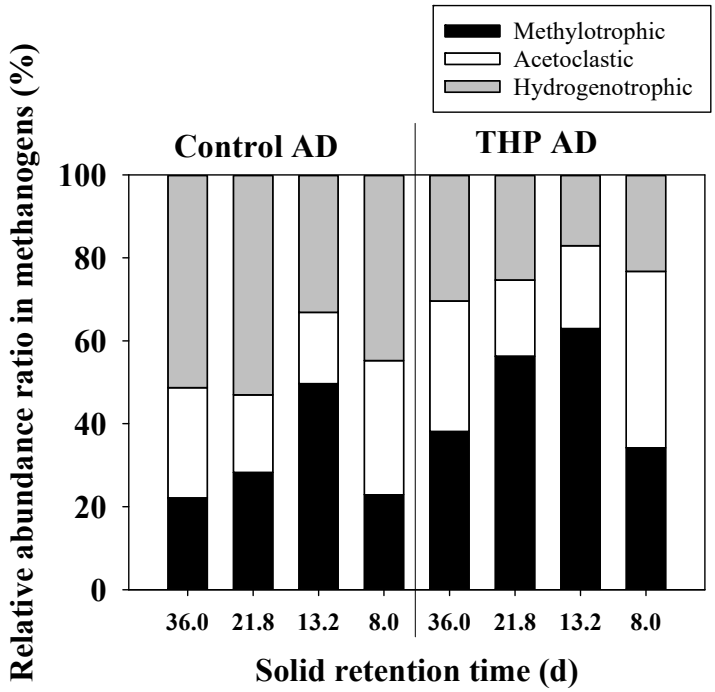

Figure 4.8 Effect of SRT and THP on relative abundance ratio in methanogens

Bathyarchaeota, a non-methanogenic archaeon, was found to dominate all SRT conditions regardless of THP with a relative abundance of at least 66.8% in archaea (Figure 4.9). The phylum *Bathyarchaeota* is usually found in anoxic sediments, and is rarely found in AD (Y. He et al., 2016; Zhou et al., 2018). In the inoculum, the relative abundances of *Bathyarchaeota* were 5%, while they were not detected in the intact CM samples. Low relative abundances of *Bathyarchaeota* have been reported in AD, such as 31% in the co-digestion of CM and corn stover (Y. Li et al., 2020; H. Wang et al., 2020). *Bathyarchaeota* are capable of hydrolysis, acidogenesis, and

acetogenesis and can coexist with methanogens through a syntrophic relationship for methane production (Evans et al., 2015; Maus et al., 2018; Zhou et al., 2018).

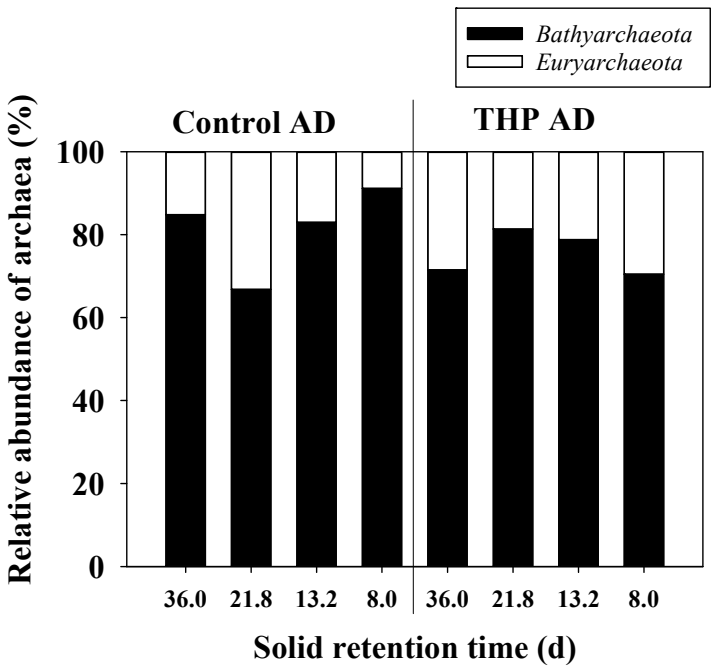

Figure 4.9 Effect of SRT and THP on relative abundance of archaea in phylum level

Figure 4.10

shows an NMDS plot of bacteria and archaea at the genus level. Both bacteria and archaea showed distinct differences in the microbial communities depending on the application of THP. This difference may be because more biodegradable organics were supplied by THP, which resulted in the selective pressure of microbial changes (Lu et al., 2018; L. Zhang et al., 2021). In bacteria

[Figure 4.10 (a)], the relative abundances of *Proteiniphilum*, *Paludibacter*, and *EF5860320_g* increased, whereas the relative abundances of *Cloacamonas*, and *Clostridium_g13* decreased when THP was applied. *Proteiniphilum* and *Paludibacter* are capable of acidogenesis by utilizing sugars and peptones (S. Chen & Dong, 2005; Ueki et al., 2006). In the archaea [Figure 4.10 (b)), the relative abundances of *Methanimicrococcus*, *Methanosaeta*, *Methanogranum*, and *Methanobacterium* increased, whereas the relative abundance of *Methanobrevibacter* decreased after applying THP. A decrease in SRT resulted in a similar shift in the bacterial and archaeal communities in both the control AD and THP AD. In terms of bacteria [Figure 4.10 (a)], the relative abundances of *AC16063_g* and *Clostridium_g13* increased, whereas the relative abundance of *BBZD_g* decreased with decreasing SRT. Among the archaea, the relative abundances of *Methanimicrococcus*, and *AF424768_g* increased, whereas the relative abundances of *Methanogranum*, *Methanobacterium*, *AF424775_g*, and *Methanobrevibacter* decreased with decreasing SRT. A positive correlation between high SRT conditions and AD performance, as indicated by the high methane yield and VS removal, was confirmed ($p < 0.05$). In contrast, a low SRT had a strong positive correlation with potential inhibitors of methanogens, such as high VFA and low pH ($p < 0.05$).

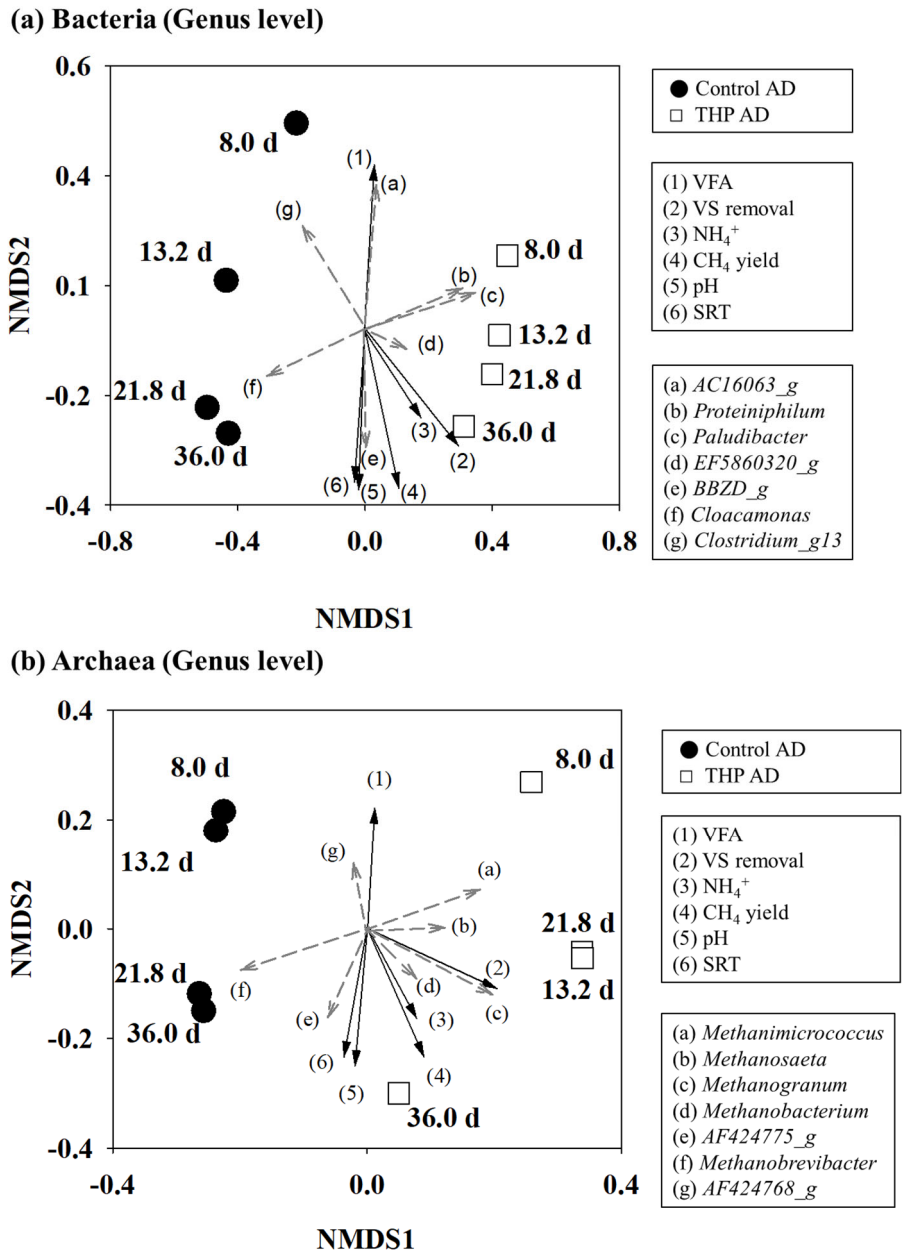

Figure 4.10 Non-metric multidimensional scaling (NMDS) plot of bacteria (a), and archaea (b) (Significant correlations ($p < 0.05$) with environmental parameters are shown as arrows, and arrow length represents the strength of the correlation)

4.4 Summary

The performance and stability of AD of CM in relation to the application of THP and variations in SRT was investigated. When THP is applied to the AD of CM, it is possible to reduce the SRT from 36.0 to 13.2 d without a reduction in performance, enabling stable operation for three SRT cycles. However, reducing the SRT of THP AD from 36.0 to 13.2 d led to a decrease in reactor stability caused by an increase in the concentration of VFA from 165 to 613 mg/L and changes in the microbial community structure to an inefficient state in terms of AD performances. Furthermore, regardless of the THP, sharp decline of methane production was observed under an SRT of 8.0 d.

References

Ahring, B. K., Biswas, R., Ahamed, A., Teller, P. J., & Uellendahl, H. 2015. Making lignin accessible for anaerobic digestion by wet-explosion pretreatment. *Bioresource Technology*, *175*, 182–188.

APHA. 2012. *Standard methods for the examination of water and wastewater*. American public health association, Washington, DC.

Björnsson, L., Mattiasson, B., & Henrysson, T. 1997. Effects of support material on the pattern of volatile fatty acid accumulation at overload in anaerobic digestion of semi-solid waste. *Applied Microbiology and Biotechnology*, *47*, 640–644.

Carrère, H., Dumas, C., Battimelli, A., Batstone, D. J., Delgenès, J. P., Steyer, J. P., & Ferrer, I. 2010. Pretreatment methods to improve sludge anaerobic degradability: A review. *Journal of Hazardous Materials*, *183*(1–3), 1–15.

Cayetano, R. D. A., Kim, G. B., Park, J. H., Kumar, G., & Kim, S. H. 2020. Waste activated sludge treatment in an anaerobic dynamic membrane bioreactor at varying hydraulic retention time: Performance monitoring and microbial community analysis. *International Journal of Energy Research*, *44*(15), 12485–12495.

Cayetano, R. D. A., Park, J., Kim, G. B., Jung, J. H., & Kim, S. H. 2021. Enhanced anaerobic digestion of waste-activated sludge via bioaugmentation strategy—Phylogenetic investigation of communities by reconstruction of unobserved states (PICRUSt2) analysis through hydrolytic enzymes and possible linkage to system performance. *Bioresource Technology*, *332*, 125014.

Chen, S., Cheng, H., Wyckoff, K. N., & He, Q. 2016. Linkages of Firmicutes and Bacteroidetes populations to methanogenic process performance. *Journal of Industrial Microbiology and Biotechnology*, *43*(6), 771–781.

Chen, S., & Dong, X. 2005. Proteiniphilum acetatigenes gen. nov., sp. nov., from a UASB reactor treating brewery wastewater. *International Journal of Systematic and Evolutionary Microbiology*, *55*(6), 2257–2261.

Devos, P., Haddad, M., & Carrère, H. 2021. Thermal Hydrolysis of Municipal Sludge: Finding the Temperature Sweet Spot: A Review. *Waste and Biomass Valorization*, *12*(5), 2187–2205.

Evans, P. N., Parks, D. H., Chadwick, G. L., Robbins, S. J., Orphan, V. J., Golding, S. D., & Tyson, G. W. 2015. Methane metabolism in the archaeal phylum Bathyarchaeota revealed by genome-centric metagenomics. *Science*, *350*(6259), 434–438.

He, Y., Li, M., Perumal, V., Feng, X., Fang, J., Xie, J., Sievert, S. M., & Wang, F. 2016. Genomic and enzymatic evidence for acetogenesis among multiple lineages of the archaeal phylum Bathyarchaeota widespread in marine sediments. *Nature Microbiology*, *1*(6), 1–9.

Henderson, C. 1973. The effects of fatty acids on pure cultures of rumen bacteria. *The Journal of Agricultural Science*, *81*(1), 107–112.

Hernández, M. A., Rodríguez Susa, M., & Andres, Y. 2014. Use of coffee mucilage as a new substrate for hydrogen production in anaerobic co-digestion with swine manure. *Bioresource*

Technology, *168*, 112–118.

Huang, W., Zhao, Z., Yuan, T., Huang, W., Lei, Z., & Zhang, Z. 2017. Low-temperature hydrothermal pretreatment followed by dry anaerobic digestion: A sustainable strategy for manure waste management regarding energy recovery and nutrients availability. *Waste Management*, *70*, 255–262.

Khan, M. U., & Ahring, B. K. 2020. Anaerobic Digestion of Digested Manure Fibers: Influence of Thermal and Alkaline Thermal Pretreatment on the Biogas Yield. *Bioenergy Research*.

Koyama, M., Yamamoto, S., Ishikawa, K., Ban, S., & Toda, T. 2017. Inhibition of anaerobic digestion by dissolved lignin derived from alkaline pre-treatment of an aquatic macrophyte. *Chemical Engineering Journal*, *311*, 55–62.

Lee, C., Ju, M., Lee, J., Kim, S., & Kim, J. Y. 2022. Long-Term Inhibition of Chlortetracycline Antibiotics on Anaerobic Digestion of Swine Manure. *SSRN Electronic Journal*, *326*(PB), 116802.

Lee, I. S., Parameswaran, P., & Rittmann, B. E. 2011. Effects of solids retention time on methanogenesis in anaerobic digestion of thickened mixed sludge. *Bioresource Technology*, *102*(22), 10266–10272.

Lee, J., & Park, K. Y. 2020. Impact of hydrothermal pretreatment on anaerobic digestion efficiency for lignocellulosic biomass: Influence of pretreatment temperature on the formation of biomass-degrading byproducts. *Chemosphere*, *256*, 127116.

Li, Y. Q., Liu, C. M., Wachemo, A. C., & Li, X. J. 2018. Effects of liquid fraction of digestate recirculation on system performance and

microbial community structure during serial anaerobic digestion of completely stirred tank reactors for corn stover. *Energy*, *160*, 309–317.

Li, Y., Zhao, J., Achinas, S., Zhang, Z., Krooneman, J., & Euverink, G. J. W. 2020. The biomethanation of cow manure in a continuous anaerobic digester can be boosted via a bioaugmentation culture containing Bathyarchaeota. *Science of the Total Environment*, *745*, 141042.

Liu, X., Lee, C., & Kim, J. Y. 2020. Thermal hydrolysis pre-treatment combined with anaerobic digestion for energy recovery from organic wastes. *Journal of Material Cycles and Waste Management, 22*, 1370-1381.

Lu, D., Sun, F., & Zhou, Y. 2018. Insights into anaerobic transformation of key dissolved organic matters produced by thermal hydrolysis sludge pretreatment. *Bioresource Technology*, *266*, 60–67.

Madigan, M. T., Bender, K. S., Buckley, D. H., Sattley, W. M., & Stahl, D. A. 2018. Brock Biology of Microorganisms. 15th Global Edition. *Boston, US: Benjamin Cummins*, *1*, 1391–1407.

Maus, I., Rumming, M., Bergmann, I., Heeg, K., Pohl, M., Nettmann, E., Jaenicke, S., Blom, J., Pühler, A., Schlüter, A., Sczyrba, A., & Klocke, M. 2018. Characterization of Bathyarchaeota genomes assembled from metagenomes of biofilms residing in mesophilic and thermophilic biogas reactors. *Biotechnology for Biofuels*, *11*(1), 167.

Miron, Y., van Lier, J. B., & Lettinga, G. 2000. The role of sludge

retention time in the hydrolysis and acidification of lipids, carbohydrates and proteins during digestion of primary sludge in CSTR systems. *Water Research*, *34*(5), 1705–1713.

Muhammad Nasir, I., & Mohd Ghazi, T. idaty. 2015. Pretreatment of lignocellulosic biomass from animal manure as a means of enhancing biogas production. *Engineering in Life Sciences*, *15*(7), 733–742.

Nagao, N., Tajima, N., Kawai, M., Niwa, C., Kurosawa, N., Matsuyama, T., Yusoff, F. M., & Toda, T. 2012. Maximum organic loading rate for the single-stage wet anaerobic digestion of food waste. *Bioresource Technology*, *118*, 210–218.

Orlando, M. Q., & Borja, V. M. 2020. Pretreatment of animal manure biomass to improve biogas production: A review. *Energies*, *13*(14), 3573.

Rittmann, B. E., & McCarty, P. L. 2001. *Environmental biotechnology: principles and applications*. McGraw-Hill Education.

Russell, J. B., & Dombrowski, D. B. 1980. Effect of pH on the efficiency of growth by pure cultures of rumen bacteria in continuous culture. *Applied and Environmental Microbiology*, *39*(3), 604–610.

Schmidt, T., Ziganshin, A. M., Nikolausz, M., Scholwin, F., Nelles, M., Kleinsteuber, S., & Pröter, J. 2014. Effects of the reduction of the hydraulic retention time to 1.5 days at constant organic loading in CSTR, ASBR, and fixed-bed reactors – Performance and methanogenic community composition. *Biomass and Bioenergy*, *69*, 241–248.

Shi, X., Lin, J., Zuo, J., Li, P., Li, X., & Guo, X. 2017. Effects of free ammonia on volatile fatty acid accumulation and process performance in the anaerobic digestion of two typical bio-wastes. *Journal of Environmental Sciences (China)*, *55*, 49–57.

Steinmetz, R. L. R., Mezzari, M. P., da Silva, M. L. B., Kunz, A., do Amaral, A. C., Tápparo, D. C., & Soares, H. M. 2016. Enrichment and acclimation of an anaerobic mesophilic microorganism's inoculum for standardization of BMP assays. *Bioresource Technology*, *219*, 21–28.

Tsapekos, P., Kougias, P. G., Frison, A., Raga, R., & Angelidaki, I. 2016. Improving methane production from digested manure biofibers by mechanical and thermal alkaline pretreatment. *Bioresource Technology*, *216*, 545–552.

Ueki, A., Akasaka, H., Suzuki, D., & Ueki, K. 2006. Paludibacter propionicigenes gen. nov., sp. nov., a novel strictly anaerobic, Gram-negative, propionate-producing bacterium isolated from plant residue in irrigated rice-field soil in Japan. *International Journal of Systematic and Evolutionary Microbiology*, *56*(1), 39–44.

Wainaina, S., Lukitawesa, Kumar Awasthi, M., & Taherzadeh, M. J. 2019. Bioengineering of anaerobic digestion for volatile fatty acids, hydrogen or methane production: A critical review. *Bioengineered*, *10*(1), 437–458.

Wandera, S. M., Westerholm, M., Qiao, W., Yin, D., Jiang, M. M., & Dong, R. 2019. The correlation of methanogenic communities' dynamics and process performance of anaerobic digestion of

thermal hydrolyzed sludge at short hydraulic retention times. *Bioresource Technology*, *272*, 180–187.

Wang, H., Li, J., Zhao, Y., Xu, C., Zhang, K., Li, J., Yan, L., Gu, J. D., Wei, D., & Wang, W. 2020. Establishing practical strategies to run high loading corn stover anaerobic digestion: Methane production performance and microbial responses. *Bioresource Technology*, *310*, 123364.

Wang, L., Zhou, Q., & Li, F. T. 2006. Avoiding propionic acid accumulation in the anaerobic process for biohydrogen production. *Biomass and Bioenergy*, *30*(2), 177–182.

Wu, D., Li, L., Zhen, F., Liu, H., Xiao, F., Sun, Y., Peng, X., Li, Y., & Wang, X. 2022. Thermodynamics of volatile fatty acid degradation during anaerobic digestion under organic overload stress: The potential to better identify process stability. *Water Research*, *214*.

Xue, Y., Liu, H., Chen, S., Dichtl, N., Dai, X., & Li, N. 2015. Effects of thermal hydrolysis on organic matter solubilization and anaerobic digestion of high solid sludge. *Chemical Engineering Journal*, *264*, 174–180.

Yang, Y., Yang, F., Huang, W., Huang, W., Li, F., Lei, Z., & Zhang, Z. 2018. Enhanced anaerobic digestion of ammonia-rich swine manure by zero-valent iron: With special focus on the enhancement effect on hydrogenotrophic methanogenesis activity. *Bioresource Technology*, *270*, 172–179.

Zhang, L., Gong, X., Wang, L., Guo, K., Cao, S., & Zhou, Y. 2021. Metagenomic insights into the effect of thermal hydrolysis pre-treatment on microbial community of an anaerobic digestion

system. *Science of the Total Environment*, *791*, 148096.

Zhang, L., Guo, K., Wang, L., Xu, R., Lu, D., & Zhou, Y. 2022. Effect of sludge retention time on microbial succession and assembly in thermal hydrolysis pretreated sludge digesters: Deterministic versus stochastic processes. *Water Research*, *209*, 117900.

Zhou, Z., Pan, J., Wang, F., Gu, J. D., & Li, M. 2018. Bathyarchaeota: Globally distributed metabolic generalists in anoxic environments. *FEMS Microbiology Reviews*, *42*(5), 639–655.

Chapter 5
Enhancement of ADM1 to incorporate changes in biochemical parameters resulting from variations in solid retention time

5.1 Introduction

Process modeling is essential for gaining a comprehensive understanding of complex systems, optimizing operations, supporting decision-making, and troubleshooting. Since the late 1960s, there have been numerous dynamic models developed for the simulation of characteristic variables of the ADM process (Angelidaki et al., 1999; Costello et al., 1991; Kalyuzhnyi & Fedorovich, 1998; Siegrist et al., 1993; Vavilin et al., 1997). The International Water Association developed Anaerobic Digestion Model No 1 (ADM1) in 2002 as a mathematical model that describes the biochemical and chemical processes that occur during AD (Batstone et al., 2002). The ADM1 is a dynamic model that considers the interaction between different microorganisms, substrates, and environmental factors that influence the anaerobic digestion process (Donoso-Bravo et al., 2011). The Model is divided into several compartments, each representing a specific biochemical reaction or microbial group involved in the process. Reactions are constructed based on the first-order kinetic for hydrolysis and the Monod equation for substrate uptake of

microorganisms. Reactions are made based on the compounds, not microorganisms. So, all microorganisms that metabolize the same compound are represented by a single biochemical parameter. Dozens of microbial species participate in AD, and multiple types of microorganisms can participate in the metabolism of the same substrate (Madigan et al., 2018). For example, various microorganisms (eg., *Pelotomaculum sp., Cryptanaerobacter sp., Cloacamonas sp.*) are involved in the degradation of propionate to acetate (Ahlert et al., 2016; Peces et al., 2021; Wu et al., 2022). Each microorganism has a unique set of characteristics that result in different substrate uptake rates and half-saturation constants, resulting in different growth rates. Numerous studies have demonstrated that alterations in the environmental variables of a reactor can lead to shifts in microbial communities, resulting in changes in the reactor's biokinetics (S. Kim et al., 2023; C. Lee et al., 2023; Ziels et al., 2017). In other words, as the microbial composition changes, substrate uptake rates and half-saturation rates may also be affected. The activity rate of three metabolic steps (hydrolysis, acetogenesis, methanogenesis) in anaerobic digestion was changed with SRT changes (Peces et al., 2021). However, the existing models do not reflect the biokinetic changes because they use the same biochemical parameter set for different conditions after the parameter calibration step. This means that the accuracy of the model

can decrease as the increase of distance from the initial parameter optimization conditions. Simulation results using the ADM1 calibrated with pig manure data at SRT condition of 35 d revealed an increasing prediction error of 4 and 8% for methane production under SRT conditions of 23.3 and 17.5 d, respectively (H. Li et al., 2020). Modeling the AD process by incorporating environmental changes, specifically, SRT, allows for more precise optimization of operational factors, process design, and overall performance improvement. Hence, it is necessary to develop a model capable of accurately capturing the changes in biochemical parameters that occur due to variations in SRT.

This chapter aims to enhance ADM1 to incorporate changes in biochemical parameters resulting from variations in SRT. In order to achieve this, four continuously stirred tank reactors were operated under three different SRT conditions. The biochemical parameters were optimized for these operational conditions, and a regression equation was applied to estimate biochemical parameters for other SRT conditions.

5.2 Materials and methods

5.2.1 Model development

The fundamental structure of the model was based on that presented by IWA (Batstone et al., 2002). However, the initial model is based on the concentration of chemical oxygen demand (COD). It was converted into a mass-based concentration using theoretical COD of the substrates and chemical stoichiometry (Weinrich et al., 2021; Weinrich & Nelles, 2021b). Symbols, and indices used in ADM1 are summarized in Table 5.1, and Table 5.2. The model maintains a mass balance between various microbial communities that interact with a heterogenous substrate within the reactor boundaries (Eq. 5.1, and 5.2).

$$\frac{dS_i}{dt} = \frac{Q}{V_{liq}}\left(S_{in,i} - S_i\right) + \sum_{j=1}^{28} \rho_j \upsilon_{i,j} \qquad \text{Eq. 5.1}$$

$$\frac{dX_i}{dt} = \frac{Q}{V_{liq}}\left(X_{in,i} - X_i\right) + \sum_{j=1}^{28} \rho_j \upsilon_{i,j} \qquad \text{Eq. 5.2}$$

Solutions were obtained for the differential equations that describe the rates of substrate consumption, metabolite production, and the growth of the microbial groups specified in the ADM1 structure (Table 5.3). Inhibition and algebraic equations, and reference biochemical parameters are summarized in Table 5.4, and Table 5.5. The equations were solved using the fourth-order Runge Kutta method implemented in MATLAB R2022b (MathWorks Inc., MA, USA).

Table 5.1 Symbols and used in ADM1

Symbols	Definition	Unit
I	Inhibition function	–
k	First–order rate constant	d^{-1}
K_a	Dissociation constant (acid)	mol/L
k_{AB}	Kinetic dissociation rate (acid/base)	L/mol/d
K_H	Henry's law constant	mol/L/bar
K_I	Inhibition constant	g/L
k_{La}	Volumetric mass transfer coefficient	d^{-1}
k_m	Maximum uptake rate	g/g/d
K_s	Half–saturation constant	g/L
K_W	Ionic product	mol/L
p	Pressure	
ρ	Process kinetic rate	g/L/d
pK_a	Negative logarithmic dissociation constant	–
pH_{LL}, pH_{LL}	Lower and upper pH limit	–
q	Volume flow	L/d
R	Ideal gas constant	bar/L/mol/K
S	Soluble component	g/L
T	Temperature	K
v	Stoichiometric coefficient	–
V	Volume	L
X	Particulate component	g/L
Y	Biomass yield coefficient	g/g
μ_m	Maximum growth rate	d^{-1}

Table 5.2 Indices used in ADM1

Indices	Definition	Indices	Definition
aa	Amino acids	*h2*	Hydrogen
ac	Acetic acid	*hyd*	Hydrolysis
an^-	Anions	*I*	inerts
atm	Atmosphere	*IC*	Inorganic carbon
bac	Microorganisms	*IN*	Inorganic nitrogen
bu	Butyric acid	*li*	Lipids
c4	Valeric acid	*liq*	Liquid phase
cat^+	Cations	*pr*	Proteins
ch	Carbohydrates	*pro*	Propionic acid
ch4	Methane	*sI*	Soluble inerts
co2	Carbon dioxide	*su*	Sugars
dec	Decay	*va*	Valeric acid
dis	Disintegration	*X*	Microorganisms
fa	Long-chain fatty acid	*xc*	Particulate composites
gas	Gas phase	*xl*	Particulate inerts

Table 5.3 Petersen matric of the mass−based ADM1

Component (i) → Process (j) ↓	1 S_{su}	2 S_{aa}	3 S_{fa}	4 S_{va}	5 S_{bu}	6 S_{pro}	7 S_{ac}	8 S_{h2}	Process rate (ρ)
1 Hydrolysis X_{ch}	1.11								$k_{ch}X_{ch}$
2 Hydrolysis X_{pr}		1							$k_{pr}X_{pr}$
3 Hydrolysis X_{li}	0.135		0.951						$k_{li}X_{li}$
4 Acidogenesis S_{su}	−13.272				0.911	2.734	4.898	0.305	$\mu_{m,su}\frac{S_{su}}{K_{S,su}+S_{su}}X_{su}I_{su}$
5 Acidogenesis S_{aa}		−11.567		1.837	2.329	0.538	6.105	0.123	$\mu_{m,aa}\frac{S_{aa}}{K_{S,aa}+S_{aa}}X_{aa}I_{aa}$
6 Acidogenesis S_{fa}			−8.214				14.555	0.838	$\mu_{m,fa}\frac{S_{fa}}{K_{S,fa}+S_{fa}}X_{su}I_{fa}$
7 Acetogenesis S_{va}				−11.576		7.915	6.446	0.419	$\mu_{m,va}\frac{S_{va}}{K_{S,va}+S_{va}}\frac{X_{va}S_{va}}{S_{va}+S_{bu}}I_{va}$
8 Acetogenesis S_{bu}					−12.982		16.635	0.558	$\mu_{m,bu}\frac{S_{bu}}{K_{S,bu}+S_{bu}}\frac{X_{bu}S_{bu}}{S_{bu}+S_{va}}I_{va}$
9 Acetogenesis S_{pro}							18.157	1.839	$\mu_{m,pro}\frac{S_{pro}}{K_{S,pro}+S_{pro}}X_{pro}I_{pro}$
10 Methanogenesis S_{ac}							−26.545		$\mu_{m,ac}\frac{S_{ac}}{K_{S,ac}+S_{ac}}X_{ac}I_{ac}$
11 Methanogenesis S_{h2}								−2.970	$\mu_{m,h2}\frac{S_{h2}}{K_{S,h2}+S_{h2}}X_{h2}I_{h2}$
12 Decay X_{su}									$k_{dec}X_{su}$
13 Decay X_{aa}									$k_{dec}X_{aa}$
14 Decay X_{fa}									$k_{dec}X_{fa}$
15 Decay X_{va}									$k_{dec}X_{va}$
16 Decay X_{bu}									$k_{dec}X_{bu}$
17 Decay X_{pro}									$k_{dec}X_{pro}$
18 Decay X_{ac}									$k_{dec}X_{ac}$
19 Decay X_{h2}									$k_{dec}X_{h2}$

Table 5.3 Petersen matric of the mass-based ADM1 (continued)

Component (i) → / Process (j) ↓	9 S_{ch4}	10 S_{IC}	11 S_{IN}	12 S_{h2o}	13 X_{ch}	14 X_{pr}	15 X_{li}	Process rate (ρ)
1 Hydrolysis X_{ch}				−0.111	−1			$k_{ch}X_{ch}$
2 Hydrolysis X_{pr}						−1		$k_{pr}X_{pr}$
3 Hydrolysis X_{li}		−0.0293		−0.0566			−1	$k_{li}X_{li}$
4 Acidogenesis S_{su}		4.4571	−0.1506	−0.4211				$\mu_{m,su}\frac{S_{su}}{K_{S,su}+S_{su}}X_{su}I_{su}$
5 Acidogenesis S_{aa}		2.8335	2.1033	−5.3026				$\mu_{m,aa}\frac{S_{aa}}{K_{S,aa}+S_{aa}}X_{aa}I_{aa}$
6 Acidogenesis S_{fa}		−0.7246	−0.1506	−7.3043				$\mu_{m,fa}\frac{S_{fa}}{K_{S,fa}+S_{fa}}X_{su}I_{fa}$
7 Acetogenesis S_{va}		−0.5594	−0.1506	−3.4940				$\mu_{m,va}\frac{S_{va}}{K_{S,va}+S_{va}}\frac{X_{va}S_{va}}{S_{va}+S_{bu}}I_{va}$
8 Acetogenesis S_{bu}		−0.3891	−0.1506	−4.6718				$\mu_{m,bu}\frac{S_{bu}}{K_{S,bu}+S_{bu}}\frac{X_{bu}S_{bu}}{S_{bu}+S_{va}}I_{va}$
9 Acetogenesis S_{pro}		13.1283	−0.1506	−10.5843				$\mu_{m,pro}\frac{S_{pro}}{K_{S,pro}+S_{pro}}X_{pro}I_{pro}$
10 Methanogenesis S_{ac}	6.737	18.4808	−0.1506	0.4778				$\mu_{m,ac}\frac{S_{ac}}{K_{S,ac}+S_{ac}}X_{ac}I_{ac}$
11 Methanogenesis S_{h2}	5.555	−17.1839	−0.1506	13.7499				$\mu_{m,h2}\frac{S_{h2}}{K_{S,h2}+S_{h2}}X_{h2}I_{h2}$
12 Decay X_{su}					0.18	0.77	0.05	$k_{dec}X_{su}$
13 Decay X_{aa}					0.18	0.77	0.05	$k_{dec}X_{aa}$
14 Decay X_{fa}					0.18	0.77	0.05	$k_{dec}X_{fa}$
15 Decay X_{va}					0.18	0.77	0.05	$k_{dec}X_{va}$
16 Decay X_{bu}					0.18	0.77	0.05	$k_{dec}X_{bu}$
17 Decay X_{pro}					0.18	0.77	0.05	$k_{dec}X_{pro}$
18 Decay X_{ac}					0.18	0.77	0.05	$k_{dec}X_{ac}$
19 Decay X_{h2}					0.18	0.77	0.05	$k_{dec}X_{h2}$

Table 5.3 Petersen matric of the mass-based ADM1 (continued)

Component (i) → Process (j) ↓	16 X_{su}	17 X_{aa}	18 X_{fa}	19 X_{va}	20 X_{bu}	21 X_{pro}	22 X_{ac}	23 X_{h2}	Process rate (ρ)
1 Hydrolysis X_{ch}									$k_{ch}X_{ch}$
2 Hydrolysis X_{pr}									$k_{pr}X_{pr}$
3 Hydrolysis X_{li}									$k_{li}X_{li}$
4 Acidogenesis S_{su}	1								$\mu_{m,su}\frac{S_{su}}{K_{S,su}+S_{su}}X_{su}I_{su}$
5 Acidogenesis S_{aa}		1							$\mu_{m,aa}\frac{S_{aa}}{K_{S,aa}+S_{aa}}X_{aa}I_{aa}$
6 Acidogenesis S_{fa}			1						$\mu_{m,fa}\frac{S_{fa}}{K_{S,fa}+S_{fa}}X_{su}I_{fa}$
7 Acetogenesis S_{va}				1					$\mu_{m,va}\frac{S_{va}}{K_{S,va}+S_{va}}\frac{X_{va}S_{va}}{S_{va}+S_{bu}}I_{va}$
8 Acetogenesis S_{bu}					1				$\mu_{m,bu}\frac{S_{bu}}{K_{S,bu}+S_{bu}}\frac{X_{bu}S_{bu}}{S_{bu}+S_{va}}I_{va}$
9 Acetogenesis S_{pro}						1			$\mu_{m,pro}\frac{S_{pro}}{K_{S,pro}+S_{pro}}X_{pro}I_{pro}$
10 Methanogenesis S_{ac}							1		$\mu_{m,ac}\frac{S_{ac}}{K_{S,ac}+S_{ac}}X_{ac}I_{ac}$
11 Methanogenesis S_{h2}								1	$\mu_{m,h2}\frac{S_{h2}}{K_{S,h2}+S_{h2}}X_{h2}I_{h2}$
12 Decay X_{su}	−1								$k_{dec}X_{su}$
13 Decay X_{aa}		−1							$k_{dec}X_{aa}$
14 Decay X_{fa}			−1						$k_{dec}X_{fa}$
15 Decay X_{va}				−1					$k_{dec}X_{va}$
16 Decay X_{bu}					−1				$k_{dec}X_{bu}$
17 Decay X_{pro}						−1			$k_{dec}X_{pro}$
18 Decay X_{ac}							−1		$k_{dec}X_{ac}$
19 Decay X_{h2}								−1	$k_{dec}X_{h2}$

Table 5.3 Petersen matric of the mass-based ADM1 (continued)

Component (i) → Process (j) ↓	8 S_{H2}	9 S_{CH4}	10 S_{IC}	24 S_{va-}	25 S_{bu-}	26 S_{pro-}	27 S_{ac-}	28 S_{hco3}	29 S_{nh3}	30 $S_{gas,h2}$	31 $S_{gas,ch4}$	32 $S_{gas,co2}$	Process rate (ρ)
20 Dissociation S_{va}				−1									$K_{AB,va}[S_{va-}(K_{a,va}+S_{H+})-K_{a,va}S_{va}]$
21 Dissociation S_{bu}					−1								$K_{AB,bu}[S_{bu-}(K_{a,bu}+S_{H+})-K_{a,bu}S_{bu}]$
22 Dissociation S_{pro}						−1							$K_{AB,pro}[S_{pro-}(K_{a,pro}+S_{H+})-K_{a,pro}S_{pro}]$
23 Dissociation S_{ac}							−1						$K_{AB,ac}[S_{ac-}(K_{a,ac}+S_{H+})-K_{a,ac}S_{ac}]$
24 Dissociation S_{IC}								−1					$K_{AB,co2}[S_{co3-}(K_{a,co2}+S_{H+})-K_{a,co2}S_{IC}]$
25 Dissociation S_{IN}									−1				$K_{AB,IN}[S_{nh3}(K_{a,IN}+S_{H+})-K_{a,IN}S_{IN}]$
26 Transition S_{h2}	−1									$\frac{V_{liq}}{V_{gas}}$			$K_{La}(S_{h2}-2K_{H,h2}P_{h2})$
27 Transition S_{ch4}		−1									$\frac{V_{liq}}{V_{gas}}$		$K_{La}(S_{ch4}-16K_{H,ch4}P_{ch4})$
28 Transition S_{co2}			−1									$\frac{V_{liq}}{V_{gas}}$	$K_{La}(S_{co2}-44K_{H,co22}P_{co2})$

Table 5.4 Inhibition and algebraic equations

Inhibition equation		
$I_{su} = I_{aa} = I_{pH,aa} I_{IN,lim}$	$I_{ac} = I_{pH,ac} I_{IN,lim} I_{nh3}$	
$I_{pro} = I_{pH,aa} I_{IN,lim} I_{h2,pro}$	$I_{va} = I_{bu} = I_{pH,aa} I_{IN,lim} I_{h2,c4}$	
$I_{fa} = I_{pH,aa} I_{IN,lim} I_{h2,fa}$	$I_{h2} = I_{pH,h2} I_{IN,lim}$	
$I_{IN,lim} = \frac{S_{IN}}{S_{IN} + K_{S,IN}}$	$I_{nh3} = \frac{K_{I,nh3}}{K_{I,nh3} + S_{nh3}}$	
$I_{H2,pro} = \frac{K_{I,h2,pro}}{K_{I,h2,pro} + S_{h2}}$	$I_{h2,c4} = \frac{K_{I,h2,c4}}{K_{I,h2,c4} + S_{h2}}$	
$I_{h2,fa} = \frac{K_{I,h2,fa}}{K_{I,h2,fa} + S_{h2}}$		
$I_{pH,aa} = \frac{K_{pH,aa}^{n_{aa}}}{K_{pH,aa}^{n_{aa}} + S_{H+}^{n_{aa}}}$	$n_{aa} = \frac{3}{pH_{UL,aa} - pH_{LL,aa}}$	$K_{pH,aa} = 10^{-\frac{pH_{UL,aa} + pH_{LL,aa}}{2}}$
$I_{pH,ac} = \frac{K_{pH,ac}^{n_{ac}}}{K_{pH,ac}^{n_{ac}} + S_{H+}^{n_{ac}}}$	$n_{ac} = \frac{3}{pH_{UL,ac} - pH_{LL,ac}}$	$K_{pH,ac} = 10^{-\frac{pH_{UL,ac} + pH_{LL,ac}}{2}}$
$I_{pH,h2} = \frac{K_{pH,h2}^{n_{h2}}}{K_{pH,aa}^{n_{h2}} + S_{H+}^{n_{h2}}}$	$n_{h2} = \frac{3}{pH_{UL,h2} - pH_{LL,h2}}$	$K_{pH,h2} = 10^{-\frac{pH_{UL,h2} + pH_{LL,h2}}{2}}$
Algebraic equation		
$S_{nh4+} = S_{IN} - S_{nh3}$	$S_{co2} = S_{IC} - S_{hco3-}$	
$\emptyset = S_{cat+} + \frac{S_{nh4+}}{17} - \frac{S_{hco3-}}{44} - \frac{S_{ac-}}{60} + \frac{S_{pro-}}{74} - \frac{S_{bu-}}{88} - \frac{S_{va-}}{102} - S_{an-}$		
$S_{H+} = -\frac{\emptyset}{2} + \frac{1}{2}\sqrt{\emptyset^2 + 4K_W}$	$pH = -\log_{10} S_{H+}$	
$P_{ch4} = S_{gas,ch4} \frac{RT}{2}$	$P_{co2} = S_{gas,co2} \frac{RT}{44}$	
$P_{h2} = S_{gas,h2} \frac{RT}{2}$	$P_{gas} = P_{ch4} + P_{co2} + P_{h2} + P_{h2o}$	
$q_{gas} = k_p(p_{gas} - p_{atm}) \frac{p_{gas}}{p_{atm}}$		

Table 5.5 Biochemical parameters of ADM1 in COD basis and mass basis

COD basis [a]			Mass basis [b]		
Hydrolysis rate constants			Hydrolysis rate constants		
$k_{c,h}$	10	d^{-1}	$k_{c,h}$	0.25	d^{-1}
k_{li}	10	d^{-1}	k_{li}	0.1	d^{-1}
k_{pro}	10	d^{-1}	k_{pro}	0.2	d^{-1}
Maximum uptake rates			Maximum growth rates [c]		
$k_{m,su}$	30	gCOD/gCOD/d	$\mu_{m,su}$	3	g/g/d
$k_{m,aa}$	50	gCOD/gCOD/d	$\mu_{m,aa}$	4	g/g/d
$k_{m,fa}$	6	gCOD/gCOD/d	$\mu_{m,fa}$	0.36	g/g/d
$k_{m,va}$	20	gCOD/gCOD/d	$\mu_{m,va}$	1.2	g/g/d
$k_{m,bu}$	20	gCOD/gCOD/d	$\mu_{m,bu}$	1.2	g/g/d
$k_{m,pro}$	13	gCOD/gCOD/d	$\mu_{m,pro}$	0.52	g/g/d
$k_{m,ac}$	8	gCOD/gCOD/d	$\mu_{m,ac}$	0.4	g/g/d
$k_{m,h2}$	35	gCOD/gCOD/d	$\mu_{m,h2}$	2.1	g/g/d
Half−saturation constants			Half−saturation constants		
$K_{S,su}$	0.5	gCOD/L	$K_{S,su}$	0.47	g/L
$K_{S,aa}$	0.3	gCOD/L	$K_{S,aa}$	0.2	g/L
$K_{S,fa}$	0.4	gCOD/L	$K_{S,fa}$	0.14	g/L
$K_{S,va}$	0.2	gCOD/L	$K_{S,va}$	0.1	g/L
$K_{S,bu}$	0.2	gCOD/L	$K_{S,bu}$	0.11	g/L
$K_{S,pro}$	0.1	gCOD/L	$K_{S,pro}$	0.07	g/L
$K_{S,ac}$	0.15	gCOD/L	$K_{S,ac}$	0.14	g/L
$K_{S,h2}$	7 E−6	gCOD/L	$K_{S,h2}$	8.8 E−7	g/L
Inhibition constants			Inhibition constants		
$K_{S,IN}$	0.0001	mol/L	$K_{S,IN}$	0.0017	g/L
$K_{I,h2,fa}$	$5x10^{-6}$	gCOD/L	$K_{I,h2,fa}$	$6.3\ x10^{-7}$	g/L
$K_{I,h2,c4}$	$1x10^{-5}$	gCOD/L	$K_{I,h2,c4}$	$1.3\ x10^{-6}$	g/L
$K_{I,h2,pro}$	$3.5x10^{-6}$	gCOD/L	$K_{I,h2,pro}$	$4.4\ x10^{-7}$	g/L
$K_{I,nh3}$	0.0018	mol/L	$K_{I,nh3}$	0.0306	g/L

a) Batstone et al., 2002
b) Huete et al., 2006; Weinrich & Nelles, 2021b
c) Calculated from a fixed biomass yield coefficient

5.2.2 Sensitivity analysis

In order to identify the biochemical parameters that significantly affect the model results, sensitivity analysis was performed. Biochemical parameters, including hydrolysis rate, maximum growth rate, and half-saturation constant, were considered, and individual parameters were adjusted to the reference values of ADM1 (Table 5.5). The parameter variations were conducted within a variability range suggested by the literature (Table 5.6).

Table 5.6 Variability of biochemical parameters

Parameter	Variability factor to the reference value [a)]	Parameter	Variability factor to the reference value [a)]
k_{ch}	0.5 – 2	$K_{S,su}$	0.5 – 2
k_{li}	0.3 – 3	$K_{S,aa}$	0.7 – 1.3
k_{pro}	0.5 – 2	$K_{S,fa}$	0.3 – 3
$\mu_{m,su}$	0.5 – 2	$K_{S,va}$	0.3 – 3
$\mu_{m,aa}$	0.5 – 2	$K_{S,bu}$	0.3 – 3
$\mu_{m,fa}$	0.3 – 3	$K_{S,pro}$	0.5 – 2
$\mu_{m,va}$	0.5 – 2	$K_{S,ac}$	0.5 – 2
$\mu_{m,bu}$	0.3 – 3	$K_{S,h2}$	0.5 – 2
$\mu_{m,pro}$	0.5 – 2		
$\mu_{m,ac}$	0.5 – 2		
$\mu_{m,h2}$	0.5 – 2		

a) Sugested by Batstone et al., 2002

Sesntivity index was calculated to quantify the model sensitivity (Eq. 5.3).

$$SI\ (\%) = \frac{|y_{min} - y_0| + |y_{max} - y_0|}{y_0} \times 100\ (\%) \qquad \text{Eq. 5.3}$$

where, SI is the sensitivity index (%), y_{min}, y_0, and y_{max} is the minimum model output, baseline model output, and maximum model output, respectively. The parameters selected through sensitivity analysis were further calibrated.

5.2.3 Parameter calibration and validation

The experimental results were separated based on their SRT conditions. The parameters were calibrated to minimize the objective function, which is the average of mean squared error (MSE) between the observed data and the model simulation results of methane production and VFAs concentration (Eq. 5.4).

$$J_{obj} = \frac{1}{i}\sum_{1}^{i}\left[\frac{1}{n}\sum_{1}^{n}(Y_{obs.} - Y_{sim.})^2\right] \quad \text{Eq. 5.4}$$

where, J_{obj} is the objective function, i is the number of components (methane production, and concentration of VFAs), n is the number of measured data points, $Y_{obs.}$ is the observed data, $Y_{sim.}$ is simulation data. The calibration of the parameters was carried out using the *fmincon* solver with an inter-point algorithm in MATLAB R2022b (MathWorks Inc., MA, USA). In order to prevent getting trapped in local minima, the initial value of the biochemical parameter was iteratively adjusted in 10 steps from the minimum to the maximum value reported in the literature (refer to Table 5.7). Furthermore, the genetic algorithm was also used, and the optimal parameter was selected based on the optimization result with the lowest objective function. The optimization process was conducted using the default tolerance and stopping criteria setting in MATLAB.

Table 5.7 Biochemical parameter of ADM1 in the literature

Substrate	Hydrolysis rate (d^{-1})			Maximum growth rate (g/g/d)							Reference
	k_{ch}	k_{li}	k_{pro}	$\mu_{m,aa}$	$\mu_{m,ac}$	$\mu_{m,bu}$	$\mu_{m,fa}$	$\mu_{m,h2}$	$\mu_{m,pro}$	$\mu_{m,su}$	$\mu_{m,va}$	
Piggery slurry	0.007	–	0.014	–	0.75	–	–	–	–	–	–	Gavala et al., 1999
Dairy slurry	0.0033	–	0.0048	–	–	–	–	–	–	–	–	
Cow manure	2.6	0.004	0.054	20	2.0	6.0	1.8	11	2.6	15	1.8	Oliveros-Munoz, 2021
Diary manure	0.0011	$9.0x10^{-4}$	0.0018	5.0	0.4	–	7.3	8.4	1.2	4.9	0.83	Zhang et al., 2009
Pig manure	0.0073	0.003	0.011	–	0.75	0.78	0.054	–	0.26	2.0	–	Li 2020
Swine manure	0.0018	$4.2x10^{-5}$	$1.4x10^{-4}$	–	2.3	0.79	0.056	–	0.26	–	–	Jurado 2016
Pig slurry	–	–	–	–	0.35	–	–	–	0.72	1.1	–	Girault 2011

a) Batstone et al., 2002

Table 5.7 Biochemical parameter of ADM1 in the literature (continued)

Substrate	Half-saturation constant (g/L)								Reference
	K_{aa}	K_{ac}	K_{bu}	K_{fa}	K_{h2}	K_{pro}	K_{su}	K_{va}	
Piggery slurry	–	0.047	–	–	–	–	–	–	Gavala et al., 1999
Dairy slurry	–	–	–	–	–	–	–	–	
Cow manure	0.2	–	–	0.14	–	–	0.47	–	Oliveros-Muñoz et al., 2021
Diary manure	0.7	0.62	–	0.26	$1.3x10^{-4}$	0.78	1.1	0.041	Bo Zhang et al., 2009
Pig manure	–	–	–	–	–	–	0.075	–	H. Li et al., 2020
Swine manure	–	–	–	–	–	–	–	–	Jurado et al., 2016
Pig slurry	0.4	1.4	–	–	–	–	1.7	–	Girault et al., 2011

a) Batstone et al., 2002

5.2.4 Dynamic ADM1

In conventional ADM1, a single biochemical parameter that was initially calibrated is used regardless of changes in simulation conditions. In order to enable the biochemical parameters to adjust accordingly with changes in SRT, the ADM1 has been improved. The overall experimental results were divided into separate datasets based on each SRT condition. The optimal biochemical parameters at each SRT condition were determined, and a regression equation was derived. This equation was then introduced into the ADM1 model instead of constant biochemical parameters, resulting in the development of Dynamic ADM1. It is difficult to apply a model calibrated to a specific substrate to different substrates. Experimental data from other reactors using the same substrate were used to validate the Dynamic ADM1. A total of four reactors were utilized for model calibration and validation simultaneously. Specifically, predictions were made for CSTR 2 using the model calibrated with CSTR 1 data, for CSTR 1 using the model calibrated with CSTR 2 data, for CSTR 4 using the model calibrated with CSTR 3 data, and for CSTR 3 using the model calibrated with CSTR 4 data.

In the ADM1, the intracellular substrate uptake processes, including acidogenesis, acetogenesis, and methanogenesis, are based on the Monod growth model. The Monod growth model is an empirical equation derived from growth experiments of pure cultures (E.coli,

and M. tuberculosis) using glucose as a substrate (Monod, 1949). The equation incorporates a half-saturation constant, determined by factors such as the affinity of enzymes for the substrate. It was developed based on experimental data under high substrate concentration conditions, which limits its applicability to low-concentration situations and limited nutrient conditions. Furthermore, it exhibits low accuracy when applied to toxic substrates (Kong, 2017). In order to investigate the feasibility of alternative kinetic models, the ADM1 model was modified and applied using the Ming, and Contois growth model, instead of the Monod growth model. A summary of the growth models is provided in Table 5.8. The Ming and Contois growth models are similar to the Monod growth model. Ming model is formulated by taking the square of the substrate concentration in the Monod growth model. In the Ming growth model, as the substrate concentration increases, the specific growth rate transitions from a first-order reaction to a zero-order reaction, and the rate of change in growth rate accelerates with the increase in substrate concentration (Kong, 2017). The Contois growth model is an equation derived from growth rate experiments of nutrient-limiting conditions (Contois, 1959). It was developed based on the assumption that the cell growth rate is influenced by cell density under nutrient-limiting conditions. To account for this, the specific growth rate equation incorporates the microbial density term. Unlike

the Monod model, which is based on batch experiments conducted during the initial growth phase, the Contois model is derived from experimental data obtained under continuous culture conditions.

Table 5.8 Kinetic models applied to ADM1 (Contois, 1959; Monod, 1949; Moser, 1983)

Model	Equation	Description
Monod	$\mu = \frac{\mu_{max} S}{K_S + S}$	−Empirical equation derived from growth experiment of pure cultures using glucose as a substrate −Monod model can overestimate microbial growth during the lag phase
Ming	$\mu = \frac{\mu_{max} S^2}{K_S + S^2}$	−Exponential term in 'S' used to describe substrate characteristics −Make a sharp switch from a first−order to zero−order when increasing 'S'
Contois	$\mu = \frac{\mu_{max} S}{K_s X + S}$	−Derived from the assumption that the specific growth rate is inversely proportional to biomass concentration in nutrient limiting condition −Saturation term is a function of biomass concentration

Figure 5.1 illustrates variations in growth rates with different microbial growth models described in Table 5.8 under the assumption of the same maximum growth rate. The half−saturation constant in the Contois model was adjusted for comparison.

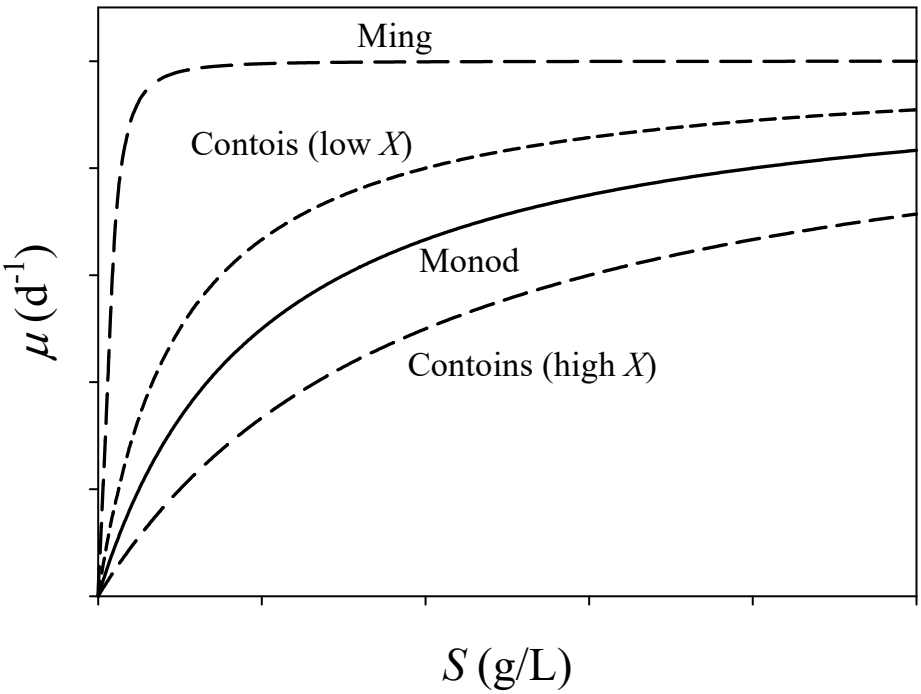

Figure 5.1 Variations in growth rates with different models

5.2.5 Reactor operation

Four CSTRs, working volumes of 3 and 6 L, respectively, were operated at different SRT conditions (Table 5.9). The reactors were operated for at least 3.1 SRT cycles under each condition to confirm the steady-state operation. The reactors were operated in a constant-temperature (35 ± 1 ℃) room for 350 d. Cattle manure samples were used as the substrate after dilution with tap water, and their characteristics are presented in Table 4.1. In order to acclimate the substrate to the inoculum, the organic loading rate was gradually increased in three stages using different dilution ratios within the same SRT during the initial 100 d. After reaching the target OLR, the reactors were operated with a shortened SRT by changing the influent flow rate while maintaining the same substrate concentration (8.0 wt.% in volatile solid). Biogas produced in the reactors were collected in a gas sampling bag and determined for volume and composition (CO_2, CH_4, N_2).

Table 5.9 Operating conditions of the reactor

CSTR	Substrate	Working volume (L)	SRT (d)			
			Start-up	Phase 1	Phase 2	Phase 3
1	Intact CM	3	18.0	18.0	10.9	6.6
2		6	36.0	36.0	21.8	13.2
3	Thermally hydrolyzed CM	3	18.0	18.0	10.9	6.6
4		6	36.0	36.0	21.8	13.2

5.2.6 Analytical methods

The gas compositions, including CH_4, CO_2, and N_2, were analyzed by gas chromatography with a thermal conductivity detector (Young Lin, Republic of Korea). The total solids (TS) and VS were determined using standard methods (APHA, 2012). Volatile fatty acids (VFAs) were analyzed via gas chromatography using a flame ionization detector (Agilent Technologies, CA, USA). The analysis of components, including carbohydrates, proteins, and lipids, was performed using the colorimetric method for sugars, the Kjeldahl method for proteins, and the ether extraction method for lipids, (APHA, 2012; Bligh & Dyer, 1959; DuBois et al., 1956)

5.3 Results and discussion

5.3.1 Sensitivity analysis

Figure 5.2 presents the sensitivity of biochemical parameters to ADM1. The hydrolysis rate constant of carbohydrates, lipids, proteins, and maximum uptake rate of acetate shows the highest sensitivity to methane production as sensitivity index of 11.0, 12.2, 6.5, and 7.6, respectively. In the case of VFAs, only specific biochemical parameters related to each VFA uptake process, such as K_{ac}, and $\mu_{m,ac}$ for acetate, K_{pro}, and $\mu_{m,pro}$ for propionate, K_{bu}, K_{va}, $\mu_{m,bu}$, and $\mu_{m,va}$ for butyrate and valerate, demonstrated high sensitivity to VFA concentration. The sensitivity index of acetogenesis, such as the uptake of sugars, amino acids, and fatty acids, and hydrogen uptake processes to model output was lower than 5%. This is likely due to the low concentrations of sugars, amino acids, and lipids present in the cattle manure used in the experiment. Biochemical parameters that exhibited a sensitivity index of 5% or higher to the model output were chosen for parameter calibration, while the excluded parameters were fixed at their reference values as indicated in Table 5.5. As a result, a total of 11 biochemical parameters were selected for calibration, which included three hydrolysis rate constants and two parameters each for the acetate, propionate, butyrate, and valerate uptake processes.

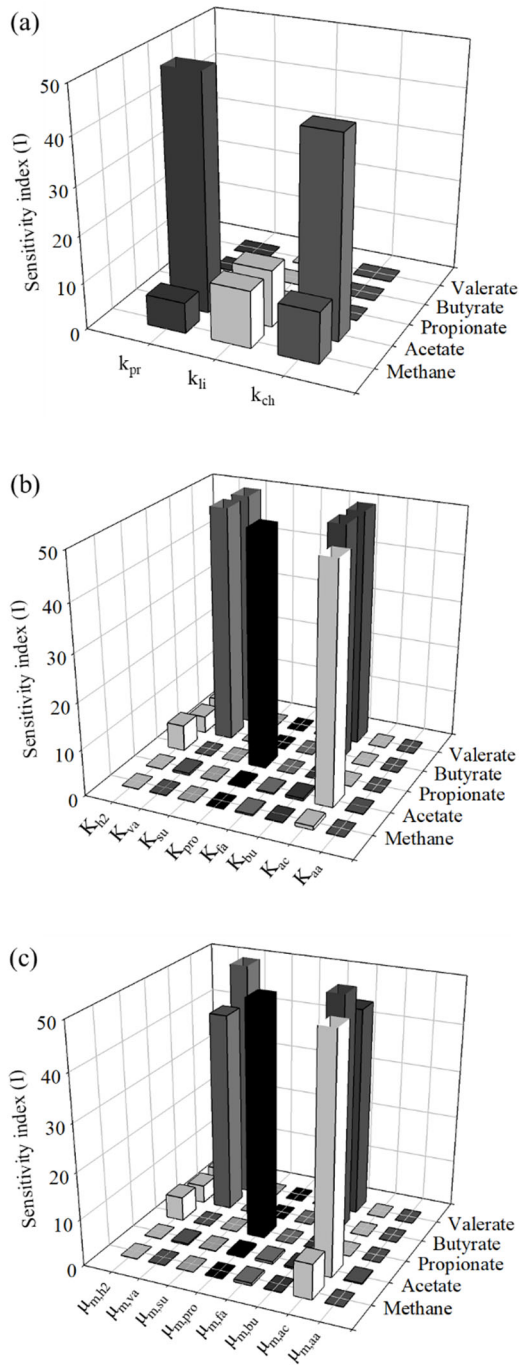

Figure 5.2 Sensitivity index of biochemical parameters to ADM1 (a: hydrolysis rate; b: half-saturation constant; c: maximum uptake rate)

5.3.2 Parameter calibration

The calibrated biochemical parameters of CSTR 1 and CSTR 2 are shown in Figure 5.3. The biochemical parameters were also calibrated for the entire set of experimental data, as shown by the solid and dotted lines in Figure 5.3. In the case of livestock manure, it is known that methane production is most sensitive to hydrolysis rate among processes involved in AD. In the biochemical parameters in CSTR 1, as the SRT increased, the hydrolysis rate constants for carbohydrates and proteins decreased, while the hydrolysis rate constant for lipids increased. As the SRT decreased from 18 d to 6.6 d, the hydrolysis rate constant for carbohydrates, lipids, and proteins were changed by 18, 45, and 76% from 0.0044, 0.0771, and 0.0137 to 0.0052, 0.0422, and 0.0241 d^{-1}, respectively. The hydrolysis rate constants calibrated for the entire dataset of CSTR 1 were determined to be 0.0046, 0.0674, and 0.0143 d^{-1} for carbohydrates, lipids, and proteins, respectively. These hydrolysis rate constants differ by up to 14, 69, and 48% for carbohydrate, lipid, and protein, respectively, compared to the hydrolysis rate constants calibrated at each SRT. In the biochemical parameters in CSTR 2, as the SRT decreased from 36.0 d to 13.2 d, the hydrolysis rate constant for carbohydrates, lipids, and proteins changed by 24, 45, and 76%, respectively. Specifically, they changed from 0.0037, 0.147, and 0.009 to 0.0046, 0.0815, and 0.0158 d^{-1}, respectively. The

hydrolysis rate constants calibrated for the entire dataset of CSTR 2 were determined to be 0.042, 0.0981, and 0.0099 d^{-1} for carbohydrates, lipids, and proteins, respectively. These hydrolysis rate constants for the entire dataset differ by up to 13, 50, and 59% for carbohydrates, lipids, and proteins, respectively, compared to the biochemical parameters calibrated at each SRT.

It has been confirmed that the metabolic rates (hydrolytic, acetogenic, and methanogenic) are influenced by SRT in the AD of model substrates (Peces et al., 2021). Additionally, alterations in kinetic parameters due to SRT changes were observed in an activated sludge system (Karlikanovaite-Balikci and Yagci, 2019). Both studies attributed the changes in kinetics to variations in the microbial composition. Consistent with these findings, Chapter 4 of this dissertation reveals a significant shift in the microbial community in response to variations in SRT, as depicted in Figure 4.10.

Hydrolysis rate

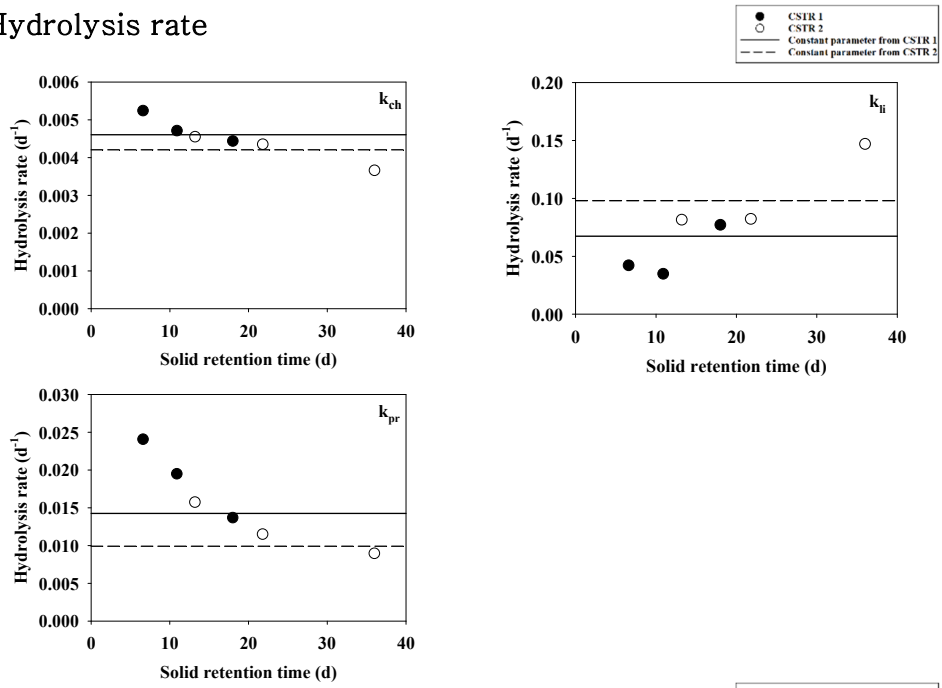

Maximum growth rate

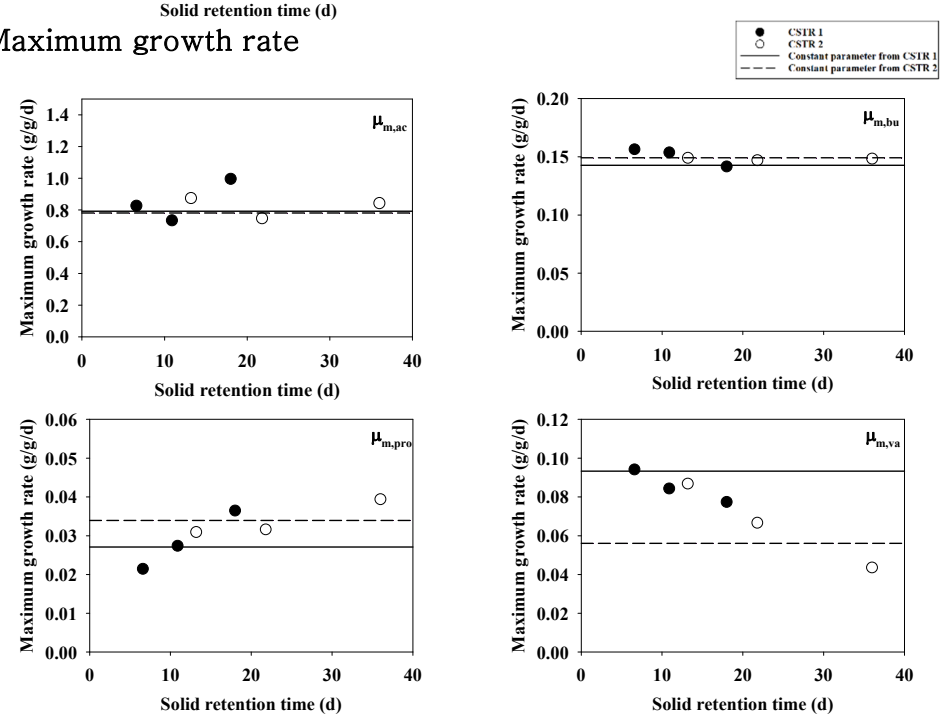

Figure 5.3 Calibrated biochemical parameters of CSTR 1 and 2

Half-saturation rate

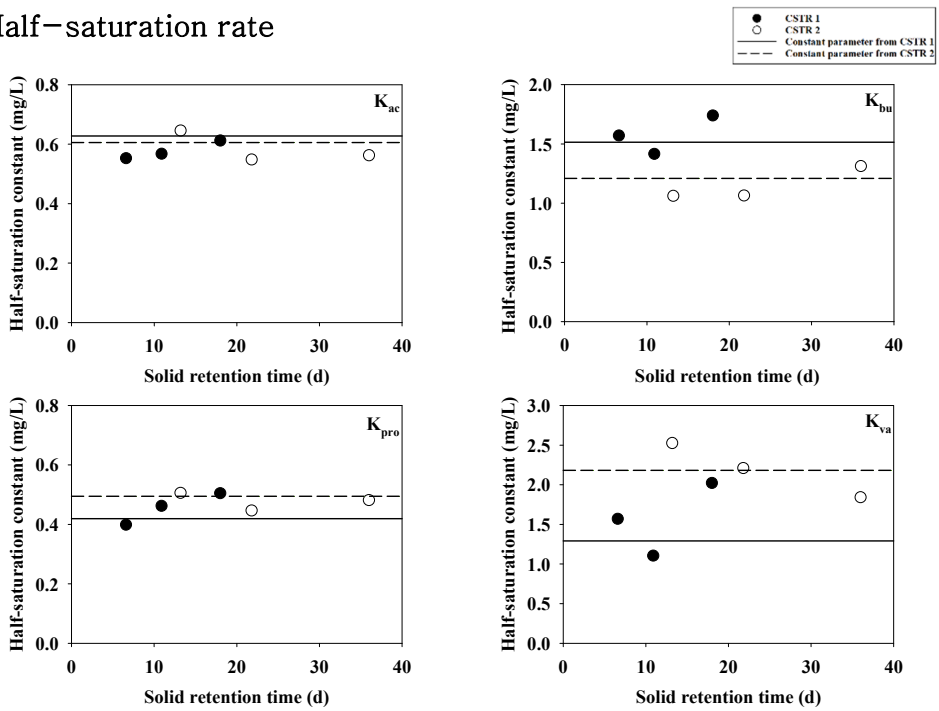

Figure 5.3 Calibrated biochemical parameters of CSTR 1 and 2 (continued)

Changes in biochemical parameters due to SRT variations can manifest in diverse ways. The relationship between SRT and biochemical parameters was interpreted using the linear regression equation, which had a higher correlation coefficient in the model than either the exponential or quadratic equation. Table 5.10 summarizes the correlation between biochemical parameters and SRT for both CSTR 1 and CSTR 2. In regression analysis, if the p-value of a coefficient is less than 0.05, the null hypothesis is rejected, indicating that the corresponding independent variable has a statistically significant influence on the dependent variable. SRT has a

statistically significant influence on the hydrolysis rates of carbohydrates, lipids, and proteins, as well as the maximum growth rates for propionate and valerate. However, the statistical analysis did not provide sufficient evidence to explain the influence of SRT on the half-saturation constants ($p > 0.05$).

The half-saturation constant, also known as the affinity constant, is commonly referred to as such because it is primarily influenced by the accessibility of the substrate, or the characteristics of the substrate, rather than the microbial properties (Arnaldos et al., 2015). Therefore, there were limitations in explaining the changes in the half-saturation constant solely based on the variations in microbial characteristics induced by SRT changes.

Table 5.10 Correlation between biochemical parameters and SRT for CSTR 1 and CSTR 2

Parameter	Regression [a)]	R^2	p−value of coefficient
k_{ch}	$y = 0.000045x + 0.005$	0.936	0.0016
k_{li}	$y = 0.004x + 0.013$	0.890	0.0047
k_{pro}	$y = -0.00048x + 0.024$	0.824	0.0124
$\mu_{m,ac}$	$y = 0.00081x + 0.823$	0.008	0.8676
$\mu_{m,bu}$	$y = -0.00025x + 0.154$	0.255	0.3071
$\mu_{m,pro}$	$y = 0.00053x + 0.022$	0.751	0.0255
$\mu_{m,va}$	$y = -0.002x + 0.106$	0.982	0.0001
$K_{S,ac}$	$y = -0.00064x + 0.593$	0.030	0.7446
$K_{S,bu}$	$y = -0.006x + 1.47$	0.056	0.6529
$K_{S,pro}$	$y = 0.001 + 0.44$	0.146	0.4548
$K_{S,va}$	$y = 0.012x + 1.667$	0.063	0.6325

a) y and x mean biochemical parameter and solid retention time, respectively.

The calibrated biochemical parameters of CSTR 3 and CSTR 4 are shown in Figure 5.4. As the SRT decreased from 18 d to 6.6 d, the hydrolysis rate constants for carbohydrates, lipids, and proteins were changed by 20, 68, and 61% from 0.0222, 0.0061, and 0.003 to 0.0179, 0.002 and 0.0012 d^{-1}, respectively. The hydrolysis rate constants calibrated for the entire dataset of CSTR 3 were determined to be 0.0219, 0.007, and 0.003 d^{-1} for carbohydrates, lipids, and proteins, respectively. These hydrolysis rate constants differ by up to 19, 72, and 61% for carbohydrate, lipid, and protein, respectively, compared to the hydrolysis rate constants calibrated at

each SRT condition. In the biochemical parameters in CSTR 4, as the SRT decreased from 36.0 d to 13.2 d, the hydrolysis rate constant for carbohydrates, lipids, and proteins changed by 13, 69, and 66%, respectively. Specifically, they changed from 0.0213, 0.005, and 0.0018 to 0.0186, 0.0084, and 0.003 d^{-1}, respectively. The hydrolysis rate constants calibrated for the entire dataset of CSTR 4 were determined to be 0.0206, 0.0055, and 0.002 d^{-1} for carbohydrates, lipids, and proteins, respectively. These hydrolysis rate constants for the entire dataset differ by up to 10, 53, and 47% for carbohydrates, lipids, and proteins, respectively, compared to the biochemical parameters calibrated at each SRT. Both CM and thermally hydrolyzed CM demonstrated changes in optimal biochemical parameters in response to variations in SRT. The parameters calibrated for each SRT condition can differ significantly from those calibrated for the entire dataset. These discrepancies in the biochemical parameters have the potential to introduce errors in a model simulation conducted at different SRT.

Hydrolysis rate

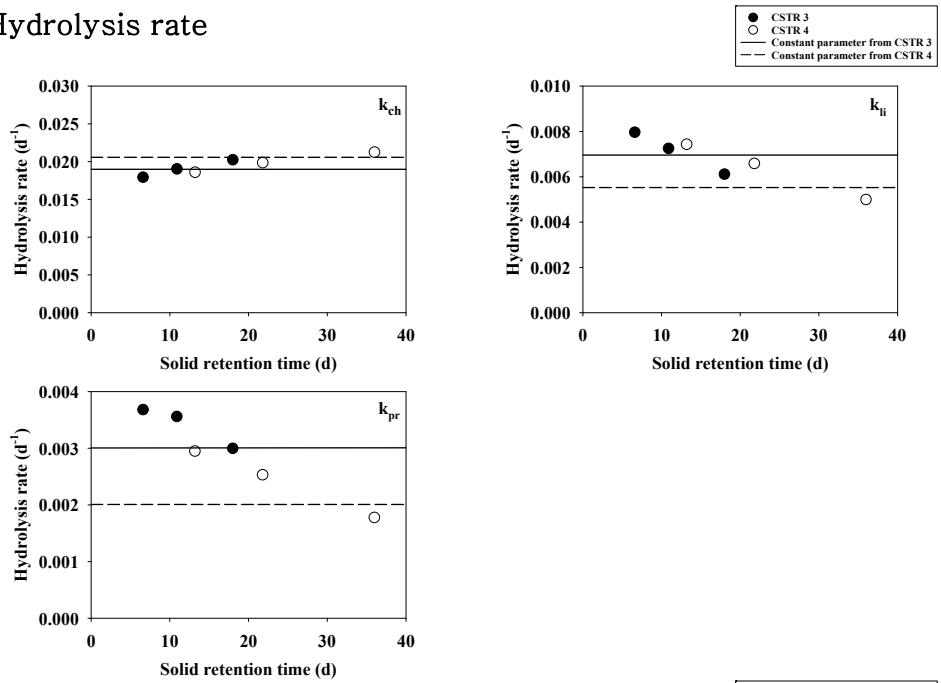

Maximum growth rate

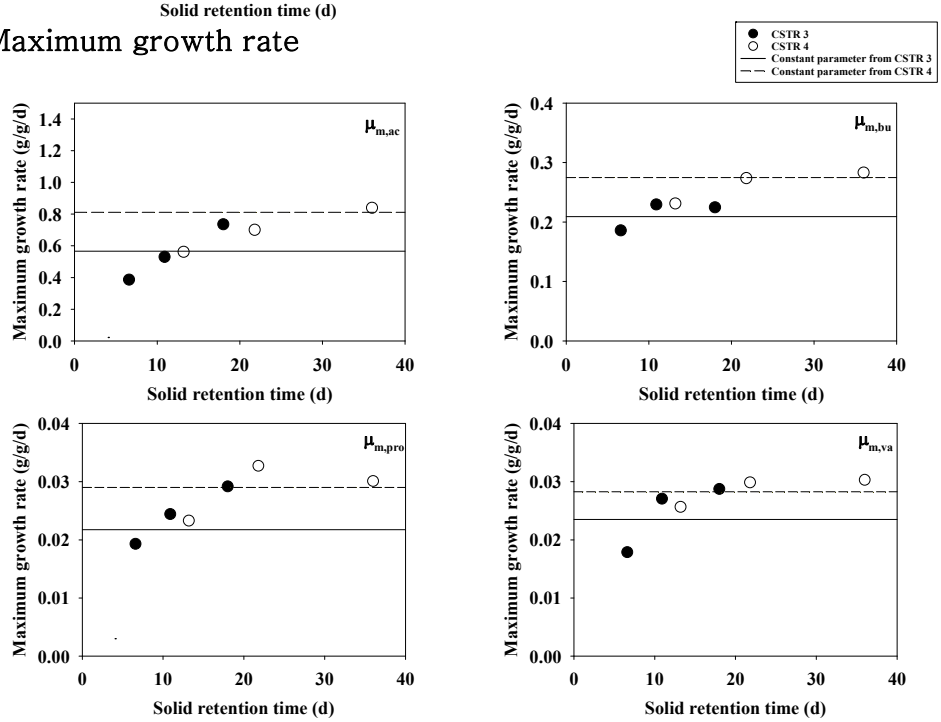

Figure 5.4 Calibrated biochemical parameters of CSTR 3 and 4

Half-saturation rate

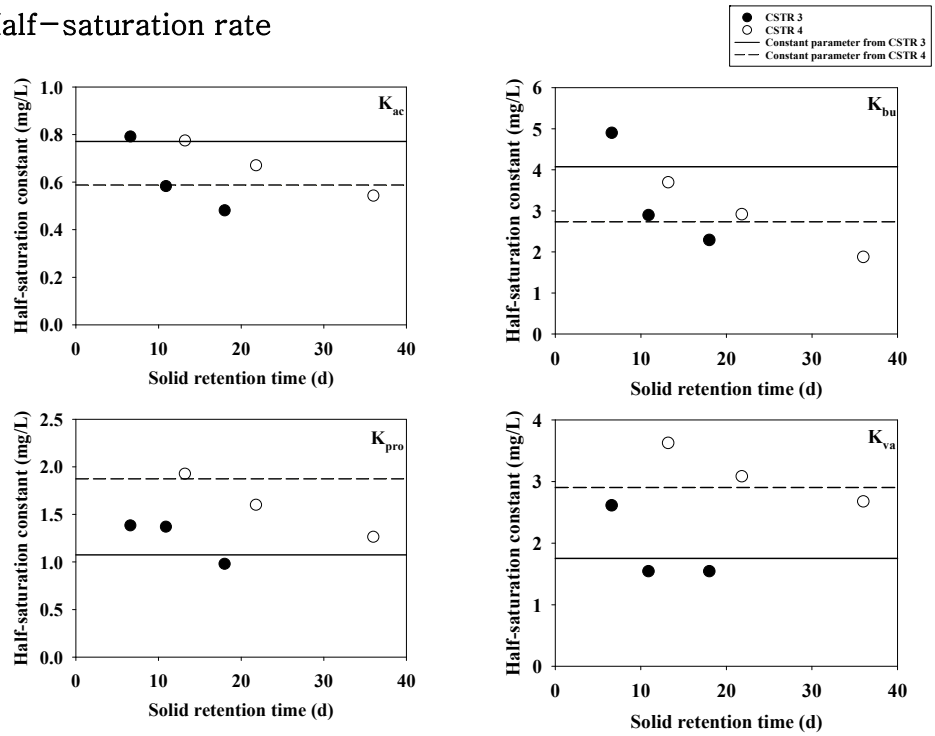

Figure 5.4 Calibrated biochemical parameters of CSTR 3 and 4 (continued)

Table 5.11 summarizes the correlation between biochemical parameters and SRT for both CSTR 3 and CSTR 4. In the case of THP AD, SRT has a statistically significant influence on the biochemical parameters for the hydrolysis rates of carbohydrates, lipids, and proteins, as well as the maximum growth rates for acetate, butyrate, propionate, and valerate ($p < 0.05$). Like CSTR 1 and CSTR 2, the statistical analysis did not provide sufficient evidence to explain the influence of SRT on the half-saturation constants ($p > 0.05$).

Table 5.11 Correlation between biochemical parameters and SRT for CSTR 3 and CSTR 4

Parameter	Regression equation [a)]	R^2	Significance of coefficient in regression [b)]
k_{ch}	$y = 0.000108x + 0.018$	0.869	0.0068
k_{li}	$y = -0.000098x + 0.0033$	0.907	0.0033
k_{pro}	$y = -0.000063x + 0.004$	0.941	0.0013
$\mu_{m,ac}$	$y = 0.014x + 0.369$	0.849	0.0090
$\mu_{m,bu}$	$y = 0.003x + 0.184$	0.781	0.0195
$\mu_{m,pro}$	$y = 0.00037x + 0.02$	0.594	0.0427
$\mu_{m,va}$	$y = 0.00033x + 0.021$	0.560	0.0470
$K_{S,ac}$	$y = -0.007x + 0.759$	0.299	0.2615
$K_{S,bu}$	$y = -0.082x + 4.559$	0.632	0.0587
$K_{S,pro}$	$y = -0.007x + 1.546$	0.052	0.6626
$K_{S,va}$	$y = 0.01x + 2.334$	0.016	0.8105

a) y and x mean biochemical parameter and solid retention time, respectively
b) null hypothesis is that the slope of the regression equation is equal to zero

The biochemical parameters based on published (Table 5.7) and calibrated data (Figure 5.3 and Figure 5.4) are illustrated in Figure 5.5. All biochemical parameters are ranged within published data.

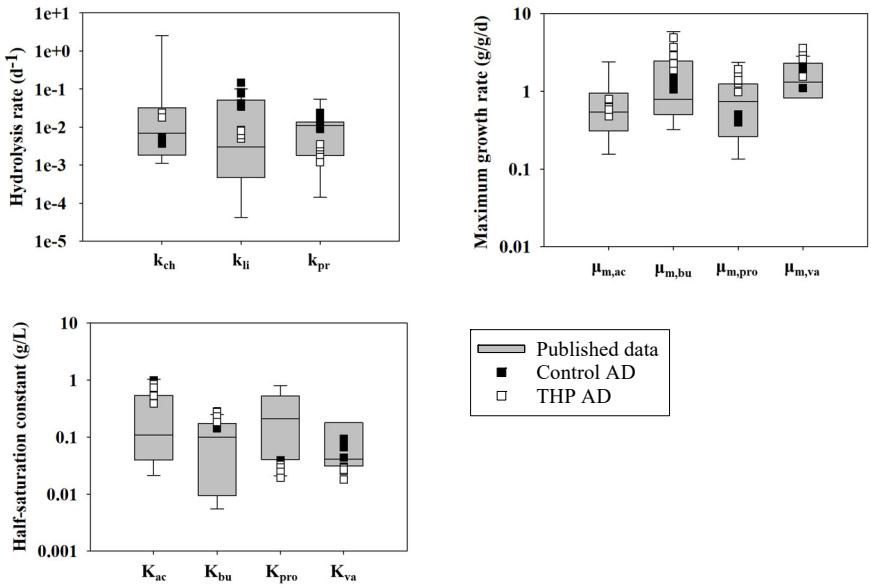

Figure 5.5 Biochemical parameters determined by calibration, and published data

Even if the parameters were calibrated using 350 d of operational data under three SRT conditions, simultaneous calibration of 11 parameters could lead to a decrease in accuracy due to mathematical limitations. However, this limitation could potentially be mitigated with an increase in the amount of available data.

5.3.3 Development of Dynamic ADM1

For the validation of Dynamic ADM1 within the same substrate, regression analysis was performed on SRT after distinguishing the biochemical parameters for each reactor. The linear regression result of biochemical parameters to SRT and single biochemical parameters for the entire dataset were shown in Table 5.12. Dynamic ADM1 was developed by introducing the regression equation to biochemical parameters in conventional ADM1.

Table 5.12 Regression result of Dynamic ADM1 to SRT, and parameters of ADM1

	Dynamic ADM1				ADM1	
	CSTR 1		CSTR 2		CSTR 1	CSTR 2
	Regression equation [a)]	R^2	Regression equation [a)]	R^2		
Hydrolysis rate (d^{-1})						
k_{ch}	$y = -0.000067x + 0.0056$	0.921	$y = -0.00004x + 0.0051$	0.972	0.0046	0.0042
k_{li}	$y = 0.0034x + 0.0117$	0.731	$y = -0.003x + 0.0317$	0.868	0.0674	0.0981
k_{pr}	$y = -0.009x + 0.0298$	0.995	$y = -0.0003x + 0.0188$	0.921	0.0143	0.0099
Maximum growth rate (g/g/d)						
$\mu_{m,ac}$	$y = 0.0171x + 0.65$	0.550	$y = -0.0006x + 0.8354$	0.499	0.7809	0.7809
$\mu_{m,bu}$	$y = -0.0013x + 0.1664$	0.957	$y = -0.00001x + 0.1485$	0.242	0.1492	0.1492
$\mu_{m,pro}$	$y = 0.013x + 0.0129$	0.998	$y = 0.0004x + 0.0248$	0.907	0.0271	0.0340
$\mu_{m,va}$	$y = -0.0014x + 0.1021$	0.944	$y = -0.0019x + 0.11$	0.990	0.0933	0.0561
Half-saturation constant (g/L)						
K_{ac}	$y = 0.0053x + 0.5147$	0.981	$y = -0.0032x + 0.6609$	0.483	0.6276	0.6058
K_{bu}	$y = 0.0179x + 1.3636$	0.405	$y = 0.0117x + 0.8706$	0.869	1.5143	1.2093
K_{pro}	$y = 0.009x + 0.3492$	0.937	$y = -0.0007x + 0.4952$	0.077	0.4195	0.4948
K_{va}	$y = 0.0486x + 0.9913$	0.372	$y = -0.0296x + 2.8939$	0.991	1.2924	2.1827

a) y and x mean biochemical parameter and solid retention time, respectively.

Table 5.12 Regression result of Dynamic ADM1 to SRT, and parameters of ADM1 (continued)

Parameter	Dynamic ADM1				ADM1	
	CSTR 3		CSTR 4		CSTR 3	CSTR 4
	Regression equation [a]	R^2	Regression equation [a]	R^2		
Hydrolysis rate (d^{-1})						
k_{ch}	$y = 0.0003x + 0.0175$	0.384	$y = 0.0001x + 0.0172$	0.986	0.0219	0.0206
k_{li}	$y = 0.0003x + 0.0009$	0.591	$y = -0.0001x + 0.0102$	0.967	0.0070	0.0055
k_{pr}	$y = 0.0001x + 0.001$	0.393	$y = -0.00005x + 0.0036$	0.999	0.0030	0.0020
Maximum growth rate (g/g/d)						
$\mu_{m,ac}$	$y = 0.0305x + 0.1905$	0.999	$y = 0.012x + 0.418$	0.980	0.5664	0.8118
$\mu_{m,bu}$	$y = 0.003x + 0.1779$	0.521	$y = 0.0021x + 0.2127$	0.775	0.2090	0.2748
$\mu_{m,pro}$	$y = 0.0008x + 0.0143$	0.974	$y = 0.0002x + 0.0228$	0.350	0.0218	0.0290
$\mu_{m,va}$	$y = 0.0009x + 0.0141$	0.752	$y = 0.0002x + 0.0242$	0.699	0.0235	0.0283
Half-saturation constant (g/L)						
K_{ac}	$y = -0.0259x + 0.9258$	0.891	$y = -0.01x + 0.9007$	0.993	0.7709	0.5884
K_{bu}	$y = -0.2146x + 5.9019$	0.819	$y = -0.0791x + 4.7021$	0.997	4.0741	2.7348
K_{pro}	$y = -0.0374x + 1.6884$	0.882	$y = -0.0286x + 2.2738$	0.982	1.0741	1.8741
K_{va}	$y = -0.0844x + 2.8991$	0.619	$y = -0.0404x + 4.0854$	0.951	1.7527	2.9045

a) y and x mean biochemical parameter and solid retention time, respectively.

5.3.4 Validation of Dynamic ADM1

The simulation results for CSTR 1 using the ADM1 and the Dynamic ADM1 calibrated with data from CSTR 2 were presented in Figure 5.6. The measured methane production values were 1.35 ± 0.19, 2.10 ± 0.20, and 2.43 ± 0.19 L/d for phases 1, 2, and 3, respectively. The ADM1 predicted the methane production as 1.59, 2.22, and 2.82 L/d for phases 1, 2, and 3, respectively. The ADM1 overestimated methane production at phase 3, which had an SRT condition (6.6 d of SRT) that was furthest from the SRT range used for model calibration (13.2 – 36.0 d of SRT). For the Dynamic ADM1, the predicted methane productions were 1.53, 1.98, and 2.46 L/d for phases 1, 2, and 3, respectively. Notably, the model showed a low error level of about 1.2% even for phase 3. The accuracy of the Dynamic ADM1 was higher than that of the ADM1 model, as evaluated by the MSE [Figure 5.6 (c)].

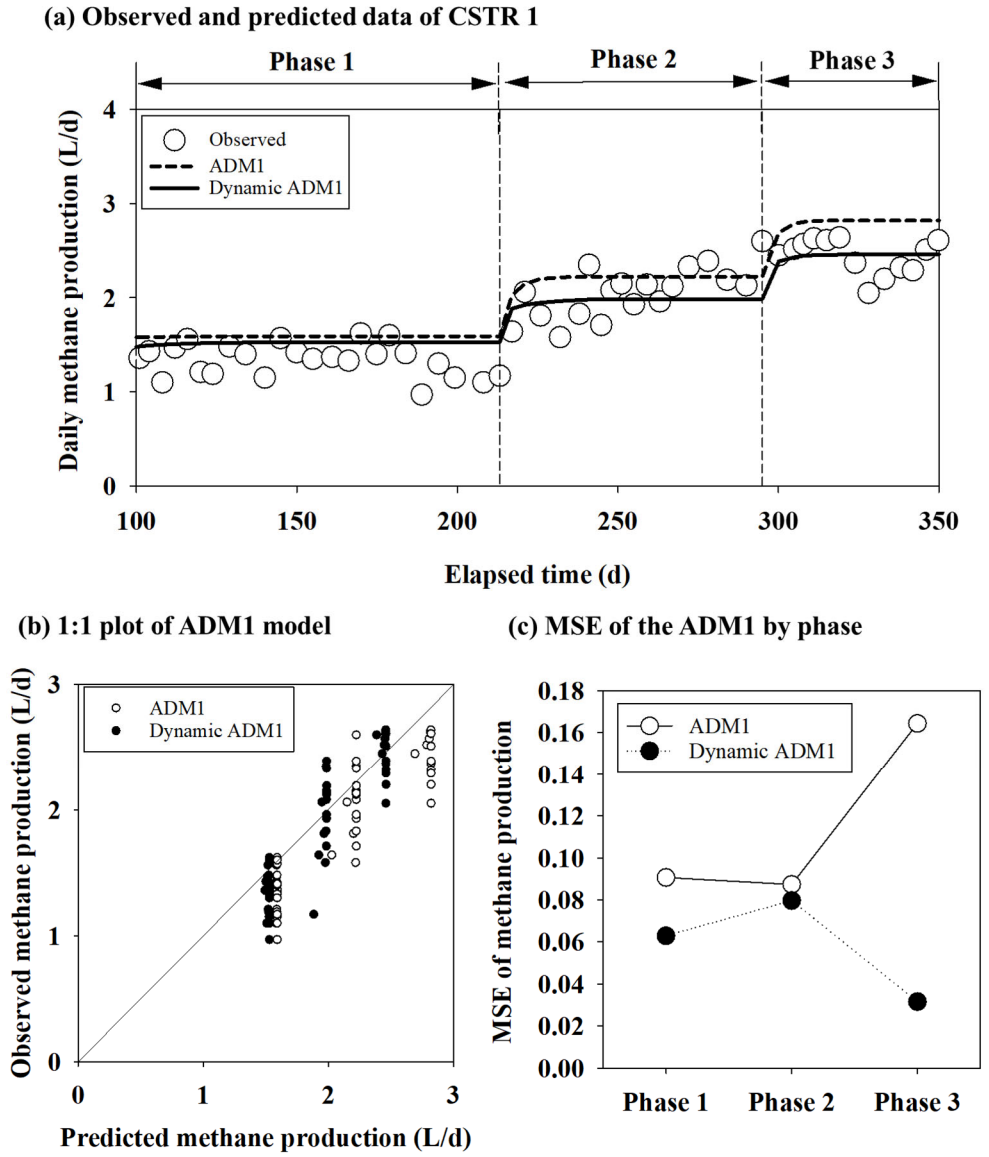

Figure 5.6 Model validation with CSTR 1 [(a) observed and predicted data of CSTR 1; (b) 1:1 plot of ADM1 models; (c) MSE of the ADM1 by phase]

The simulation results for CSTR 2 using the ADM1 and the Dynamic ADM1 calibrated with data from CSTR 1 were presented in Figure 5.7. The measured methane production values were 1.71 ± 0.25, 2.88 ± 0.21, and 3.32 ± 0.39 L/d for phases 1, 2, and 3, respectively. The ADM1 predicted the methane production as 2.58, 3.18, and 3.71 L/d for phases 1, 2, and 3, respectively. For the dynamic ADM1, the predicted methane productions were 1.92, 2.66, and 3.45 L/d for phases 1, 2, and 3, respectively. Similar to CSTR 1, the ADM1 model showed an increase in prediction error as the SRT condition moved further away from the range used for model calibration, while the Dynamic ADM1 exhibited improved accuracy compared to the ADM1 model [Figure 5.7 (c)].

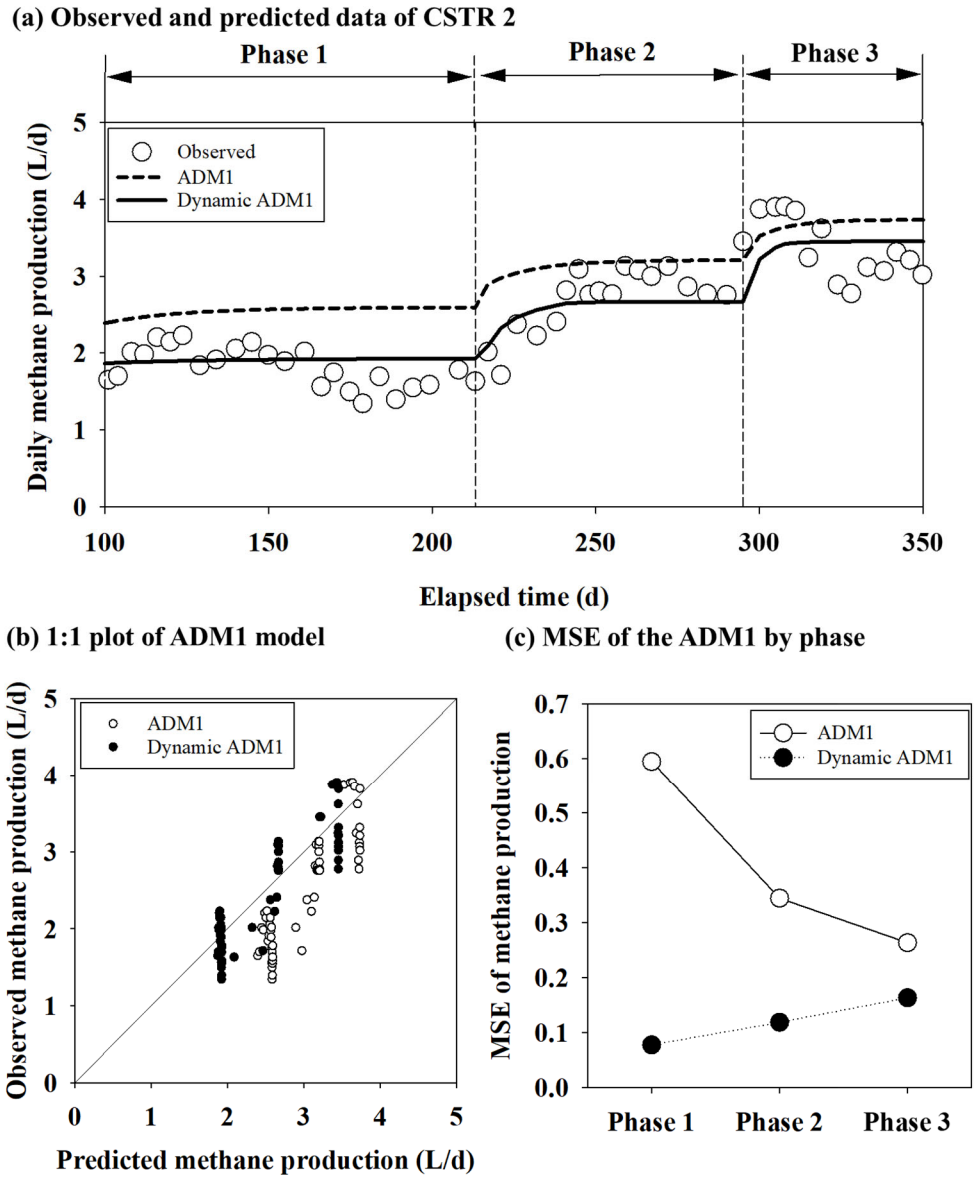

Figure 5.7 Model validation with CSTR 2 [(a) observed and predicted data of CSTR 2; (b) 1:1 plot of ADM1 models; (c) MSE of the ADM1 models by phase]

Coefficient of determination and mean squared error of VFA concentration predicted by the model for CSTR 1 and CSTR 2 are summarized in Table 5.13. The prediction accuracy of not only methane production but also VFA concentration is higher in Dynamic ADM1 compared to conventional ADM1.

Table 5.13 Coefficient of determination and mean squared error of VFA concentration

		CSTR1		CSTR2	
		ADM1	Dynamic ADM1	ADM1	Dynamic ADM1
R^2	Acetate	0.481	0.606	0.390	0.482
	Propionate	0.202	0.372	0.282	0.320
	Butyrate	0.330	0.455	0.269	0.332
	Valerate	0.189	0.463	0.292	0.329
Mean squared error	Acetate	0.032	0.024	0.007	0.004
	Propionate	0.561	0.099	0.020	0.017
	Butyrate	0.128	0.114	0.022	0.012
	Valerate	0.132	0.112	0.017	0.010

Model development and validation were also conducted on CSTR 3 and CSTR 4, both of which were fed with thermally hydrolyzed cattle manure. The optimized parameter and regression result are shown in Appendix. The simulation results for CSTR 3 using the ADM1 and the Dynamic ADM1 calibrated with data from CSTR 4 were presented in Figure 5.8. The measured methane production values were 2.21 ± 0.22, 3.30 ± 0.26, and 2.94 ±

0.18 L/d for phases 1, 2, and 3, respectively. The ADM1 predicted the methane production as 2.24, 3.15, and 3.76 L/d for phases 1, 2, and 3, respectively. For the Dynamic ADM1, the predicted methane productions were 2.27, 3.18, and 3.10 L/d for phases 1, 2, and 3, respectively.

Methane production decreased then the SRT was set to 6.6 d. Specifically, the VFA concentration reached a peak of 6,464 mg/L in THP AD under the SRT of 6.6 d, while it was only 1,462 mg/L in control AD at the same SRT. The accumulation of VFA can lead to process inhibition, and the extent of inhibition varies depending on the substrate and operating conditions (Y. Chen et al., 2008; Y. Han et al., 2020; Van Ginkel & Logan, 2005). Despite ADM1 incorporating microbial inhibition by free acids, it does not consider the inhibition caused by accumulated VFA since it is formulated as a function of pH, independent of VFA concentrations. Consequently, the prediction accuracy was low for the THP AD with accumulated VFA, specifically at an SRT of 6.6 d.

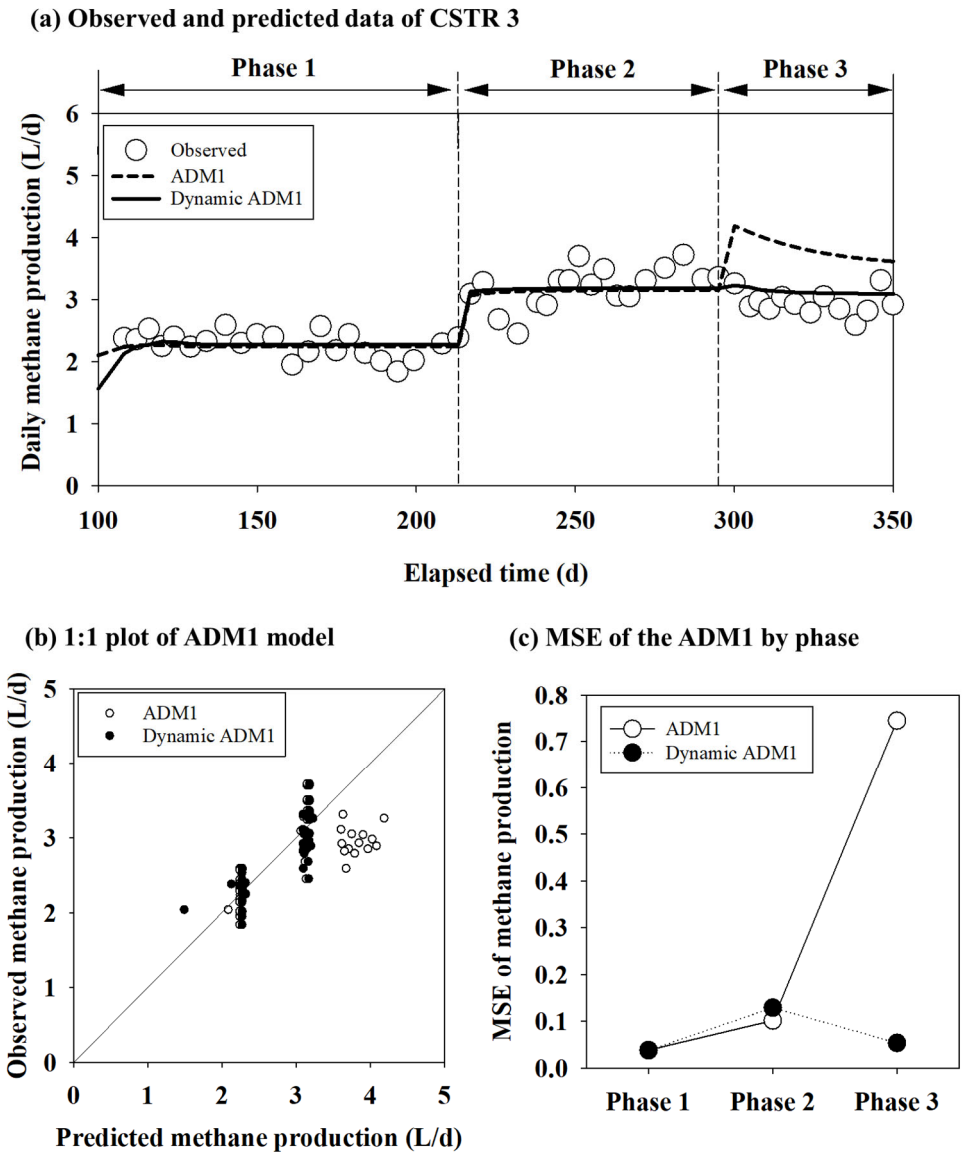

Figure 5.8 Model validation with CSTR 3 [(a) observed and predicted data of CSTR 4; (b) 1:1 plot of ADM1 models; (c) MSE of the ADM1 models by phase]

The simulation results for CSTR 4 using the ADM1 and the Dynamic ADM1 calibrated with data from CSTR 3 were presented in Figure 5.9. The measured methane production values were 2.74 ± 0.16, 4.01 ± 0.31, and 5.54 ± 0.35 L/d for phases 1, 2, and 3, respectively. The ADM1 predicted the methane production as 2.50, 3.90, and 6.22 L/d for phases 1, 2, and 3, respectively. For the Dynamic ADM1, the predicted methane productions were 2.77, 3.87, and 5.43 L/d for phases 1, 2, and 3, respectively. Similar to CSTR 1 and 2, the ADM1 model showed an increase in prediction error as the SRT condition moved further away from the range used for model calibration, while the Dynamic ADM1 exhibited improved accuracy compared to the ADM1 model.

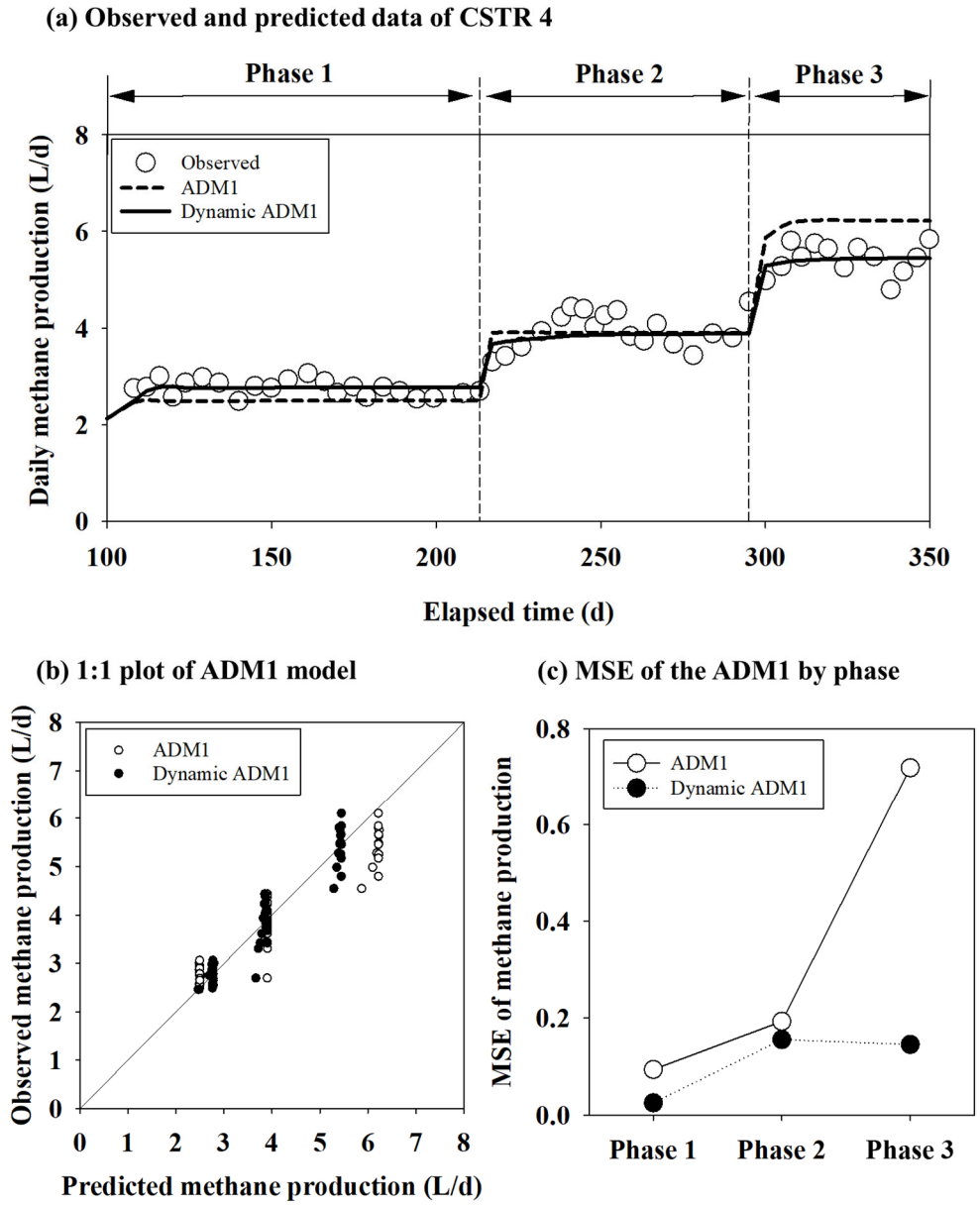

Figure 5.9 Model validation with CSTR 4 [(a) observed and predicted data of CSTR 4 (b) 1:1 plot of ADM1 models; (c) MSE of the ADM1 models by phase]

Table 5.14 summarizes the coefficient of determination and mean squared error of VFA concentration predictions by the model for CSTR 3 and CSTR 4. It is observed that the accuracy of predicting both methane production and VFA concentration is higher in Dynamic ADM1 as compared to conventional ADM.

Table 5.14 Coefficient of determination and mean squared error of VFA concentration prediction in THP AD

		CSTR 3		CSTR 4	
		ADM1	Dynamic ADM1	ADM1	Dynamic ADM1
R^2	Acetate	0.766	0.826	0.203	0.461
	Propionate	0.721	0.781	0.050	0.034
	Butyrate	0.753	0.742	0.052	0.084
	Valerate	0.633	0.732	0.008	0.038
Mean squared error	Acetate	0.127	0.022	0.044	0.008
	Propionate	1.371	0.701	0.043	0.040
	Butyrate	0.283	0.172	0.032	0.016
	Valerate	0.301	0.264	0.031	0.021

The ADM1 model was developed using the Ming and Conotis growth models instead of the Monod growth model. The simulation results of CSTR 1 (fed with intact CM), and CSTR 3 (fed with thermally hydrolyzed CM) are shown in Figure 5.10, and Figure 5.12, respectively. Similar to the Monod growth-based ADM1, both the Ming and Contois growth-based ADM1 exhibited low prediction accuracy for phase 3, which represents operating conditions significantly different from the parameter calibration conditions.

Among the three models, the Monod growth-based ADM1 shows the highest prediction accuracy. The implementation of the Dynamic ADM1 resulted in improved prediction accuracy for all growth models, including phase 3.

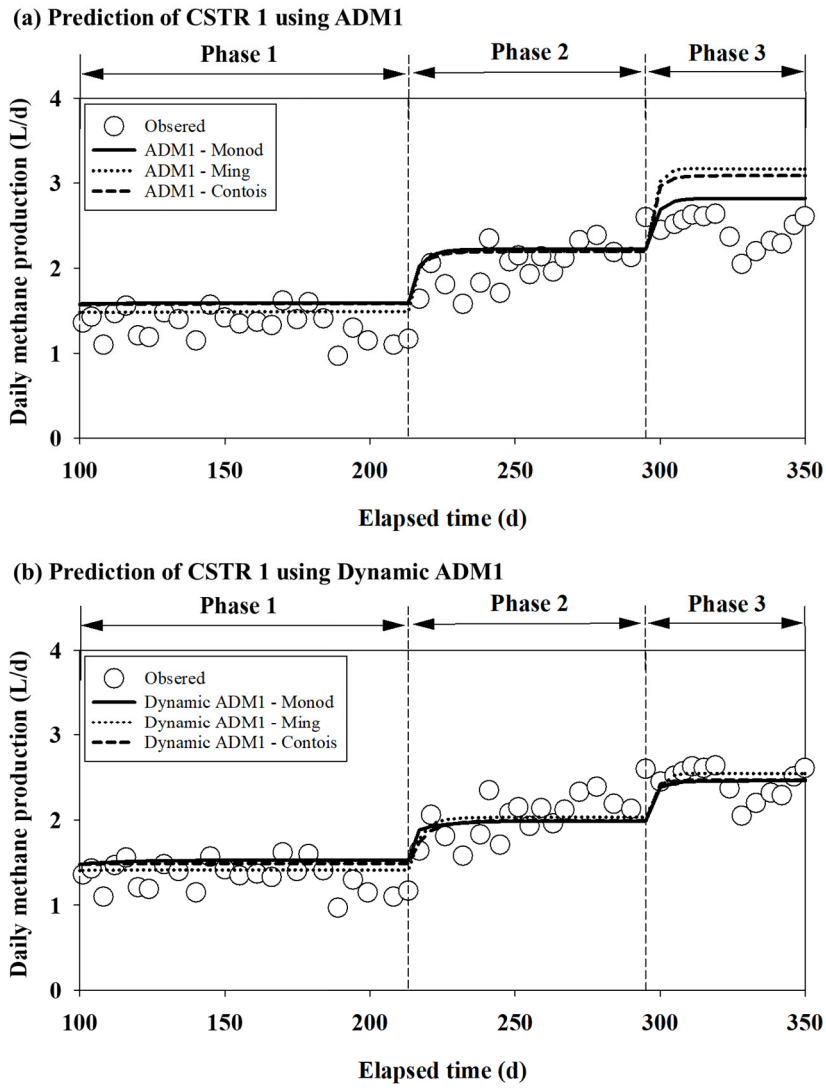

Figure 5.10 Simulation result of CSTR 1 using various microbial growth models with (a) ADM1, and (b) Dynamic ADM1

Figure 5.11 illustrates the MSE of methane production predicted by the model using various growth kinetic models for CSTR 1, broken down by phase. It can be observed that the prediction error of the model increases at Phase 3 in all conventional ADM1, regardless of the growth kinetic models used. Among these models, the Monod model demonstrates a lower MSE compared to the Ming and Contois models. On the other hand, in the case of Dynamic ADM1, the prediction accuracy does not decrease with each phase, indicating robustness of Dynamic ADM1 throughout the phase and growth kinetic models.

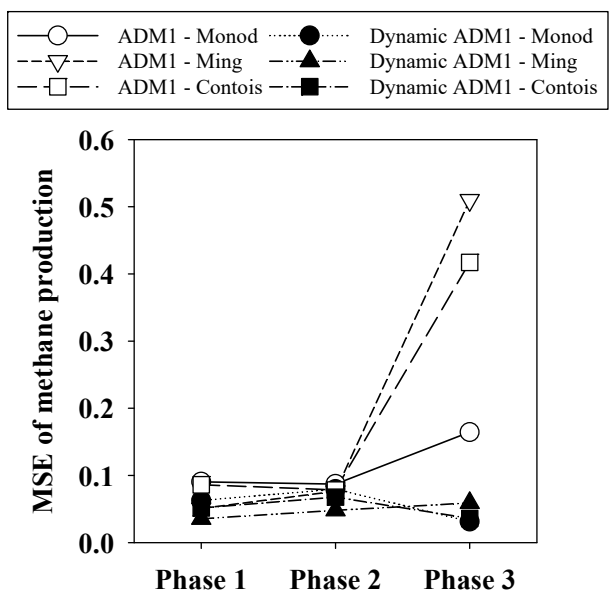

Figure 5.11 Mean squared error of methane production predicted by the model using various growth kinetic models for CSTR 1

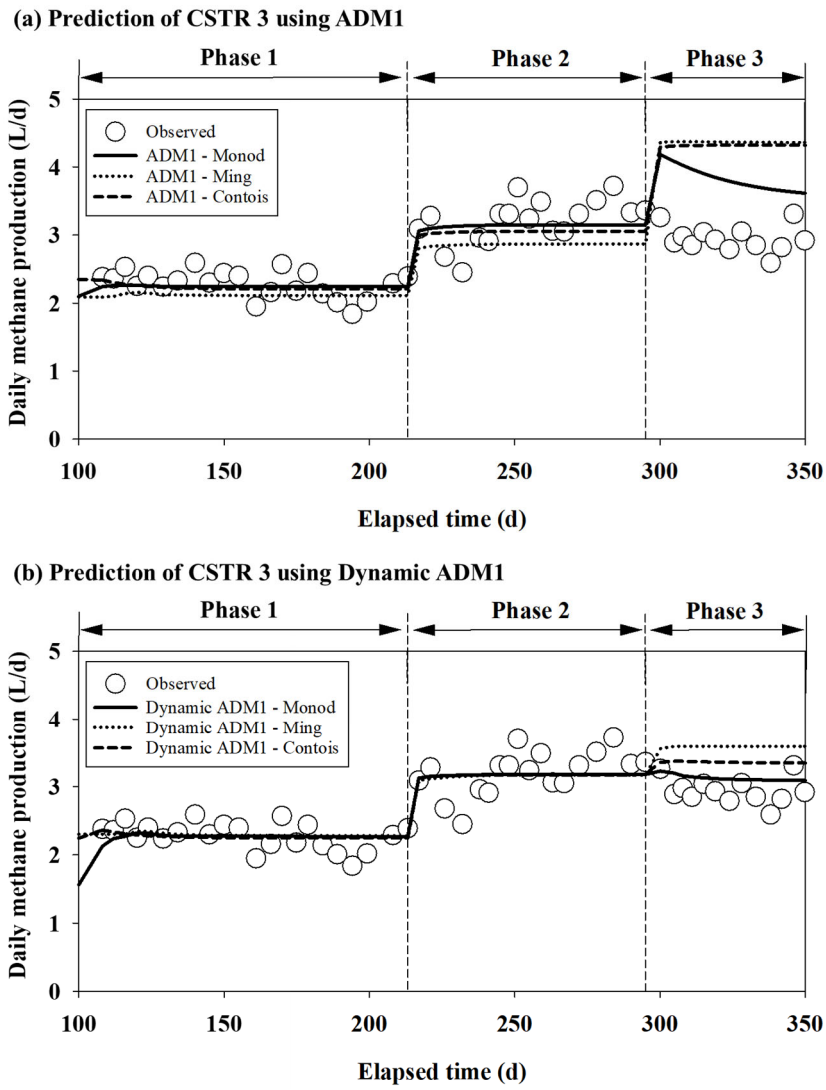

Figure 5.12 Simulation result of CSTR 3 using various microbial growth models with (a) ADM1), and (b) Dynamic ADM1

Figure 5.11 presents the MSE of methane production predicted by the model using various growth kinetic models for CSTR 3, categorized by phases. Similar to CSTR 1, an increase in prediction error at Phase 3 is observed across all growth kinetic models in conventional ADM1. However, in the case of Dynamic ADM1, the model exhibits lower prediction errors regardless of the growth kinetic model used.

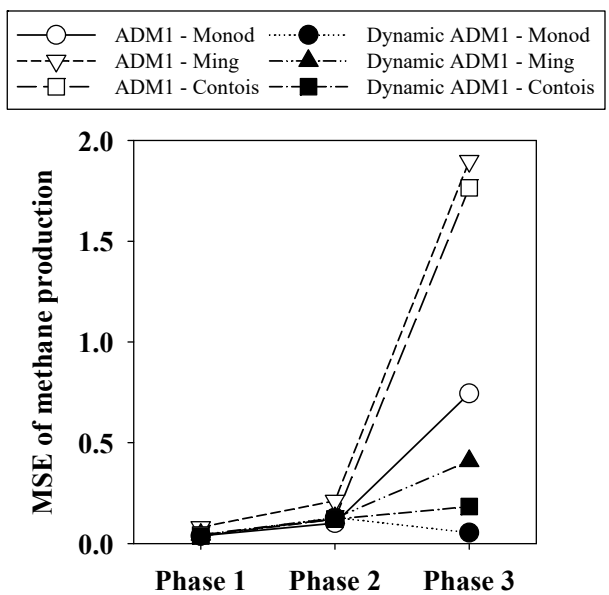

Figure 5.13 Mean squared error of methane production predicted by the model using various growth kinetics for CSTR 3

5.3.5 Simulation of Dynamic ADM1

Figure 5.14 illustrates the simulation results of methane production and VFA concentration. The simulation showed over 90% accuracy in predicting methane production, except for THP AD at an SRT of 6.6 d. The low accuracy is likely due to the limited biokinetic parameter set used for model training. The reactor operating results showed dramatic changes in reactor conditions at short SRT conditions like 6.6 d of SRT, but the biokinetic parameters around these conditions were insufficient. Therefore, the regression model used to predict biokinetic parameters showed low accuracy at an SRT of 6.6 d, which had an impact on the prediction of methane production. Simulation results for VFA concentration showed a similar trend.

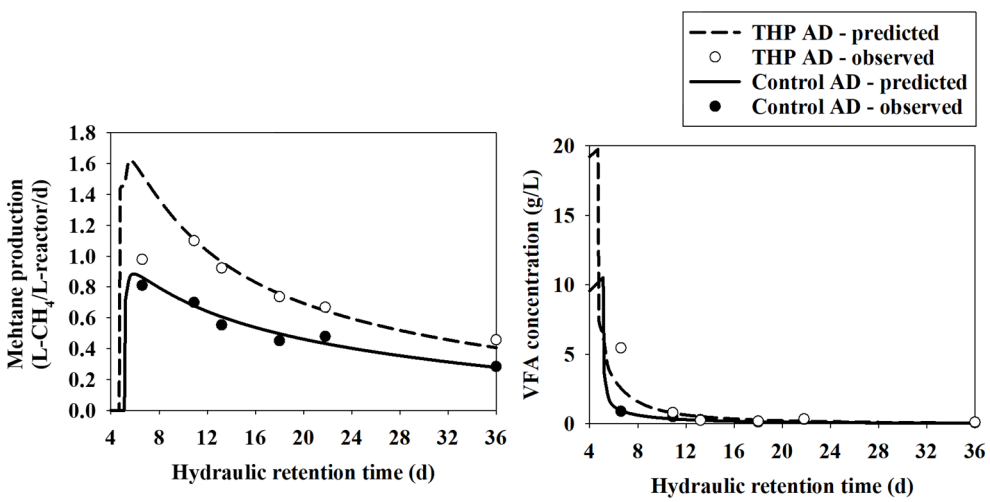

Figure 5.14 Model simulation result of methane production and VFA concentration

The simulation results of microorganisms are presented in

Figure 5.15. The concentrations of acidogens, acetogens, and methanogens were found to be increased by 1.6,1.8, and 1.5 times, respectively, compared to the control AD under SRT conditions of 6.6 – 36.0 d. This increase was attributed to the higher availability of easily accessible substrate resulting from the THP treatment. With the shortening of THP from 36.0 d to 16.3 d, the concentration of acidogens increased due to a sufficient supply of substrate resulting from an increase in OLR. AD of livestock manure or agricultural residues may encounter problems due to low OLR, which limits the availability of substrate (Bi et al., 2019; D. Li et al., 2015; Menardo et al., 2011). SRT conditions shorter than 16.3 d, the concentration of acidogens decreased, primarily because of the predominant increase in microorganisms discharge due to the shortening of SRT compared to the increase in microorganisms resulting from the increase in OLR. The acetogens and methanogens also exhibit a similar trend, but the SRT conditions where changes occurred were different. The SRT points, which represent the SRT condition at maximum microorganism concentration, were lower in THP AD than in control AD. This implies that the community of microorganisms was altered to favor faster-growing microorganisms due to THP treatment.

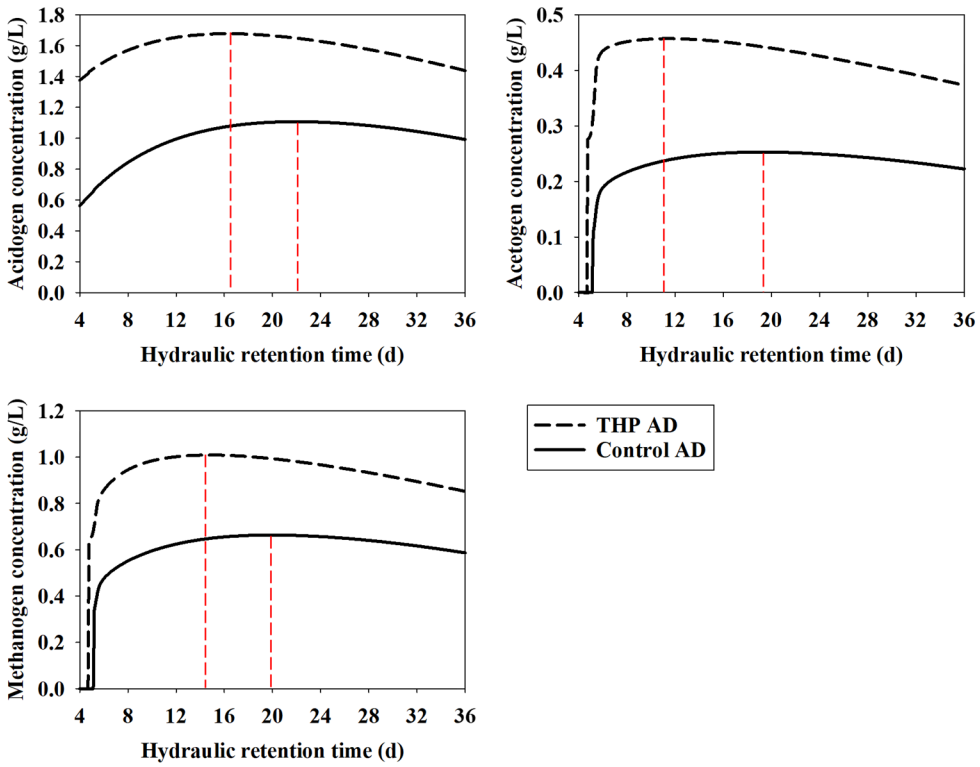

Figure 5.15 Model simulation result of acidogens, acetogens, and methanogens concentration

Unlike acetogens, the washout of acetogens and methanogens was predicted to occur at an SRT of 4 – 5 d. This was due to the influence of a slow maximum growth rate compared to acidogens (Table 5.5, and Table 5.12). Figure 5.16 shows the simulation results for individual microbial concentrations in the range of SRT 4 – 6 d. For acetogens, regardless of THP, the propionate uptake microorganism was the first to wash out, followed by the remaining valerate and butyrate uptake microorganisms. The

concentration of methanogens also decreased slightly in the range of SRT 5 – 5.5 d. This was due to the interruption of acetogenesis, which is responsible for acetate and hydrogen production, as the propionate uptake microorganism was washed out. As a result, the concentration of methanogens decreased slightly due to the decrease in feedstock.

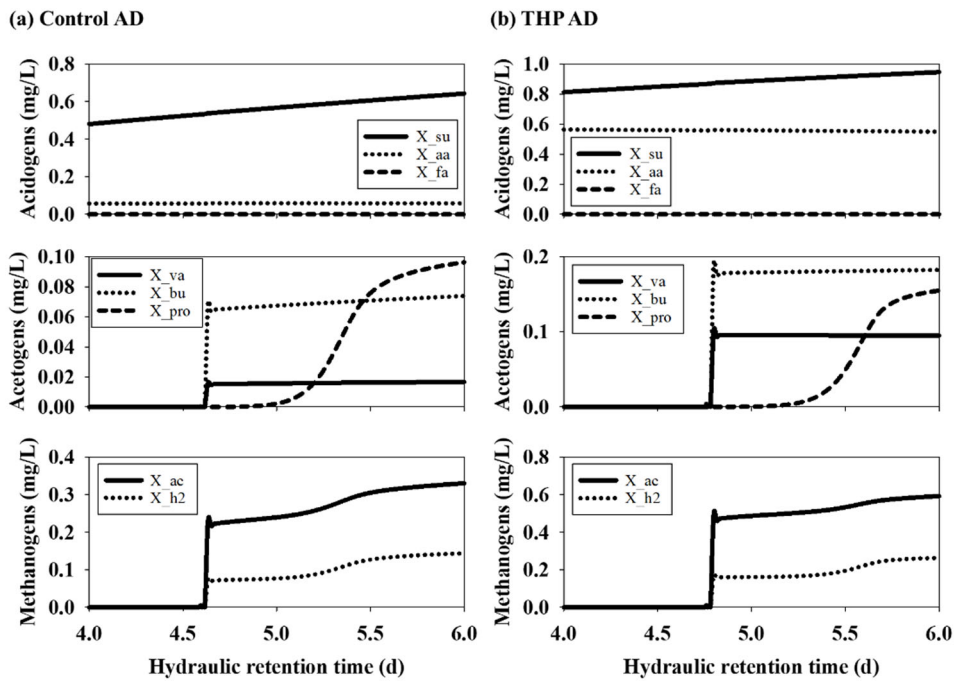

Figure 5.16 Model simulation result of microorganism characterized by substrate [(a) control AD and (B) THP AD]

5.4 Summary

The Dynamic ADM1 was proposed and validated for substrate of intact CM and thermally hydrolyzed CM, enabling the prediction of biokinetic parameters under varying SRT conditions. The dynamic ADM1 exhibited higher prediction accuracy than the conventional ADM1 when predicting methane production during SRT changes. Model simulations indicated that THP application resulted in a 1.5−fold enhancement in average methane production under SRT conditions ranging from 6.6 to 36.0 d, due to an increase in a biodegradable substrate and maximum growth rate of microorganisms. Furthermore, THP shortened the SRT condition which demonstrated the maximum concentration of microorganisms. The Dynamic ADM1 enables more accurate prediction of reactor behavior in response to changes in SRT by predicting biochemical parameters at each SRT. This can be beneficial in deriving operational conditions, improving design, and reducing operating costs.

References

Ahlert, S., Zimmermann, R., Ebling, J., & König, H. 2016. Analysis of propionate-degrading consortia from agricultural biogas plants. *MicrobiologyOpen*, *5*(6), 1027–1037.

Angelidaki, I., Ellegaard, L., & Ahring, B. K. 1999. A comprehensive model of anaerobic bioconversion of complex substrates to biogas. *Biotechnology and Bioengineering*, *63*(3), 363–372.

APHA. 2012. *Standard methods for the examination of water and wastewater*. American public health association Washington, DC.

Batstone, D. J., Keller, J., Angelidaki, I., Kalyuzhnyi, S. V., Pavlostathis, S. G., Rozzi, A., Sanders, W. T., Siegrist, H., & Vavilin, V. A. 2002. The IWA Anaerobic Digestion Model No 1 (ADM1). *Water Science and Technology : A Journal of the International Association on Water Pollution Research*, *45*(10), 65–73.

Bi, S., Qiao, W., Xiong, L., Ricci, M., Adani, F., & Dong, R. 2019. Effects of organic loading rate on anaerobic digestion of chicken manure under mesophilic and thermophilic conditions. *Renewable Energy*, *139*, 242–250.

Bligh, E. G., & Dyer, W. J. 1959. A rapid method of total lipid extraction and purification. *Canadian Journal of Biochemistry and Physiology*, *37*(8), 911–917.

Bo Zhang, Kathleen R Fowler, Matthew D Grace, Sumona Mondal, & Stefan J Grimberg. 2009. *Optimization of Anaerobic Digestion Model No. 1 (ADM1) : Simulation of Dairy Manure Digestion*. *1*(1),

1–13.

Chen, Y., Cheng, J. J., & Creamer, K. S. 2008. Inhibition of anaerobic digestion process: A review. *Bioresource Technology*, *99*(10), 4044–4064.

Contois, D. E. 1959. Kinetics of Bacterial Growth: Relationship between Population Density and Specific Growth Rate of Continuous Cultures. *Journal of General Microbiology*, *21*(1), 40–50.

Costello, D. J., Greenfield, P. F., & Lee, P. L. 1991. Dynamic modelling of a single-stage high-rate anaerobic reactor—II. Model verification. *Water Research*, *25*(7), 859–871.

Donoso-Bravo, A., Mailier, J., Martin, C., Rodríguez, J., Aceves-Lara, C. A., & Wouwer, A. Vande. 2011. Model selection, identification and validation in anaerobic digestion: A review. *Water Research*, *45*(17), 5347–5364.

DuBois, Michel., Gilles, K. A., Hamilton, J. K., Rebers, P. A., & Smith, Fred. 1956. Colorimetric Method for Determination of Sugars and Related Substances. *Analytical Chemistry*, *28*(3), 350–356.

Gavala, H. N., Skiadas, I. V, & Lyberatos, G. 1999. On the performance of a centralised digestion facility receiving seasonal agroindustrial wastewaters. *Water Science and Technology*, *40*(1), 339–346.

Girault, R., Rousseau, P., Steyer, J. P., Bernet, N., & Béline, F. 2011. Combination of batch experiments with continuous reactor data for ADM1 calibration: Application to anaerobic digestion of pig slurry. *Water Science and Technology*, *63*(11), 2575–2582.

Han, Y., Green, H., & Tao, W. 2020. Reversibility of propionic acid inhibition to anaerobic digestion: Inhibition kinetics and microbial mechanism. *Chemosphere*, *255*, 126840.

Jurado, E., Antonopoulou, G., Lyberatos, G., Gavala, H. N., & Skiadas, I. V. 2016. Continuous anaerobic digestion of swine manure: ADM1–based modelling and effect of addition of swine manure fibers pretreated with aqueous ammonia soaking. *Applied Energy*, *172*, 190–198.

Kalyuzhnyi, S. V, & Fedorovich, V. V. 1998. Mathematical modelling of competition between sulphate reduction and methanogenesis in anaerobic reactors. *Bioresource Technology*, *65*(3), 227–242.

Kong, J. D. 2017. Modeling Microbial Dynamics: Effects on Environmental and Human Health, Doctoral dissertation, University of Alberta, Canada.

Li, D., Liu, S., Mi, L., Li, Z., Yuan, Y., Yan, Z., & Liu, X. 2015. Effects of feedstock ratio and organic loading rate on the anaerobic mesophilic co–digestion of rice straw and cow manure. *Bioresource Technology*, *189*, 319–326.

Li, H., Chen, Z., Fu, D., Wang, Y., Zheng, Y., & Li, Q. 2020. Improved ADM1 for modelling C, N, P fates in anaerobic digestion process of pig manure and optimization approaches to biogas production. *Renewable Energy*, *146*(422), 2330–2336.

Madigan, M. T., Bender, K. S., Buckley, D. H., Sattley, W. M., & Stahl, D. A. 2018. Brock Biology of Microorganisms. 15th Global Edition. *Boston, US: Benjamin Cummins*, *1*, 1391–1407.

Menardo, S., Gioelli, F., & Balsari, P. 2011. The methane yield of

digestate: Effect of organic loading rate, hydraulic retention time, and plant feeding. *Bioresource Technology*, *102*(3), 2348–2351.

Monod, J. 1949. The growth of bacterial cultures. *Annual Review of microbiology, 3*, 371–394.

Oliveros-Muñoz, J. M., Martínez-Villalba, J. A., Jiménez-Islas, H., Luna-Porres, M. Y., Escamilla-Alvarado, C., & Ríos-Fránquez, F. J. 2021. Luus-Jaakola method and ADM1 based optimization of hydrogen sulfide in anaerobic digestion of cow manure. *Biochemical Engineering Journal*, *171*, 108012.

Peces, M., Astals, S., Jensen, P. D., & Clarke, W. P. 2021. Transition of microbial communities and degradation pathways in anaerobic digestion at decreasing retention time. *New Biotechnology*, *60*, 52–61.

Siegrist, H., Renggli, D., & Gujer, W. 1993. Mathematical modelling of anaerobic mesophilic sewage sludge treatment. *Water Science and Technology*, *27*(2), 25–36.

Van Ginkel, S., & Logan, B. E. 2005. Inhibition of biohydrogen production by undissociated acetic and butyric acids. *Environmental Science and Technology*, *39*(23), 9351–9356.

Vavilin, V. A., Lokshina, L. Y., Rytov, S. V, Kotsyurbenko, O. R., Nozhevnikova, A. N., & Parshina, S. N. 1997. Modelling methanogenesis during anaerobic conversion of complex organic matter at low temperatures. *Water Science and Technology*, *36*(6–7), 531–538.

Weinrich, S., Mauky, E., Schmidt, T., Krebs, C., Liebetrau, J., & Nelles, M. 2021. Systematic simplification of the Anaerobic

Digestion Model No. 1 (ADM1) – Laboratory experiments and model application. *Bioresource Technology*, *333*(1), 125104.

Weinrich, S., & Nelles, M. 2021. Systematic simplification of the Anaerobic Digestion Model No. 1 (ADM1) – Model development and stoichiometric analysis. *Bioresource Technology*, *333*(1), 125124.

Wu, D., Li, L., Zhen, F., Liu, H., Xiao, F., Sun, Y., Peng, X., Li, Y., & Wang, X. 2022. Thermodynamics of volatile fatty acid degradation during anaerobic digestion under organic overload stress: The potential to better identify process stability. *Water Research*, *214*, 118187.

Chapter 6
Conclusions

The primary objective of this study is to evaluate the biokinetics dynamics of anaerobic digestion of thermally hydrolyzed cattle manure. Detailed objectives and a summary of the results are given in each chapter. The conclusions of this thesis corresponding to each goal are as follows:

(1) Effects of THP conditions on the AD of CM was investigated. Increasing the amount of NaOH addition during the THP enhances lignin removal and solubilization of cattle manure. The thermally hydrolyzed cattle manure (at 160 ℃ with 2% (dry wt.) NaOH addition) showed a significantly higher biochemical methane potential of 227.0 ± 11.0 mL-CH_4/g-volatile solid compared to that of intact CM (182.2 ± 2.5 mL-CH_4/g-volatile solid). The concentration of melanoidins reached its highest level of 135.3 mg/g-VS of CM treated at THP condition of 200 ℃ with 6 wt.% NaOH addition, and it increased with elevated temperature and higher NaOH dosage under the tested conditions. Energy balance analysis showed that additional 278.2 ± 43.9 MJ of energy can be gained per tonne of CM by applying THP (at 180 ℃ with 6% NaOH addition). Among the THP conditions without NaOH addition aimed at reducing by-

product formation, the THP at 160 ℃ demonstrated the highest net energy gain.

(2) The performance and stability of AD of CM in relation to the application of THP and variations in SRT was investigated. The THP AD outperformed the control AD by over 1.4 times in terms of methane yield and VS removal at the same SRT. The THP AD operated at an SRT of 13.2 d exhibited higher performance compared to the control AD operated at an SRT of 36.0 d and demonstrated stable operation throughout three HRT cycles. However, reducing the SRT of THP AD from 36.0 to 13.2 d may lead to a decrease in reactor stability. This was evidenced by an increase in the concentration of VFA and changes in the microbial community structure, which became inefficient in terms of AD performance. Further confirmation is required to evaluate the long-term stability of THP AD.

(3) The proposed Dynamic ADM1was validated for intact CM and thermally hydrolyzed CM, enabling the representation of biokinetic parameters variations caused by changes in SRT. Compared to the conventional ADM1, the Dynamic ADM1 demonstrated superior accuracy in predicting

methane production during SRT changes. Model simulations revealed that the application of THP resulted in a 1.5–fold increase in average methane production under SRT conditions ranging from 6.6 to 36.0 d. Additionally, THP led to a reduction in the required SRT for achieving maximum microbial concentration. The Dynamic ADM1 provides more precise prediction of reactor behavior in response to changes in SRT, offering benefits in determining operational conditions, enhancing design, and reducing operating costs.

국문 초록 (ABSTRACT IN KOREAN)

열가수분해 처리된 우분의 혐기성 소화기작 이해와 성능 모사

김 승 환

건설환경공학부

서울대학교 대학원

가축분뇨는 국내 유기성 폐자원 중 80%(습윤중량 기준)를 차지하고 있다. 가축분뇨의 약 86%가 퇴비화로 처리되고 있지만, 퇴비의 수요는 지속적으로 감소할 것으로 전망된다. 혐기성 소화는 유기물을 처리함과 동시에 에너지를 생산할 수 있는 공정으로, 유기성 폐자원의 처리를 위한 방법으로 최근 수십 년간 주목받아 왔다. 혐기성 소화를 통해 가축분뇨를 에너지화 할 경우 그 잠재량은 약 1.7 million TOE/year로 보고되었지만, 가축분뇨의 낮은 혐기성 소화 효율로 인해 공정 운영에 한계가 있다. 본 연구에서는 혐기성 소화 효율 향상을 위한 목적으로 우분 시료를 대상으로 열가수분해 전처리를 적용하고, 혐기성 소화에 대한 영향을 분석하였다.

우분 시료를 대상으로 다양한 온도와 NaOH 주입조건에 대하여 열가수분해 전처리를 수행하고 생화학적 메탄 잠재량을 측정하였다.

또한, 전처리과정 중 발생할 수 있는 난분해성 및 독성 물질(예를 들어, melanoidin과 furfural)의 생성을 확인하고, 공정의 에너지 수지를 계산하였다. 그 결과, 우분의 열가수분해 과정 중 NaOH 농도의 증가는 섬유질 내 리그닌 함량을 감소시켰으며 우분의 가용화율을 증가시켰다. 우분을 2% NaOH, 160도 조건에서 처리한 경우 메탄잠재량이 227.0 ± 11.0 mL−CH_4/g−VS로 가장 높았으며, 전처리하지 않은 우분의 메탄잠재량 (182.2 ± 2.5 mL−CH_4/g−VS) 대비 약 25% 높았다. 180도 이상의 고온 처리조건에서 난분해성 물질과 furfural의 급격한 증가를 확인하였으며, NaOH 주입량이 증가함에 따라 난분해성 물질의 생성이 촉진되었다. THP 적용에 따른 추가 에너지 생산량은 실험 조건 중 6% NaOH, 180도 조건에서 278.2 ± 43.9 MJ/tonne−CM으로 가장 높았다. 난분해성 물질의 생성을 줄이기 위해 NaOH 주입을 제한할 경우 추가 에너지 생산량은 160도 처리 조건에서 161.4 ± 39.3 MJ/tonne−CM으로 가장 높았다.

실험실 규모의 연속식 완전혼합반응조를 중온의 혐기성 조건에서 고형물체류시간을 점차 단축시키며 약 400일 동안 운전함으로써 열가수분해 전처리 적용에 따른 우분 혐기성 소화조의 고형물체류시간 단축 가능성을 평가하였다. 열가수분해 전처리는 NaOH 주입 없이 160 ℃, 6.1 atm 조건에서 30분간 수행하였으며, 소화조의 고형물체류시간은 36.0일을 시작으로 21.8, 13.2, 8.0일로 점차 단축시켰다. 실험 결과, 열가수분해 전처리를 적용함에 따라 동일한 고형물체류시간을 갖는 대조군 대비 1.4배 이상의 메탄 수율과 휘발성 고형물 제거 성능을 나타내었다. 열가수분해 전처리가 적용된 소화조의

경우 13.2일의 고형물체류시간 조건으로 운전하더라도 36일 조건에서 운전한 대조군 소화조보다 높은 성능을 나타내었다. 하지만, 열가수분해 전처리가 적용된 소화조의 고형물체류시간을 36.0일에서 13.2일로 단축함에 따라 저해 가능성이 있는 휘발성유기산의 농도가 165 mg/L에서 613 mg/L로 상승하였으며, 소화조 미생물 군집이 소화조 성능에 비효율적인 방향으로 변화하였다. 이를 통해 소화조 안정성이 감소할 수 있음을 확인하였다. 본 실험에서는 13.2일 조건에서 세 주기 만큼의 고형물체류시간 동안 안정적인 반응을 확인하였다. 장기 운전에 대한 안정성 확인이 필요하다.

마지막으로, 소화조의 거동 예측 모형인 Anaerobic Digestion Model No.1(ADM1) 모형이 소화조의 고형물체류시간 변화에 따른 미생물의 생물화학적 상수 변화를 예측하여 반영할 수 있도록 개선하였다. 고형물체류시간과 생물화학적 상수 간의 관계를 선형회귀분석한 후 모형에 도입하여 미생물의 생물화학적 상수를 고형물체류시간에 대한 함수로 변경하여 Dynamic ADM1 모형을 구축하였다. 우분 혐기성 소화조의 운전 데이터로 교정한 모델을 이용하여 다른 조건에서 운전된 별도의 소화조 메탄 발생량을 모사하고, 결과를 비교하여 모형의 유효성(validation)을 확인하였다. 기존 ADM1 모형과 새로 개발한 Dynamic ADM1의 비교를 통해 모형의 정확도가 향상되었음을 확인하였다. 열가수분해가 결합된 우분 혐기성 소화조에 대하 동일한 과정을 수행하여 모형의 유효성을 확인하였고, 모사 실험을 통해 열가수분해 전처리에 의한 혐기성 소화조의 영향을 해석하였다. ADM1 모형 개선을 통해 변화하는 고형물체류시간에 대한 예측

정확도가 향상되었으며, 이는 소화조 운전 조건 최적화, 설계 개선, 운영비용 절감에 활용될 수 있다.